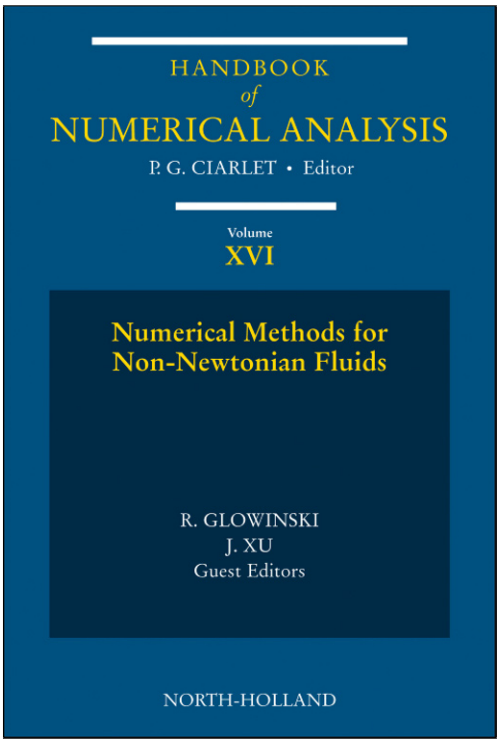

From Young-Ju Lee, Jinchao Xu, and Chen-Song Zhang, Stable Finite Element Discretizations for Viscoelastic Flow Models.
In: P.G. Ciarlet, editor, Handbook of Numerical Analysis, Vol XVI,
Special Volume: Numerical Methods for Non-Newtonian Fluids,
Guest Editors: R. Glowinski and J. Xu.
The Netherlands: North-Holland, 2011, pp. 371–432.
ISBN: 978-0-444-53047-9

Stable Finite Element Discretizations for Viscoelastic Flow Models

Young-Ju Lee
Department of Mathematics, Rutgers, The State University of New Jersey, NJ 08901, USA
E-mail: leeyoung@math.rutgers.edu

Jinchao Xu
Department of Mathematics and Center for Computational Mathematics and Application, the Pennsylvania State University, PA 16802, USA
E-mail: xu@math.psu.edu

Chen-Song Zhang
Department of Mathematics and Center for Computational Mathematics and Application, the Pennsylvania State University, PA 16802, USA
E-mail: zhangchensong@gmail.com

Numerical Methods for Non-Newtonian Fluids
Special Volume (R. Glowinski and Jinchao Xu, Guest Editors) of
HANDBOOK OF NUMERICAL ANALYSIS, VOL. XVI
P.G. Ciarlet (Editor)

ISSN 1570-8659
DOI 10.1016/B978-0-444-53047-9.00004-6

1. Introduction

A complex fluid, also called a non-Newtonian fluid, is "a fluid made up of a lot of different kinds of stuff" as described by Gelbart and Ben-Shaul [1996]. This high number of complexities and their interactions can produce a variety of new nontrivial physical phenomena (Bird, Curtiss, Armstrong and Hassager [1987]), including, for example, the rod-climbing Weissenberg effect (Dealy and Vu [1977]) and the die swell (Clermont and Pierrard [1976]). Among the phenomena that have been of particular research interest in recent years are the flow behaviors in highly elastic complex fluid with a vanishingly small Reynolds number (Groisman and Steinberg [1998], Thomases and Shelley [2009]). It is agreed that the peculiar behavior of the highly elastic fluids flow, known as "elastic turbulence," originates in the strong nonlinear mechanical properties of the polymer solutions (Groisman and Steinberg [1998]), and it is similar to the phenomena observed from the strong inertial effects in Newtonian fluids. During the past decade, these phenomena have been the subject of many theoretical and experimental studies.

The controlling parameter of the strength of the nonlinearity of complex fluid models is the Weissenberg number or the Deborah number. Roughly speaking, the larger the Weissenberg number, the stronger the elasticity of the polymer solutions (see Groisman and Steinberg [1998]). One crucial outstanding problem in computational rheology is that computations for complex fluid models with a high Weissenberg number have encountered great difficulty due to a breakdown in the convergence of the algorithms at critical values of the Weissenberg number. Although some significant progress has been made in recent years (e.g., Fattal and Kupferman [2004]), the level of fundamental correctness in the relevant regimes of large Weissenberg number has yet to be obtained. The main aim of this article is to focus on the issues that arise in simulating highly elastic and high Weissenberg number flows.

After briefly reviewing recent progress regarding the theoretical and numerical study of generic polymeric fluids in high Weissenberg number regimes, we will give a detailed presentation of a family of algorithms originally proposed by Lee and Xu's [2006] and some new results developed in the last few years. In particular, we will give a more refined presentation of the positivity-preserving discretization schemes proposed in Lee and Xu's [2006] and present some preliminary numerical experiments. In our discussion, we will

- demonstrate how a general macroscopic viscoelastic fluid model can be reformulated, in terms of the conformation tensor, as a Riccati differential equation;
- use this reformulation to establish the positive definiteness of the conformation tensor;
- use key numerical methods based on the Eulerian–Lagrangian method, which discretizes the momentum equation and constitutive equations by solving the nonlinear ordinary differential equations that define the characteristics related to the transport part of the equation;
- discuss how the resulting discrete system can be effectively solved iteratively by combining multigrid and parallel computing techniques; and
- show that the nonlinear iterations uniformly converge and the computational costs of the methods are uniformly optimal with respect to relevant physical parameters (such as the Reynolds number and the Weissenberg number) as well as time step and mesh sizes (see Lee, Xu and Zhang [To appear]).

The rest of the article is organized as follows. In Section 2, we review the basic properties of the flow maps, the generalized Lie derivatives, and the algebraic Riccati differential equations. In Section 3, we introduce the connection between the algebraic Riccati differential equations and the macroscopic constitutive relations for viscoelastic fluids. In Section 4, we discuss the properties of various macroscopic models for viscoelastic fluids. In Section 5, we briefly review the existing numerical schemes designed for simulating viscoelastic fluids at high Weissenberg number regimes. In Section 6, we discuss the numerical discretization schemes that preserve the positive definiteness of the conformation tensor. In Section 7, we briefly consider the solution techniques for the resulting discrete systems. In Section 8, we show the energy estimate, the long-term stability, and the well posedness, of the discrete solution, and then in Section 9, we present the implementation details and corresponding numerical results. Finally, in Section 10, we offer concluding remarks.

2. Flow maps, generalized Lie derivatives, and Riccati equations

2.1. Notation

Throughout this article, we use the standard notation for Sobolev spaces: $H^k(\Omega)$ denotes the classical Sobolev space of scalar functions on a bounded domain $\Omega \subset \mathbb{R}^d$ whose derivatives up to order k are square integrable, with the full norm $\|\cdot\|_k$ and the corresponding seminorm $|\cdot|_k$. The symbol $H_0^1(\Omega)$ denotes the subspace of $H^1(\Omega)$ whose trace vanishes on the boundary $\partial\Omega$. We will also discuss the corresponding spaces restricted to the subdomain of Ω. For any $\omega \subset \Omega$, we denote $\|\cdot\|_{k,\omega}$ and $|\cdot|_{k,\omega}$ as the norm and the seminorm, respectively, on the domain ω. The usual L^∞-norm and L^2-norm will be denoted by $\|\cdot\|_\infty$ and $\|\cdot\|_0$, respectively. The symbol $L_0^2(\Omega)$ denotes a subspace of $L^2(\Omega)$ consisting of functions that have a zero average. $(\cdot,\cdot)$ and $\langle\cdot,\cdot\rangle$ denote the classical L^2-inner product and the dual pairing, respectively. The space $L^p(0,T;H^1(\Omega))$ for $1 \le p < \infty$ is the Hilbert space consisting of functions $f(x,t) : \Omega \times [0,T] \mapsto \mathbb{R}$ such that

$$\left(\int_0^T \|f(\cdot,\nu)\|_1^p \, \mathrm{d}\nu \right)^{1/p} < \infty.$$

The symbol $\mathbb{M}$ denotes the space of matrix-valued functions whose ranges are in $\mathbb{R}^{d\times d}$, and $\mathbb{S}$ denotes the subspace of $\mathbb{M}$ consisting of the symmetric matrices. In addition, $\mathbb{S}^+$ denotes the subset of $\mathbb{S}$ consisting of positive-definite matrices. Finally, following (Xu [1992]), the symbol $A \lesssim B$ means $A \le CB$ with a constant C independent of space mesh size h and time step k, and $A \lesssim B$ is an abbreviation of $A \lesssim B \lesssim A$.

2.2. Flow maps and the deformation tensor

Consider a bounded domain $\Omega \subset \mathbb{R}^d$ ($d = 2$ or 3) and a velocity field of flow $\mathbf{u} = (u_i) \in \mathbb{R}^d$. The motion of a particle can be described by the flow map $\phi_{t,s} : \Omega \mapsto \Omega$ such that

$$\frac{\partial}{\partial s}\phi_{t,s}(x) = \mathbf{u}(\phi_{t,s}(x), s), \quad \phi_{t,t}(x) = x. \tag{2.1}$$

We note that by $\phi_{t,t}(x) = x$, we mean that the Eulerian coordinate is coincident with the Lagrangian (or material) coordinate at time t. As in classical mechanics, the flow map $\phi_{t,s}$ is assumed to be a diffeomorphism. Moreover, the flow map satisfies the composition rule, i.e., $\phi_{t_1,t_2}\phi_{t,t_1} = \phi_{t,t_2}$, for any $t_1, t_2 \geq 0$.

By means of this flow map, with an abuse of notation, we define

$$v(t,s) = v(x,t;s) := v(\phi_{t,s}(x), s) \quad \text{and} \quad v(t,t) = v(t) = v(x,t;t) = v(x,t),$$

where v can be any (scalar, vector, or tensor) function. Furthermore, for any $v(x,t)$, we have the following definition of the material derivative:

$$\frac{Dv}{Dt}(x,t) := \frac{\partial}{\partial s} v(\phi_{t,s}(x), s)\Big|_{s=t} = \big(v_t + (\mathbf{u}\cdot\nabla)v\big)(x,t). \tag{2.2}$$

Of the different conventions to define the gradient of velocity $\mathbf{u}$, denoted by $\nabla\mathbf{u}$ (or $\nabla_x\mathbf{u}$), we use the convention that $(\nabla\mathbf{u})_{i,j} = (\partial_j u_i)_{i,j}$, i.e.,

$$\nabla\mathbf{u} := \begin{pmatrix} \nabla u_1^T \\ \nabla u_2^T \\ \vdots \\ \nabla u_d^T \end{pmatrix} = \begin{pmatrix} \partial_1 u_1 & \partial_2 u_1 & \cdots & \partial_d u_1 \\ \partial_1 u_2 & \partial_2 u_2 & \cdots & \partial_d u_2 \\ \vdots & \vdots & \ddots & \vdots \\ \partial_1 u_d & \partial_2 u_d & \cdots & \partial_d u_d \end{pmatrix}.$$

For any two time variables, t_1 and t_2, we define the relative deformation gradient $\boldsymbol{F}(x,t;t_1,t_2)$ ($\boldsymbol{F}(t;t_1,t_2)$ in short) as follows:

$$\boldsymbol{F}(t;t_1,t_2) := \nabla_z \phi_{t_1,t_2}(z), \quad \text{with } z = \phi_{t,t_1}(x). \tag{2.3}$$

In case $t_1 = t$, we have $\boldsymbol{F}(t;t,t_2) = \nabla_x \phi_{t,t_2}(x)$. Geometrically, the deformation gradient $\boldsymbol{F}(t;t_1,t_2)$ measures the relative deformation between two configurations at t_1 and t_2.

From the definition of $\boldsymbol{F}(t;t_1,t_2)$ and the chain rule, we can derive the following ordinary differential equation:

$$\begin{aligned} \frac{\partial \boldsymbol{F}(t;t_1,t_2)}{\partial t_2} &= \frac{\partial}{\partial t_2}\nabla_z \phi_{t_1,t_2}(z) = \nabla_z \mathbf{u}(\phi_{t,t_2}(x), t_2) = \nabla_z \mathbf{u}(\phi_{t_1,t_2}(z), t_2) \\ &= \nabla\mathbf{u}(\phi_{t_1,t_2}(z), t_2)\boldsymbol{F}(t;t_1,t_2) = \nabla\mathbf{u}(t,t_2)\boldsymbol{F}(t;t_1,t_2) \end{aligned} \tag{2.4}$$

and the initial condition $\boldsymbol{F}(t;t_1,t_1) = \boldsymbol{\delta}$, where $\boldsymbol{\delta}$ is the identity tensor.

Throughout this article, we will only consider incompressible fluids, namely, $\nabla\cdot\mathbf{u} = 0$, which implies the determinant of $\boldsymbol{F}(t;t_1,t_2)$ is one, i.e., $\det \boldsymbol{F}(t;t_1,t_2) = 1$. Therefore, it is invertible. Furthermore, the inverse of $\boldsymbol{F}(t;t_1,t_2)$ is given by $\boldsymbol{F}(t;t_2,t_1)$ unambiguously because we have the following relation:

$$\boldsymbol{F}(t;t_2,t_1) = \nabla_{z'} \phi_{t_2,t_1}(z'), \quad \text{with } z' = \phi_{t,t_2}(x). \tag{2.5}$$

Using (2.5), we can derive the following relation that

$$\begin{aligned} 0 = \frac{\partial\big(\boldsymbol{F}(t;t_1,t_2)\boldsymbol{F}(t;t_2,t_1)\big)}{\partial t_2} &= \frac{\partial \boldsymbol{F}(t;t_1,t_2)}{\partial t_2}\boldsymbol{F}(t;t_2,t_1) + \boldsymbol{F}(t;t_1,t_2)\frac{\partial \boldsymbol{F}(t;t_2,t_1)}{\partial t_2} \\ &= \nabla\mathbf{u}(t,t_2) + \boldsymbol{F}(t;t_1,t_2)\frac{\partial \boldsymbol{F}(t;t_2,t_1)}{\partial t_2}. \end{aligned}$$

Therefore, we obtain

$$\frac{\partial \boldsymbol{F}(t;t_2,t_1)}{\partial t_2} = -\boldsymbol{F}(t;t_2,t_1)\nabla \mathbf{u}(t,t_2) \quad \text{and} \quad \boldsymbol{F}(t;t_1,t_1) = \boldsymbol{\delta}. \tag{2.6}$$

2.3. *Generalized Lie derivatives*

We will now introduce the generalized Lie derivative. For any given continuous function $\boldsymbol{\Phi}(t) = \boldsymbol{\Phi}(x,t)\colon \Omega \times (0,+\infty) \mapsto \mathbb{M}$, we define $\boldsymbol{L}(t;t_1,t_2)$ to be the transition matrix (or evolution matrix) that satisfies the following ordinary differential equation:

$$\frac{\partial \boldsymbol{L}(t;t_1,t_2)}{\partial t_2} = \boldsymbol{\Phi}(t,t_2)\boldsymbol{L}(t;t_1,t_2) \quad \text{and} \quad \boldsymbol{L}(t;t_1,t_1) = \boldsymbol{\delta}. \tag{2.7}$$

We can view this transition matrix $\boldsymbol{L}(t;t_1,t_2)$ as a generalization of the deformation gradient $\boldsymbol{F}(t;t_1,t_2)$; when $\boldsymbol{\Phi}(t,t_2) = \nabla \mathbf{u}(t,t_2)$, $\boldsymbol{L}(t;t_1,t_2)$ reduces to $\boldsymbol{F}(t;t_1,t_2)$.

The following lemma gives a fundamental property of the transition matrices (see, for example, Brockett [1970, theorem 2, section 1.4].)

Lemma 2.1 (Composition Rule). *For any time levels, $t, t_0, t_1, t_2 \geq 0$, we have the following property*

$$\boldsymbol{L}(t;t_1,t_2)\boldsymbol{L}(t;t_0,t_1) = \boldsymbol{L}(t;t_0,t_2). \tag{2.8}$$

In particular, we also have

$$\boldsymbol{L}(t;t_1,t_0)\boldsymbol{L}(t;t_0,t_1) = \boldsymbol{\delta}.$$

Furthermore, we have that $\boldsymbol{L}(t;t_2,t_1)$ is the inverse of $\boldsymbol{L}(t;t_1,t_2)$ and it satisfies:

$$\frac{\partial \boldsymbol{L}(t;t_2,t_1)}{\partial t_2} = -\boldsymbol{L}(t;t_2,t_1)\boldsymbol{\Phi}(t,t_2) \quad \textit{and} \quad \boldsymbol{L}(t;t_1,t_1) = \boldsymbol{\delta}. \tag{2.9}$$

Proof. Given any point $y \in \Omega$, we consider the ordinary differential equation:

$$\frac{\partial y(s)}{\partial s} = \boldsymbol{\Phi}(t,s)y(s) \quad \text{and} \quad y(t_1) = y. \tag{2.10}$$

Then, by definition (2.7), we obtain $y(s) = \boldsymbol{L}(t;t_1,s)y$. Similarly, let $z(s)$ satisfy the following ODE:

$$\frac{\partial z(s)}{\partial s} = \boldsymbol{\Phi}(t,s)z(s) \quad \text{and} \quad z(t_0) = y(t_0). \tag{2.11}$$

We have the relation:

$$z(s) = \boldsymbol{L}(t;t_0,s)y(t_0) = \boldsymbol{L}(t;t_0,s)\boldsymbol{L}(t;t_1,t_0)y.$$

It follows that $z(t_1) = \boldsymbol{L}(t;t_0,t_1)\boldsymbol{L}(t;t_1,t_0)y$, which implies that

$$z(s) = \boldsymbol{L}(t;t_1,s)z(t_1) = \boldsymbol{L}(t;t_1,s)\boldsymbol{L}(t;t_0,t_1)\boldsymbol{L}(t;t_1,t_0)y.$$

Consequently, by the definition and the uniqueness of the transition matrix $\boldsymbol{L}$, we have

$$\boldsymbol{L}(t;t_0,s)\boldsymbol{L}(t;t_1,t_0)y=\boldsymbol{L}(t;t_1,s)\boldsymbol{L}(t;t_0,t_1)\boldsymbol{L}(t;t_1,t_0)y,\quad \forall\, y\in\Omega,\ s\geq 0.$$

Hence, we can get the composition rule. Furthermore, by simply taking $t_2=t_0$, we obtain the second equation in this lemma.

Hence, we immediately see that $\boldsymbol{L}(t;t_1,t_2)\boldsymbol{L}(t;t_2,t_1)=\boldsymbol{L}(t;t_2,t_2)=\boldsymbol{\delta}$. By taking derivatives with respect to t_2 on both sides, we can obtain

$$\frac{\partial \boldsymbol{L}(t;t_1,t_2)}{\partial t_2}\boldsymbol{L}(t;t_2,t_1)+\boldsymbol{L}(t;t_1,t_2)\frac{\partial \boldsymbol{L}(t;t_2,t_1)}{\partial t_2}=0.$$

By plugging (2.7) into the equation above, we can see that $\boldsymbol{L}(t;t_2,t_1)$ is the inverse of $\boldsymbol{L}(t;t_1,t_2)$ and it satisfies the following ODE:

$$\frac{\partial \boldsymbol{L}(t;t_2,t_1)}{\partial t_2}=-\boldsymbol{L}(t;t_2,t_1)\big(\boldsymbol{\Phi}(t,t_2)\boldsymbol{L}(t;t_1,t_2)\big)\boldsymbol{L}(t;t_2,t_1)=-\boldsymbol{L}(t;t_2,t_1)\boldsymbol{\Phi}(t,t_2)$$

and the initial condition $\boldsymbol{L}(t;t_1,t_1)=\boldsymbol{\delta}$. □

Now, we are ready to introduce to the definition and the properties of the generalized Lie derivative.

DEFINITION 2.1 (Generalized Lie Derivative). We define the generalized Lie derivative of a symmetric tensor with respect to $\boldsymbol{\Phi}$ in the Lagrangian frame as follows: for $t,s\geq 0$,

$$\mathcal{L}_{\mathbf{u},\boldsymbol{\Phi}}\boldsymbol{\zeta}(t,s):=\boldsymbol{L}(t;t,s)\frac{\partial\left(\boldsymbol{L}(t;s,t)\boldsymbol{\zeta}(t,s)\boldsymbol{L}(t;s,t)^T\right)}{\partial s}\boldsymbol{L}(t;t,s)^T. \tag{2.12}$$

In the Eulerian coordinates, we let $s=t$ and

$$\mathcal{L}_{\mathbf{u},\boldsymbol{\Phi}}\boldsymbol{\zeta}(t):=\boldsymbol{L}(t;t,s)\frac{\partial\left(\boldsymbol{L}(t;s,t)\boldsymbol{\zeta}(t,s)\boldsymbol{L}(t;s,t)^T\right)}{\partial s}\boldsymbol{L}(t;t,s)^T\Big|_{s=t}. \tag{2.13}$$

The following lemma then gives the generalized Lie derivative defined above in the Eulerian frame:

LEMMA 2.2 (The Generalized Lie Derivative in the Eulerian Frame). *For any* $\boldsymbol{\zeta}=\boldsymbol{\zeta}(x,t)\colon \Omega\times(0,+\infty)\mapsto\mathbb{S}$, *we have*

$$\mathcal{L}_{\mathbf{u},\boldsymbol{\Phi}}\boldsymbol{\zeta}(t)=\frac{D\boldsymbol{\zeta}(t)}{Dt}-\boldsymbol{\Phi}(t)\boldsymbol{\zeta}(t)-\boldsymbol{\zeta}(t)\boldsymbol{\Phi}(t)^T. \tag{2.14}$$

PROOF. Using Eqn (2.9) and the product rule, we have

$$\begin{aligned}\frac{\partial\left(\boldsymbol{L}(t;s,t)\boldsymbol{\zeta}(t,s)\boldsymbol{L}(t;s,t)^T\right)}{\partial s}&=\frac{\partial \boldsymbol{L}(t;s,t)}{\partial s}\boldsymbol{\zeta}(t,s)\boldsymbol{L}(t;s,t)^T+\boldsymbol{L}(t;s,t)\frac{\partial\boldsymbol{\zeta}(t,s)}{\partial s}\boldsymbol{L}(t;s,t)^T\\&\quad+\boldsymbol{L}(t;s,t)\boldsymbol{\zeta}(t,s)\frac{\partial \boldsymbol{L}(t;s,t)^T}{\partial s}.\end{aligned}$$

Hence, we can immediately obtain

$$\begin{aligned}\mathcal{L}_{\mathbf{u},\boldsymbol{\Phi}}\boldsymbol{\zeta}(t,s) &= \boldsymbol{L}(t;t,s)\frac{\partial(\boldsymbol{L}(t;s,t)\boldsymbol{\zeta}(t,s)\boldsymbol{L}(t;s,t)^T)}{\partial s}\boldsymbol{L}(t;t,s)^T \\ &= \boldsymbol{L}(t;t,s)\frac{\partial \boldsymbol{L}(t;s,t)}{\partial s}\boldsymbol{\zeta}(t,s) + \frac{\partial \boldsymbol{\zeta}(t,s)}{\partial s} + \boldsymbol{\zeta}(t,s)\frac{\partial \boldsymbol{L}(t;s,t)^T}{\partial s}\boldsymbol{L}(t;t,s)^T.\end{aligned}$$

Using the relation (2.9), we observe that

$$\mathcal{L}_{\mathbf{u},\boldsymbol{\Phi}}\boldsymbol{\zeta}(t,s) = \frac{\partial \boldsymbol{\zeta}(t,s)}{\partial s} - \boldsymbol{\Phi}(t,s)\boldsymbol{\zeta}(t,s) - \boldsymbol{\zeta}(t,s)\boldsymbol{\Phi}(t,s)^T. \tag{2.15}$$

Now, by letting $s = t$, we get Eqn (2.14) in this lemma. □

The derivative $\mathcal{L}_{\mathbf{u},\boldsymbol{\Phi}}\boldsymbol{\zeta}$ is known as the Truesdell stress rate (Simo and Hughes [1998]). The notion of generalized Lie derivatives makes it possible to treat many complicated time derivatives in a unified way. This observation has been used in developing numerical schemes effectively in the pioneering work by Hughes and Winget [1980]. The main advantage that had been obtained was that the temporal discretization induced from this type of Lie derivative-based algorithms can have the numerical frame indifference, which is called the *incrementally objective discretization*. A key observation in Lee and Xu's [2006] is that many macroscopic constitutive equations can be reformulated into a well-known symmetric matrix Riccati differential equation in terms of the aforementioned generalized Lie derivatives. Many new numerical methods can be obtained based on this observation. This will be further explored in Sections 3 and 6.

2.4. *A few examples of generalized Lie derivatives*

With some appropriate choices of transition matrices, one can consider many types of generalized Lie derivatives; see especially Hughes [1984] and Simo and Hughes [1998]. For example, if $\boldsymbol{\Phi}(t)$ is the zero matrix, then the transition matrix $\boldsymbol{L}(t;s,t) \equiv \boldsymbol{\delta}$ and the corresponding generalized Lie derivative are reduced to the usual material derivative (2.2).

We now give a few more examples that will be used in the next section.

Example 2.1 (Upper Convective Maxwell Derivative). If $\boldsymbol{\Phi}(t) = \nabla\mathbf{u}(t)$, then the transition matrix $\boldsymbol{L}(t;s,t) = \boldsymbol{F}(t;s,t)$ is the deformation gradient. From Lemma 2.2, the generalized Lie derivative with respect to $\boldsymbol{\Phi}(t)$ is just the upper convective Maxwell derivative (Oldroyd [1950]):

$$\mathcal{L}_{\mathbf{u},\boldsymbol{\Phi}}\boldsymbol{\zeta}(t) = \frac{D\boldsymbol{\zeta}(t)}{Dt} - \nabla\mathbf{u}(t)\,\boldsymbol{\zeta}(t) - \boldsymbol{\zeta}(t)\nabla\mathbf{u}(t)^T, \qquad \forall \boldsymbol{\zeta}(t) \in \mathbb{M}. \tag{2.16}$$

Example 2.2 (Lower Convective Maxwell Derivative). If $\boldsymbol{\Phi}(t) = -\nabla\mathbf{u}(t)^T$, then the transition matrix $\boldsymbol{L}(t;s,t) = \boldsymbol{F}(t;t,s)$, the inverse of $\boldsymbol{F}(t;s,t)$ (cf. Eqn (2.6)). In this case, we have that

$$\mathcal{L}_{\mathbf{u},\boldsymbol{\Phi}}\boldsymbol{\zeta}(t) = \frac{D\boldsymbol{\zeta}(t)}{Dt} + \nabla\mathbf{u}(t)^T\,\boldsymbol{\zeta}(t) + \boldsymbol{\zeta}(t)\,\nabla\mathbf{u}(t), \qquad \forall \boldsymbol{\zeta}(t) \in \mathbb{M}. \tag{2.17}$$

This is the well-known lower convective Maxwell derivative.

These two examples above have been studied in terms of the Lie derivative by THIFFEAULT [2001].

EXAMPLE 2.3 (Gordon–Schowalter Derivative). We can also take $\boldsymbol{\Phi}(t) = \boldsymbol{R}(t)$ with

$$\boldsymbol{R}(t) := \frac{\mathsf{a}+1}{2}\nabla\mathbf{u}(t) + \frac{\mathsf{a}-1}{2}\nabla\mathbf{u}^T(t),$$

where $\mathsf{a} \in [-1, 1]$ is some parameter. In this case, the generalized Lie derivative with respect to $\boldsymbol{R}(t)$ can be given as follows:

$$\mathcal{L}_{\mathbf{u},\boldsymbol{R}}\boldsymbol{\zeta}(t) = \frac{D\boldsymbol{\zeta}(t)}{Dt} - \boldsymbol{R}(t)\,\boldsymbol{\zeta}(t) - \boldsymbol{\zeta}(t)\,\boldsymbol{R}(t)^T. \tag{2.18}$$

This is known as the Gordon–Schowalter derivative (GORDON and SCHOWALTER [1972]), in which the transition matrix is often denoted by $\boldsymbol{E}$ (JOHNSON and SEGALMAN [1977]), and we also use this convention in the rest of this article.

2.5. *Riccati differential equations*

The classical symmetric matrix Riccati differential equation (ABOU-KANDIL, FREILING, IONESCU and JANK [2003]) for a symmetric tensor $\boldsymbol{\zeta} : \Omega \times (0, +\infty) \mapsto \mathbb{S}$ has this form:

$$\frac{D\boldsymbol{\zeta}(t)}{Dt} = \boldsymbol{A}(t)\boldsymbol{\zeta}(t) + \boldsymbol{\zeta}(t)\boldsymbol{A}(t)^T - \boldsymbol{\zeta}(t)\boldsymbol{B}(t)\boldsymbol{\zeta}(t)^T + \boldsymbol{G}(t), \tag{2.19}$$

with a symmetric positive semidefinite initial condition $\boldsymbol{\zeta}(t, 0) = \boldsymbol{\zeta}_0$. Typically, it is assumed that the coefficient matrices $\boldsymbol{A}$, $\boldsymbol{B}$, and $\boldsymbol{G}$ are bounded and that the matrices $\boldsymbol{B}$ and $\boldsymbol{G}$ are both symmetric and positive semidefinite.

In particular, in this study, we are interested in two important properties of the Riccati differential equation (2.19):

- Equation (2.19) has a certain closed-form solution, from which the solution $\boldsymbol{\zeta}$ can be proved to be symmetric positive definite under certain conditions.
- The positivity-preserving schemes for such equations can easily be devised, especially in time, as investigated in the literature, as well as in terms of the solution to the Riccati form of the ODE (DIECI and EIROLA [1996]).

The following theorem shows further how this view can be exploited to establish the property of the solution to a symmetric matrix Riccati differential equation.

THEOREM 2.1 (Solution of Riccati Equations). *Equation (2.19) is equivalent to*

$$\mathcal{L}_{\mathbf{u},\boldsymbol{\Phi}}\boldsymbol{\zeta}(t) = \boldsymbol{G}(t), \quad \textit{with} \quad \boldsymbol{\Phi}(t) = \boldsymbol{A}(t) - \frac{1}{2}\boldsymbol{B}(t)\boldsymbol{\zeta}(t). \tag{2.20}$$

Furthermore, we can write $\boldsymbol{\zeta}$ in a closed form as follows: for any $t, s \geq 0$,

$$\boldsymbol{\zeta}(t) = \boldsymbol{L}(t; s, t)\boldsymbol{\zeta}(t, s)\boldsymbol{L}(t; s, t)^T + \int_s^t \boldsymbol{L}(t; \nu, t)\boldsymbol{G}(t, \nu)\boldsymbol{L}(t; \nu, t)^T \mathrm{d}\nu, \tag{2.21}$$

where the transition matrix $\boldsymbol{L}$ *satisfies the following ODE:*

$$\frac{\partial \boldsymbol{L}(t;t_1,t_2)}{\partial t_2} = \boldsymbol{\Phi}(t,t_2)\boldsymbol{L}(t;t_1,t_2) \quad \textit{and} \quad \boldsymbol{L}(t;t_1,t_1) = \boldsymbol{\delta}.$$

PROOF. We first rewrite Eqn (2.19) in the Lagrangian frame:

$$\frac{\partial \boldsymbol{\zeta}(t,s)}{\partial s} = \boldsymbol{A}(t,s)\boldsymbol{\zeta}(t,s) + \boldsymbol{\zeta}(t,s)\boldsymbol{A}(t,s)^T - \boldsymbol{\zeta}(t,s)\boldsymbol{B}(t,s)\boldsymbol{\zeta}(t,s)^T + \boldsymbol{G}(t,s). \tag{2.22}$$

Hence, the equivalence between two Eqns (2.19) and (2.20) is straightforward from the definition of generalized Lie derivatives and (2.15). We can write Eqn (2.20) as follows:

$$\boldsymbol{L}(t;t,s)\frac{\partial(\boldsymbol{L}(t;s,t)\boldsymbol{\zeta}(t,s)\boldsymbol{L}(t;s,t)^T)}{\partial s}\boldsymbol{L}(t;t,s)^T = \boldsymbol{G}(t,s). \tag{2.23}$$

This relation can also be cast into the following form:

$$\frac{\partial(\boldsymbol{L}(t;\nu,t)\boldsymbol{\zeta}(t,\nu)\boldsymbol{L}(t;\nu,t)^T)}{\partial \nu} = \boldsymbol{L}(t;\nu,t)\boldsymbol{G}(t,\nu)\boldsymbol{L}(t;\nu,t)^T. \tag{2.24}$$

By taking integration (from s to t) with respect to ν on both sides of the equality above, we obtain the desired result. This completes the proof. □

REMARK 2.1 (Positive Definiteness of the Solution). Notice that the expression of $\boldsymbol{\zeta}$ given in Eqn (2.21) suggests that $\boldsymbol{\zeta}$ is always positive definite if $\boldsymbol{G}$ and $\boldsymbol{\zeta}_0$ are positive definite.

In the rest of this article, we drop the first variable of the transition matrix $\boldsymbol{L}(t;t_1,t_2)$ when t_1 or t_2 is equal to t. For example, $\boldsymbol{L}(t;s,t)$ is denoted simply by $\boldsymbol{L}(s,t)$. Same notation applies to the deformation gradient $\boldsymbol{F}(s,t) = \boldsymbol{F}(t;s,t)$ as well.

3. General macroscopic viscoelastic models

Most macroscopic complex fluid models are given by three fundamental equations: the momentum balance equation, the continuity equation, and a constitutive law. In this section, as stated earlier, we will reformulate various constitutive equations from viscoelastic fluid models into symmetric matrix Riccati differential equations (ABOU-KANDIL, FREILING, IONESCU and JANK [2003]). This new formulation will be a key ingredient in understanding viscoelastic fluid models and in developing new numerical algorithms. The link between viscoelastic fluid models and symmetric matrix Riccati differential equations was first established by LEE and XU's [2006]. It is then successfully used by LEE [2004] to compute the falling sphere simulation through the Johnson–Segalman fluids. The close relation between the general macroscopic viscoelastic fluid models and the symmetric matrix Riccati differential equations in this section leads to a number of important numerical schemes for solving non-Newtonian equations in a unified framework, and it opens new doors to further development.

3.1. Basic fluid models

Consider fluids that occupy a bounded domain $\Omega \subset \mathbb{R}^d$. Define the Reynolds number $\mathsf{Re} := \bar{U}\bar{L}/\eta_0$ where η_0 is the zero shear viscosity and $\bar{U}$ and $\bar{L}$ are the characteristic velocity scale and the length scale, respectively. The dimensionless form of the momentum balance and continuity equations in these models can be written as follows:

$$\mathsf{Re}\left(\frac{\partial \mathbf{u}}{\partial t} + \mathbf{u}\cdot\nabla\mathbf{u}\right) = -\nabla p + \nabla\cdot\boldsymbol{T}, \tag{3.1}$$

and

$$\nabla\cdot\mathbf{u} = 0, \tag{3.2}$$

where $\mathbf{u}$ is the velocity of the fluids, p is the pressure, and $\boldsymbol{T}$ is the extra-stress tensor that can be decomposed into two parts (Groisman and Steinberg [1998]) in the dilute polymeric fluids as

$$\boldsymbol{T} = 2\eta_s\mathcal{D}(\mathbf{u}) + \boldsymbol{\tau}, \tag{3.3}$$

where η_s is the Newtonian viscosity and $\mathcal{D}(\mathbf{u})$ is the symmetric part of the gradient of velocity,

$$\mathcal{D}(\mathbf{u}) = \frac{\nabla\mathbf{u} + (\nabla\mathbf{u})^T}{2}. \tag{3.4}$$

We remark that $2\eta_s\mathcal{D}(\mathbf{u})$ is the solvent contribution of the stress. We note also that the tensor $\boldsymbol{\tau}$ is the polymeric contribution of the stress, which arises from the high-molecular-weight viscoelastic macromolecules and enters the equation of motion linearly.

3.2. The Oldroyd-B model

Most complex fluid models share the same mathematical form for the momentum and continuum equations as (3.1) and (3.2); different constitutive equations for the polymeric stress $\boldsymbol{\tau}$ lead to different complex fluid models. One basic model for complex fluids that introduces the outstanding challenge for high Weissenberg number regimes is called the Oldroyd-B model (Oldroyd [1950]).

The Oldroyd-B model (Oldroyd [1958]) obeys the following constitutive relation for $\boldsymbol{\tau}$:

$$\boldsymbol{\tau} + \mathsf{Wi}\left(\frac{\partial\boldsymbol{\tau}}{\partial t} + \mathbf{u}\cdot\nabla\boldsymbol{\tau} - \nabla\mathbf{u}\,\boldsymbol{\tau} - \boldsymbol{\tau}(\nabla\mathbf{u})^T\right) = 2\eta_p\mathcal{D}(\mathbf{u}), \tag{3.5}$$

where η_p is the polymeric viscosity and the Weissenberg number $\mathsf{Wi} = \lambda\bar{U}/\bar{L}$, where λ, $\bar{U}$, and $\bar{L}$ are the relaxation time, the characteristic velocity scale, and the length scale, respectively. The Weissenberg number is proportional to the material relaxation time.

The Oldroyd-B constitutive model (3.5) can be viewed as the simplest nonlinear extension of Maxwell's idea of formulating a system of ordinary differential equations to determine the stress in terms of the velocity gradient and the time derivative. It is easy to see that

the upper convective Maxwell time derivative $\frac{\partial \boldsymbol{\tau}}{\partial t} + \mathbf{u} \cdot \nabla \boldsymbol{\tau} - \nabla \mathbf{u} \boldsymbol{\tau} - \boldsymbol{\tau} \nabla \mathbf{u}^T$ that appears in the model can be identified to be $\mathcal{L}_{\mathbf{u}, \nabla \mathbf{u}}$ (see Example 2.1); therefore, the Oldroyd-B constitutive law can simply be written as

$$\boldsymbol{\tau} + \mathsf{Wi}\, \mathcal{L}_{\mathbf{u}, \nabla \mathbf{u}} \boldsymbol{\tau} = 2\eta_p \mathcal{D}(\mathbf{u}). \tag{3.6}$$

It is well known that the Oldroyd-B model reduces to the upper convected Maxwell (UCM) model for the special case in which $\eta_s = 0$. It has been proved that Eqns (3.1), (3.2), and (3.6) are stable in the sense of Hadamard (Owens and Phillips [2002]).

Writing the constitutive equation as in Eqn. (3.6) is an attempt to relate the stress $\boldsymbol{\tau}$ and the rate of strain $\mathcal{D}(\mathbf{u})$. For instance, when Wi becomes zero, the stress is linearly proportional to the rate of strain, which is the Newtonian constitutive relation; in this case, the Eqns (3.1), (3.2), and (3.3) become the Navier–Stokes equations. The Weissenberg number Wi is thus the characteristic constant that distinguishes the polymeric fluids from the Newtonian fluids.

3.3. A reformulation of the Oldroyd-B model in terms of the conformation tensor

We now take the Oldroyd-B model (Oldroyd [1950]) as an illustrative example to show how the Oldroyd-B constitutive law can be reformulated in terms of the conformation tensor and viewed as a symmetric matrix Riccati differential equation.

The constitutive law (3.5) is frequently written in terms of the conformation tensor

$$\boldsymbol{c} := \boldsymbol{\tau} + \frac{\eta_p}{\mathsf{Wi}} \boldsymbol{\delta}. \tag{3.7}$$

From a physical point of view, the conformation tensor can be regarded as a molecular deformation tensor on a continuum level. More precisely, the conformation tensor is the ensemble average of the dyadic product of the end-to-end vector of the dumbbell. It is, therefore, symmetric and positive definite, and it is often used as a primary variable in viscoelastic flow calculations (Carreau and Grmela [1987]).

We recall that the rate of the strain tensor $\mathcal{D}(\mathbf{u})$ can be expressed in terms of the upper convected derivative of the identity tensor $\boldsymbol{\delta}$:

Lemma 3.1 (Lie Derivative of the Identity). *Let $\boldsymbol{\delta}$ be the identity tensor. Then, we have*

$$\mathcal{L}_{\mathbf{u}, \nabla \mathbf{u}} \boldsymbol{\delta} = -2\mathcal{D}(\mathbf{u}). \tag{3.8}$$

This is a direct consequence of the definition of $\mathcal{L}_{\mathbf{u}, \nabla \mathbf{u}}$, and this simple identity plays a significant role in understanding various constitutive equations. We can reformulate the model (3.6) as follows:

$$\boldsymbol{\tau} + \mathsf{Wi} \left(\mathcal{L}_{\mathbf{u}, \nabla \mathbf{u}} \boldsymbol{\tau} + \frac{\eta_p}{\mathsf{Wi}} \mathcal{L}_{\mathbf{u}, \nabla \mathbf{u}} \boldsymbol{\delta} \right) = 0. \tag{3.9}$$

By adding $\frac{\eta_p}{\mathsf{Wi}} \boldsymbol{\delta}$ to both sides of the equation above and using the fact that the operator $\mathcal{L}_{\mathbf{u}, \nabla \mathbf{u}}$ is linear, we obtain

$$\left(\boldsymbol{\tau} + \frac{\eta_p}{\mathsf{Wi}} \boldsymbol{\delta} \right) + \mathsf{Wi}\, \mathcal{L}_{\mathbf{u}, \nabla \mathbf{u}} \left(\boldsymbol{\tau} + \frac{\eta_p}{\mathsf{Wi}} \boldsymbol{\delta} \right) = \frac{\eta_p}{\mathsf{Wi}} \boldsymbol{\delta}. \tag{3.10}$$

In terms of the conformation tensor, the constitutive equation (3.6) becomes

$$\boldsymbol{c} + \mathrm{Wi}\,\mathcal{L}_{\mathbf{u},\nabla\mathbf{u}}\boldsymbol{c} = \frac{\eta_p}{\mathrm{Wi}}\boldsymbol{\delta}, \tag{3.11}$$

and we observe that Eqn (3.11) can be written such that for $\mathrm{Wi} \neq 0$,

$$\frac{D\boldsymbol{c}}{Dt} - \nabla\mathbf{u}\,\boldsymbol{c} - \boldsymbol{c}\,\nabla\mathbf{u}^T + \frac{1}{\mathrm{Wi}}\boldsymbol{c} = \frac{\eta_p}{\mathrm{Wi}^2}\boldsymbol{\delta}. \tag{3.12}$$

REMARK 3.1 (Algebraic Riccati Form of Oldroyd-B). Equation (3.12) can be further reformulated into the following form:

$$\frac{D\boldsymbol{c}}{Dt} + \left(\frac{1}{2\mathrm{Wi}} - \nabla\mathbf{u}\right)\boldsymbol{c} + \boldsymbol{c}\left(\frac{1}{2\mathrm{Wi}} - \nabla\mathbf{u}\right)^T = \frac{\eta_p}{\mathrm{Wi}^2}\boldsymbol{\delta}. \tag{3.13}$$

This form can be immediately identified with the symmetric matrix Riccati differential equation for $\boldsymbol{c}$ as introduced in the general form (2.19) with the choice of the coefficient matrices that

$$\boldsymbol{A}(t) = \frac{1}{2\mathrm{Wi}}\boldsymbol{\delta} - \nabla\mathbf{u}, \quad \boldsymbol{B}(t) \text{ is a zero matrix, and } \boldsymbol{G}(t) = \frac{\eta_p}{\mathrm{Wi}^2}\boldsymbol{\delta}. \tag{3.14}$$

REMARK 3.2 (Positivity of the Conformation Tensor for the Oldroyd-B Model). The positive definiteness of $\boldsymbol{c}$ is thought to have been first established by HULSEN [1990] directly from the differential model (3.11). From the Riccati form of the Oldroyd-B constitutive law (3.13) and Lemma 2.1, it is easy to establish that if $\boldsymbol{c}(0)$ is given to be a positive definite tensor, then the conformation tensor $\boldsymbol{c}$ is always positive definite since $\boldsymbol{G}$ is non-negative. In fact, this technique will allow us to provide an integral equivalent equation of the differential equation given by Eqn (3.12) and establish the positive definiteness of the conformation tensor $\boldsymbol{c}$ in a transparent manner as well. See Eqn (3.30).

3.4. *Conformation tensor formulation of the Johnson–Segalman model*

The Oldroyd-B model (3.6) is a basic constitutive model for complex fluids. Many improvements for constitutive equations have been developed from the Oldroyd-B model, e.g., by modifying the upper convective derivative or by adding additional terms to better fit the rheological property of the fluids. A few such examples will be discussed in this section.

Let us first consider the Johnson–Segalman model (JOHNSON and SEGALMAN [1977]):

$$\boldsymbol{\tau} + \mathrm{Wi}\,\mathcal{L}_{\mathbf{u},\boldsymbol{R}}\boldsymbol{\tau} = 2\eta_p\mathcal{D}(\mathbf{u}), \tag{3.15}$$

where $\mathcal{L}_{\mathbf{u},\boldsymbol{R}}$ is the Gordon–Schowalter derivative as in Example 2.3. The Johnson–Segalman model is often the model of choice for studying material instability, such as shark-skin and spurt, which have been the subject of considerable research interest in recent years.

Similar to our approach with the Oldroyd-B model, we first reformulate Eqn (3.15) in terms of the conformation tensor $\boldsymbol{c}$. We obtain

$$\mathcal{L}_{\mathbf{u},\boldsymbol{R}}\boldsymbol{\delta} = -\left(\frac{\mathrm{a}+1}{2}\nabla\mathbf{u} + \frac{\mathrm{a}-1}{2}\nabla\mathbf{u}\right) - \left(\frac{\mathrm{a}+1}{2}\nabla\mathbf{u} + \frac{\mathrm{a}-1}{2}\nabla\mathbf{u}\right)^T = -2\mathrm{a}\mathcal{D}(\mathbf{u}).$$

Therefore, for nonzero Wi and a, the model (3.15) can be written as follows:

$$\boldsymbol{\tau} + \mathsf{Wi}\,\mathcal{L}_{\mathbf{u},\boldsymbol{R}}\boldsymbol{\tau} = -\frac{\eta_p}{\mathsf{a}}\mathcal{L}_{\mathbf{u},\boldsymbol{R}}\boldsymbol{\delta} \implies \boldsymbol{\tau} + \frac{\eta_p}{\mathsf{aWi}} + \mathsf{Wi}\,\mathcal{L}_{\mathbf{u},\boldsymbol{R}}\left(\boldsymbol{\tau} + \frac{\eta_p}{\mathsf{aWi}}\boldsymbol{\delta}\right) = \frac{\eta_p}{\mathsf{aWi}}\boldsymbol{\delta}.$$

Defining $\boldsymbol{c} = \boldsymbol{\tau} + \frac{\eta_p}{\mathsf{aWi}}\boldsymbol{\delta}$, we arrive at the following reformulation of the Johnson–Segalman model (3.15):

$$\boldsymbol{c} + \mathsf{Wi}\,\mathcal{L}_{\mathbf{u},\boldsymbol{R}}\boldsymbol{c} = \frac{\eta_p}{\mathsf{aWi}}\boldsymbol{\delta}. \tag{3.16}$$

Recall that the generalized Lie derivative $\mathcal{L}_{\mathbf{u},\boldsymbol{R}}$ is determined by the transition matrix $\boldsymbol{E}(s,t)$ that satisfies the following ODE:

$$\frac{D\boldsymbol{E}(s,t)}{Dt} = \left(\frac{\mathsf{a}+1}{2}\nabla\mathbf{u} + \frac{\mathsf{a}-1}{2}\nabla\mathbf{u}^T\right)\boldsymbol{E}(s,t) \quad \text{and} \quad \boldsymbol{E}(s,s) = \boldsymbol{\delta}. \tag{3.17}$$

The tensor $\boldsymbol{E}(s,t)$ obeying (3.17) was first introduced by Johnson and Segalman [1977] as a deformation tensor for viscoelastic fluids that have certain degree of nonaffinity. The parameter a is related to the so-called slippage parameter $\xi = 1 - \mathsf{a}$, which measures the nonaffinity in the reaction of macromolecules under the exerted force from the surrounding fluids.

3.5. *Conformation reformulation for a general viscoelastic model*

To summarize, we now discuss macroscopic models that can be written in the following general form:

$$\mathcal{L}_{\mathbf{u},\boldsymbol{R}}\boldsymbol{c} + \alpha\boldsymbol{c} = \beta\boldsymbol{\delta}, \tag{3.18}$$

where $\alpha \geq 0$ and $\beta > 0$ may depend on t and/or $\boldsymbol{c}$. For instance, the Johnson–Segalman model can be recovered from Eqn (3.18) by choosing $\alpha = \frac{1}{\mathsf{Wi}}$ and $\beta = \frac{\eta_p}{\mathsf{aWi}^2}$. It would be of interest to consider Eqn (3.18) as it is, which is because the generalized Lie derivative $\mathcal{L}_{\mathbf{u},\boldsymbol{R}}$ is ubiquitous in general macroscopic equations. We can, in fact, derive the solution expression $\boldsymbol{c}$ in terms of the transition matrix $\boldsymbol{E}$ as follows.

Theorem 3.1 (Explicit Solution of the Constitutive Equation). *The solution to the constitutive equation in Riccati form (3.18) satisfies*

$$\begin{aligned}\boldsymbol{c}(t) = {} & \exp\left(-\int_s^t \alpha(\varsigma)\mathrm{d}\varsigma\right)\boldsymbol{E}(s,t)\boldsymbol{c}(t,s)\boldsymbol{E}(s,t)^T \\ & + \int_s^t \exp\left(-\int_\nu^t \alpha(\varsigma)\mathrm{d}\varsigma\right)\beta(\nu)\boldsymbol{E}(\nu,t)\boldsymbol{E}(\nu,t)^T\mathrm{d}\nu.\end{aligned} \tag{3.19}$$

PROOF. Note that Eqn (3.18) can be reformulated as follows:

$$\mathcal{L}_{\mathbf{u},\boldsymbol{\Phi}}\boldsymbol{c} = \beta\boldsymbol{\delta},$$

where the generalized Lie derivative is with respect to

$$\boldsymbol{\Phi}(t) := \frac{\mathsf{a}+1}{2}\nabla\mathbf{u} + \frac{\mathsf{a}-1}{2}\nabla\mathbf{u}^T - \frac{\alpha(t)}{2}.$$

From the Lemma 2.1, we arrive at the following expression for $\boldsymbol{c}$:

$$\boldsymbol{c}(t) = \boldsymbol{L}(s,t)\boldsymbol{c}(t,s)\boldsymbol{L}(s,t)^T + \int_s^t \beta(\nu)\boldsymbol{L}(\nu,t)\boldsymbol{L}(\nu,t)^T \mathrm{d}\nu. \tag{3.20}$$

On the other hand, the matrix $\boldsymbol{L}(s,t)$ can be expressed as follows:

$$\boldsymbol{L}(s,t) = \exp\left(-\int_s^t \frac{\alpha(\nu)}{2}\mathrm{d}\nu\right)\boldsymbol{E}(s,t). \tag{3.21}$$

To see this, we note that $\boldsymbol{L}_1(s,t) = \boldsymbol{E}(s,t)$ is the solution to the following ODE:

$$\frac{\partial\boldsymbol{L}_1(s,t)}{\partial t} = \left(\frac{\mathsf{a}+1}{2}\nabla\mathbf{u}(t) + \frac{\mathsf{a}-1}{2}\nabla\mathbf{u}(t)^T\right)\boldsymbol{L}_1(s,t)$$

and the solution to the equation

$$\frac{\partial\boldsymbol{L}_2(s,t)}{\partial t} = -\frac{\alpha(t)}{2}\boldsymbol{L}_2(s,t)$$

is given by

$$\boldsymbol{L}_2(s,t) = \exp\left(-\int_s^t \frac{\alpha(\nu)}{2}\mathrm{d}\nu\right)\boldsymbol{\delta}. \tag{3.22}$$

The simple observation that $\boldsymbol{L}(s,t) = \boldsymbol{L}_1(s,t)\boldsymbol{L}_2(s,t)$ completes the proof. □

The simple formulation (3.18) can, in fact, represent many existing models. For example, it can represent the well-known Phan-Thien and Tanner (PTT) model THIEN and TANNER [1977] and other models that belong to the finitely extensible nonlinear elastic (FENE) models (CHILCOTT and RALLISON [1988], ILG, KARLIN and ÖTTINGER [2002], LIELENS, HALIN, JAUMAIN, KEUNINGS and LEGAT [1998], REMMELGAS, SINGH and LEAL [1999], SZERI [2000]).

EXAMPLE 3.1 (The Phan-Thien and Tanner Model). The Phan-Thien and Tanner (PTT) model can be given in the following expression:

$$\mathcal{F}(\boldsymbol{\tau})\boldsymbol{\tau} + \mathrm{Wi}\,\mathcal{L}_{\mathbf{u},\boldsymbol{R}}\boldsymbol{\tau} = 2\eta_p\mathcal{D}(\mathbf{u}), \tag{3.23}$$

where $\mathcal{F}$ is a scalar function defined by

$$\mathcal{F}(\boldsymbol{\tau}) = \exp\left(\frac{\epsilon \mathsf{Wi}}{\eta_p}\,\mathrm{tr}(\boldsymbol{\tau})\right), \tag{3.24}$$

where ϵ is a parameter. The model (3.23) can easily be transformed in terms of the conformation tensor $\boldsymbol{c}$ as follows:

$$\mathcal{L}_{\mathbf{u},\boldsymbol{R}}\boldsymbol{c} + \frac{\mathcal{G}(\boldsymbol{c})}{\mathsf{Wi}}\boldsymbol{c} = \eta_p \frac{\mathcal{G}(\boldsymbol{c})}{\mathsf{aWi}^2}\boldsymbol{\delta}, \quad \text{with } \mathcal{G}(\boldsymbol{c}) = \mathcal{F}\Big(\boldsymbol{c} - \frac{\eta_p}{\mathsf{aWi}}\boldsymbol{\delta}\Big). \tag{3.25}$$

Therefore, the PTT model belongs to the class of models that can be represented by Eqn (3.18).

Example 3.2 (General Single-Variable Models). We note that the general single-variable models as introduced by Hulsen (e.g., Beris and Edwards [1994], Hulsen [1990]) can be given in terms of the conformation tensor $\boldsymbol{c}$ as follows:

$$\frac{D\boldsymbol{c}}{Dt} = \boldsymbol{a}(t)\,\boldsymbol{c} + \boldsymbol{c}\,\boldsymbol{a}(t)^T + g_0\boldsymbol{\delta} + g_1\boldsymbol{c} + g_2\boldsymbol{c}^2, \tag{3.26}$$

where g_i's $(i = 0, 1, 2)$ are given functions that may depend on time and/or $\boldsymbol{c}$. Hulsen [1990] provided a sufficient condition that $g_0 > 0$ for which the conformation tensor $\boldsymbol{c}$ for models of the form (3.26) remains positive definite for all time if it is positive initially. His arguments were based on the rate of change in the determinant of $\boldsymbol{c}$ along the trajectory. Our framework cast (3.26) into the general Riccati equation

$$\frac{D\boldsymbol{c}}{Dt} - \boldsymbol{A}(t)\boldsymbol{c} - \boldsymbol{c}\boldsymbol{A}(t)^T = \boldsymbol{G}(t), \tag{3.27}$$

with the coefficient matrices

$$\boldsymbol{A}(t) := \boldsymbol{a}(t) + \frac{g_1}{2}\boldsymbol{\delta} + \frac{g_2\boldsymbol{c}}{2} \quad \text{and} \quad \boldsymbol{G}(t) := g_0\boldsymbol{\delta}.$$

An alternative reformulation of (3.27) can be given by

$$\mathcal{L}_{\mathbf{u},\boldsymbol{A}}\boldsymbol{c} = \boldsymbol{G}(t). \tag{3.28}$$

This reformulation in terms of the generalized Lie derivative with respect to $\boldsymbol{\Phi}$ immediately proves the positivity of $\boldsymbol{c}$ under the assumption that $g_0 > 0$.

It should be note here that the analytic expression (3.19) of the conformation tensor $\boldsymbol{c}$ can be used to derive the corresponding integral models. Indeed, under some appropriate assumption (such as $\alpha \geq \alpha_0$ for some positive constant α_0 and $\boldsymbol{E}(s, t)$ is bounded for $s \leq t$), we formally obtain the following integral models by taking $s \to -\infty$,

$$\boldsymbol{c}(t) = \int_{-\infty}^{t} \exp\left(-\int_{\nu}^{t} \frac{\alpha(\nu)}{2}\mathrm{d}\nu\right)\beta(\nu)\boldsymbol{E}(\nu, t)\boldsymbol{E}(\nu, t)^T\mathrm{d}\nu. \tag{3.29}$$

In particular, this includes the Johnson–Segalman integral model, which does not seem to be known in the literature; see Joseph [1990]. Furthermore, as an immediate consequence of $\mathsf{a} = 1$, we obtain the well-known integral expression for the Oldroyd-B model (3.12) as follows:

$$\boldsymbol{c}(t) = \frac{\eta_p}{\mathrm{Wi}^2} \int_{-\infty}^{t} \exp\left(-\frac{t-\nu}{\mathrm{Wi}}\right) \boldsymbol{F}(\nu, t)\boldsymbol{F}(\nu, t)^T \mathrm{d}\nu. \tag{3.30}$$

Although it has been widely believed that the integral expression (3.30) of the conformation tensor is equivalent to (3.11) (see, e.g., Renardy [2000b]), a rigorous justification for this equivalence is missing in the literature (see relevant remarks made both by Joseph [1990, p.15], Renardy [2000b, p.18]). Note that it is easy to establish that the integral model can result in the differential model (3.11) by taking the (material) time derivative. With the help of the Riccati formulation, the justification that the differential model results in the integral model is completed with ease, which would have been difficult otherwise.

4. Basic mathematical and physical properties of the models

In this section, we give a brief overview of the existing mathematical analysis of basic theoretical issues such as the existence and stability of the solution to complex fluid models. While these theoretical works are obviously of interest themselves, they are also instrumental to designing of appropriate numerical methods for these models.

4.1. Existence theory

On the mathematical theory for complex fluid models, many fundamental questions, such as whether (weak) solutions exist, are still open (Chemin and Masmoudi [2001], Lin, Liu and Zhang [2007], Lions and Masmoudi [2000]). On the Oldroyd-B model, the existence of global weak solutions even at regimes of low Weissenberg number has not been fully understood yet. The global existence of weak solutions was established by Barrett and Süli [2008] for the corotational models, under the assumption that the velocity field is regularized. For the noncorotational models, like the Oldroyd-B model, both the velocity and the extra-stress fields are assumed to be mollified in the weak formulations in order to obtain the global existence of weak solutions (Barrett and Süli [2008]).

Some studies have been published on short-time existence (Guillope and Saut [1990a,b], Jourdain, Lelivre and Bris [2004], Li and Zhang [2004], Renardy [1991]) and global existence with small initial data (Guillope and Saut [1990a,b], Lin, Liu and Zhang [2005]) of the solutions. In particular, Lin, Liu and Zhang [2005] established the existence of classical solutions for the Oldroyd-B model at infinite Weissenberg number with small initial data. In another notable work, Lions and Masmoudi [2000] proved the existence of global weak solutions for the corotational Jeffreys model based on the L^2-norm energy estimate for both velocity and stress fields. This type of energy estimate does not, however, hold for the Oldroyd-B model; therefore, the global existence of the Oldroyd-B model is still an open problem for general initial data. A stability result has also been obtained by He and Zhang [2009]: if the initial data is sufficiently close to the equilibrium, the solution approaches to the equilibrium with a certain decaying rate measured in the

L^2-norm. The main idea behind the existence and stability proof in He and Zhang [2009] and Lin, Liu and Zhang [2005] is to take full advantage of the *Divergence-free condition* imposed at the velocity field, which is shown to generate a dissipation mechanism and hence stabilize the equation. This work strongly indicates that incompressibility plays an important role in the stability of the system. It hints at the importance of preserving incompressibility on the discrete level in order to obtain stable numerical schemes.

While the global existence of the Oldroyd-B model for general "large" data is missing, there are several global-in-time existence results of some complex fluid models for simple shear flows. Engler [1987] and Guillope and Saut [1990a,b] obtained global existence results for shear flows obeying a class of nonlinear integro-differential models and the Johnson–Segalman model, respectively. This problem has recently been revisited by Renardy [2009], in which the global existence for shear flow under the PTT (Giesekus [1982], Thien and Tanner [1977]), and Johnson–Segalman models (Johnson and Segalman [1977]) has been established for some parameters, although not for the Oldroyd-B model. As Renardy stated in Renardy [2009] that the positive definiteness of the conformation tensor is crucial to his proof.

In addition, several studies indicate that the Oldroyd-B model might produce nonsmooth stress fields; for example, see Renardy [2006] and Bajaj, Pasquali and Prakash [2008]. Renardy's (Renardy [2006]) results have been correlated with the numerical results of Thomases and Shelley [2007], where certain numerical evidence of singularity formation is provided. The latter study tried to explain why the flow-past-cylinder benchmark problem presents numerical challenges. We note that these singular solutions are obtained for the steady-state Oldroyd-B model, and it is unclear whether or not singularity will form for the time-dependent equations.

While global-in-time existence remains illusive for continuous problems, we will establish the global existence of the discrete solutions for macroscopic viscoelastic models in this article; see Section 8. Similar to the theories on the continuous level, the strong divergence-free condition and the positivity of the conformation tensors play critical roles in our analysis. As suggested by these successful theoretical efforts, our guiding principle is that the positivity of the conformation tensors and the strong divergence-free condition for the velocity fields should be both preserved in the fully discrete level. Both ingredients are crucial in deriving the discrete energy estimates and global existence for the numerical solutions.

4.2. *Energy estimates*

Energy estimates are basic ingredients in the analysis of well posedness of the equations, and they are also crucially important in designing well-posed numerical discretization schemes as well. We will present some basic energy estimates (Lee and Xu's [2006], Lozinski and Owens [2003]) for the continuous equations in this section, and we will later extend these estimates to the discrete level.

To state the energy estimate, let us first introduce an energy norm for the conformation tensor:

$$\|\boldsymbol{\sigma}\|_{L^1} := \int_\Omega \operatorname{tr}(\boldsymbol{\sigma})\,\mathrm{d}x, \qquad \forall \boldsymbol{\sigma} \in \boldsymbol{S}_h. \tag{4.1}$$

This obviously defines a norm on the space of positive-definite tensors. We note that for the conformation tensor $\boldsymbol{c}$, the norm $\|\boldsymbol{c}\|_{L^1}$ has its own physical meaning as well. The trace of the conformation tensor $\boldsymbol{c}$ can be viewed as the length from the tail to the head of a macromolecule: the longer the length, the more elastic energy it stores. We can view $\|\boldsymbol{c}\|_{L^1}$ as the total elastic energy due to the interaction between the macromolecules and surrounding fluids.

Based on this, we can define the total energy (kinetic and elastic) of the fluid at time level t to be

$$\mathcal{E}(t) := \mathsf{Re}\|\mathbf{u}(\cdot,t)\|_0^2 + \frac{1}{2}\|\boldsymbol{c}(\cdot,t)\|_{L^1}. \tag{4.2}$$

For all the estimates presented in this section, the following *bridging identity* is crucial:

$$(\boldsymbol{c}(\cdot,t) : \mathcal{D}(\mathbf{u})(\cdot,t)) = \int_\Omega \operatorname{tr}(\nabla\mathbf{u}(\cdot,t)\boldsymbol{c}(\cdot,t))\,\mathrm{d}x. \tag{4.3}$$

This identity plays a role in bridging the energy term in the momentum equation and its counterpart in the constitutive equation.

Now, we take the Oldroyd-B model (in terms of the conformation tensor) in the Riccati form as an example:

$$\mathsf{Re}\left(\frac{\partial\mathbf{u}}{\partial t} + \mathbf{u}\cdot\nabla\mathbf{u}\right) = -\nabla p + 2\mu_s\nabla\cdot\mathcal{D}(\mathbf{u}) + \nabla\cdot\boldsymbol{c}, \tag{4.4}$$

$$\nabla\cdot\mathbf{u} = 0, \tag{4.5}$$

$$\frac{\partial\boldsymbol{c}}{\partial t} + \mathbf{u}\cdot\nabla\boldsymbol{c} - \nabla\mathbf{u}\,\boldsymbol{c} - \boldsymbol{c}\,\nabla\mathbf{u}^T + \frac{1}{\mathsf{Wi}}\boldsymbol{c} = \frac{\eta_p}{\mathsf{Wi}^2}\boldsymbol{\delta}. \tag{4.6}$$

From (4.3), we can easily establish the following energy law for Eqns (4.4)–(4.6):

$$\frac{\mathrm{d}}{\mathrm{d}t}\mathcal{E}(t) = -\eta_s\|\mathcal{D}(\mathbf{u}(\cdot,t))\|_0^2 - \frac{1}{2\mathsf{Wi}}\|\boldsymbol{c}(\cdot,t)\|_{L^1} + \frac{d}{2}\frac{1-\eta_s}{\mathsf{Wi}^2}|\Omega|, \tag{4.7}$$

where $|\Omega|$ and d are the measure and spatial dimension of the domain Ω, respectively. From the energy law (4.7), we can derive the following energy estimate for the Oldroyd-B model.

THEOREM 4.1 (Continuous Energy Estimate). *For* $\mathsf{Wi} \neq 0$*, the Oldroyd-B model (4.4)–(4.6) admits the following energy estimate:*

$$\mathcal{E}(t) \le \mathrm{e}^{-\mathsf{C}_1 t}\mathcal{E}(0) + \frac{\mathsf{C}_2}{\mathsf{C}_1}\left(1 - \mathrm{e}^{-\mathsf{C}_1 t}\right) \tag{4.8}$$

$$\eta_s\int_0^t \|\mathcal{D}(\mathbf{u}(\cdot,\nu))\|_0^2\,\mathrm{d}\nu \le \mathcal{E}(0) + \mathsf{C}_2\,t, \tag{4.9}$$

with the constants

$$\mathsf{C}_1 = \min\left(\frac{\mathsf{C}_\Omega\eta_s}{\mathsf{Re}}, \frac{1}{\mathsf{Wi}}\right) \quad \textit{and} \quad \mathsf{C}_2 = \frac{d}{2}\frac{1-\eta_s}{\mathsf{Wi}^2}|\Omega|, \tag{4.10}$$

where C_Ω *is a positive constant depending on* Ω *only. For the special case when* $\mathsf{Wi} = \infty$, *we have*

$$\mathcal{E}(t) \le \mathcal{E}(0) \qquad \textit{and} \qquad \eta_s \int_0^t \|\mathcal{D}(\mathbf{u}(\cdot, \nu))\|_0^2 \le \mathcal{E}(0). \tag{4.11}$$

Proof. From Korn's inequality, we have the following inequality $\mathsf{C}_\Omega \|\mathbf{u}\|_0 \le \|\mathcal{D}(\mathbf{u})\|_0$, where C_Ω depends only on Ω. The energy law (4.7) then leads to

$$\frac{d}{dt}\Big(\mathsf{Re}\|\mathbf{u}(\cdot, t)\|_0^2 + \frac{1}{2}\|\boldsymbol{c}(\cdot, t)\|_{L^1}\Big) \le -\eta_s \mathsf{C}_\Omega \|\mathbf{u}(\cdot, t)\|_0^2 - \frac{1}{2\mathsf{Wi}}\|\boldsymbol{c}(\cdot, t)\|_{L^1} + \frac{d}{2}\frac{1-\eta_s}{\mathsf{Wi}^2}|\Omega|.$$

We define $\mathsf{C}_1 = \min(\mathsf{C}_\Omega \eta_s/\mathsf{Re}, 1/\mathsf{Wi})$ and $\mathsf{C}_2 = \frac{d}{2}\frac{1-\eta_s}{\mathsf{Wi}^2}|\Omega|$ to obtain the following inequality:

$$\frac{d}{dt}\Big(\mathsf{Re}\|\mathbf{u}(\cdot, t)\|_0^2 + \frac{1}{2}\|\boldsymbol{c}(\cdot, t)\|_{L^1}\Big) \le -\mathsf{C}_1\Big(\mathsf{Re}\|\mathbf{u}(\cdot, t)\|_0^2 + \frac{1}{2}\|\boldsymbol{c}(\cdot, t)\|_{L^1}\Big) + \mathsf{C}_2. \tag{4.12}$$

This estimate gives the desired estimate (4.8) immediately by Gronwall's inequality. We take integration with respect to time on both sides of (4.7) to get

$$\begin{aligned}
&\mathsf{Re}\|\mathbf{u}(\cdot, t)\|_0^2 + \frac{1}{2}\|\boldsymbol{c}(\cdot, t)\|_{L^1} + \eta_s \int_0^t \|\mathcal{D}(\mathbf{u}(\cdot, \nu))\|_0^2 \, d\nu \\
&\qquad \le \mathsf{Re}\|\mathbf{u}(\cdot, 0)\|_0^2 + \frac{1}{2}\|\boldsymbol{c}(\cdot, 0)\|_{L^1} - \frac{1}{2\mathsf{Wi}}\int_0^t \|\boldsymbol{c}(\cdot, \nu)\|_{L^1} \, d\nu + \mathsf{C}_2 t \\
&\qquad \le \mathsf{Re}\|\mathbf{u}(\cdot, 0)\|_0^2 + \frac{1}{2}\|\boldsymbol{c}(\cdot, 0)\|_{L^1} + \mathsf{C}_2 t.
\end{aligned}$$

This completes the proof. □

Remark 4.1 (The Effect of the Weissenberg Number). The parameter Wi is the ratio between the relaxation time of the macromolecules and the characteristic time. The longer the relaxation time, the longer it takes for the macromolecules to return to their original states; this can be interpreted as showing that the fluid is less dependent on its initial state. This has been correlated in the energy estimate (4.8); that is, the coefficient function multiplied to the initial data decays slowly when Wi becomes larger.

5. Existing numerical methods for viscoelastic fluid models

In this section, we offer a brief overview of numerical methods for solving viscoelastic fluid models, especially in regard to studies focused on the well-known high Weissenberg number problem (HWNP). The problem is associated with the breakdown of the numerical solutions to the complex fluid models when the Weissenberg numbers are *moderately* large. This outstanding problem has been one of the driving forces for developing new numerical techniques for complex fluids (see Owens and Phillips [2002]).

5.1. Mixed formulations

To numerically achieve mesh convergence and long-time stability beyond certain critical Weissenberg numbers for various viscoelastic models has proven difficult. Numerous attempts have been made to overcome the high Weissenberg number problem with mixed finite element methods. Most of the early work on viscoelastic flow analysis is based on the mixed finite element formulations for $(\mathbf{u}, p, \boldsymbol{\tau})$; see Baaijens's Baaijens [1998] review for more details. Two basic problems have been encountered with the above formulations. First, as the value of the Weissenberg number increases, the importance of the convective term grows, which makes Galerkin discretizations not suitable. Second, the discretization spaces for the three variables must be carefully selected with respect to each other in order to satisfy appropriate stability conditions for the three fields.

Numerical success in the early stage of computational rheology can be found in Marchal and Crochet [1987], which introduced a new mixed finite element method for the numerical simulation of viscoelastic flows. In Marchal and Crochet [1987], the authors showed that the streamline-upwinding (SU) method by Hughes and Brooks [1982] could be used for viscoelastic fluid simulation in order to stabilize the hyperbolic constitutive equation. Further, Fortin and Pierre [1989] analyzed the finite element spaces employed in Marchal and Crochet [1987]. Another approach, introduced by Fortin and Fortin [1989], used the discontinuous Galerkin (DG) method by Lesaint Raviart [1979] for the constitutive equation combined with the element-wise streamline-upwinding method for the momentum equation.

Much work has been done in this line of research. To stabilize the numerical simulation, these algorithms focus on adding more diffusion to the momentum equation in order to make the ellipticity of the equation explicit. Sun, Smith, Armstrong and Brown [1999] summarized the main ideas as follows:

(1) reformulating the momentum and the constitutive equation to make the elliptic character of this equation explicit with respect to the velocity field;
(2) splitting the formulation into the solution of the velocity-pressure saddle point problem equations for an incompressible fluid and the calculation of the extra-stress field from the hyperbolic constitutive equation;
(3) applying numerically stable and accurate methods, like SUPG or DG methods, for solution of the hyperbolic constitutive equations; and
(4) introducing accurate and smooth interpolation of velocity gradients for additional numerical stability in solution of the constitutive equation.

King, Apelian, Armstrong and Brown [1988] made the first effort in this direction; they introduced the explicitly elliptic momentum equation (EEME) and gave a reformulation of the momentum equation that makes its ellipticity explicit for the upper convected Maxwell (UCM) models. This method was later generalized by Beris, Armstrong and Brown [1984, 1986]: their elastic-viscous split-stress (EVSS) formulation splits the extra-stress $\boldsymbol{T}$ into a viscous part and an elastic part; i.e., $\boldsymbol{T} = \boldsymbol{\tau}_v + \boldsymbol{\tau}_e$, where $\boldsymbol{\tau}_v = 2\eta_a \mathcal{D}(\mathbf{u})$ and η_a is a parameter for viscosity; in this way, the formulation introduces another variable, the rate-of-strain $\mathcal{D}(\mathbf{u})$. The application of this method has been limited to a few models; furthermore, it introduced a new term containing convected derivatives of $\mathcal{D}(\mathbf{u})$. Rajagopalan,

Armstrong and Brown [1990] modified this method by using a least square approximation of $\mathcal{D}(\mathbf{u})$ and generalized it to the Oldroyd-B model, as well as the Giesekus models.

The EEME and EVSS formulations are significant improvements over previous methods based on the standard viscous model in terms of numerical stability. They allow numerically stable and accurate calculations at moderately high Wi values. However, almost every flow problem has levels of elasticity that cannot be calculated with these methods for any given finite element mesh. Sun, Phan-Thien and Tanner [1996] argued that the failure is due to a steep stress gradient and introduced an adaptive way for choosing the viscosity parameter η_a to tackle the difficulty; this is known as the adaptive viscoelastic stress splitting (AVSS) method. An alternative EVSS method was proposed in Brown, Szady, Northey and Armstrong [1993] and Szady et al. [1995], who applied least square approximation for the gradient $\nabla\mathbf{u}$ instead of $\mathcal{D}(\mathbf{u})$; this type of methods is called EVSS-G. Guenette and Fortin [1995] and Liu, Bornside, Armstrong and Brown [1998] applied the stress splitting at the discrete level, which gives the discrete elastic-viscous split-stress (DEVSS) and DEVSS-G, respectively. Sun, Smith, Armstrong and Brown [1999] combined all these techniques to create the discrete adaptive viscoelastic stress splitting–discontinuous Galerkin (DAVSS-G/DG) method, which does exactly what the name suggests.

Besides the finite element formulation, other related discretization schemes, such as finite volume method and the spectral methods, have been applied to viscoelastic fluids. Just to mention a few, Hu and Joseph [1990] designed a finite volume (FV) discretization based on the semi-implicit method for pressure-linked equations revised (SIMPLER) for the UCM model on orthogonal staggered grids. Oliveira, Pinho and Pinto [1998] generalized this method to nonorthogonal collocated grids. Alves, Oliveira and Pinho [2003] and Alves, Pinho and Oliveira [2001] discussed FVM on nonorthogonal grids combined with a high-resolution scheme (HRS) instead of usual upwind difference schemes for the Oldroyd-B model and the PTT model for the planar contraction benchmark problem. Chauviére and Owens [2001] applied the spectral method for viscoelastic flows and introduced the streamline-upwind Petrov/Galerkin (SUPG) for constitutive equations.

5.2. *Steep stress layers and log-conformation formulation*

The breakdown of the numerical algorithms for high Weissenberg numbers has often been associated with the steep stress gradients in the narrow regions of the flow domain. Even for the well-known flow-past-cylinder problem, which has no geometric singularities and generates smooth flows, the numerical simulation is still difficult. Observed in many numerical simulations is that this difficulty inheres in the thin stress layers that develop around the cylinder and in the wake along the centerline, where the flow is purely elongational; see the review by Baaijens [1998] for example. Beris, Armstrong and Brown [1983, 1987] have demonstrated the formation of elastic boundary layers in both asymptotic analysis and spectral/finite-element calculations for the flow between two eccentric rotating cylinders. Renardy [2000a] analyzed the width of the boundary layer and the wake for the UCM model with fixed Newtonian kinematics. Based on this work, Wapperom and Renardy [2005] applied a Lagrangian technique to simulate viscoelastic flow past a cylinder benchmark problem; they showed that for an ultradilute solution, the governing equations for the Oldroyd-B model can be solved for arbitrarily large values of Wi under the assumption that the underlying velocity field is fixed to be Newtonian.

By far the most successful method is (Fattal and Kupferman's [2004]) matrix-logarithm formulation of the conformation tensor for the constitutive laws; this method introduces a new variable $\boldsymbol{\Psi} = \ln \boldsymbol{c}$ and rewrite the constitutive equations in terms of $\boldsymbol{\Psi}$ for numerical calculations. The main motivation relies on the fact that the stress tensor is exponential in regions of high deformation rates or stagnation points; numerical instabilities are caused by failure to balance exponential growth with convection. In Fattal and Kupferman [2004], the authors pointed out the inappropriateness of polynomial-based approximations to represent the stress.

Let the conformation tensor be $\boldsymbol{c} = \boldsymbol{\delta} + \frac{\mu_p}{\mathrm{Wi}}\boldsymbol{\tau}$. Notice that the conformation tensor is different from that defined in (3.7) by a constant multiplier. We can then write the Oldroyd-B constitutive equation (3.5) in terms of $\boldsymbol{c}$:

$$\frac{\partial \boldsymbol{c}}{\partial t} + \mathbf{u}\cdot\nabla\boldsymbol{c} - \nabla\mathbf{u}\,\boldsymbol{c} - \boldsymbol{c}(\nabla\mathbf{u})^T = \frac{1}{\mathrm{Wi}}(\boldsymbol{\delta} - \boldsymbol{c}). \tag{5.1}$$

The core feature of the transformation is the decomposition of the velocity gradient into a traceless extensional component $\boldsymbol{B}$ and a pure rotational component $\boldsymbol{R}$:

$$\nabla\mathbf{u} = \boldsymbol{R} + \boldsymbol{B} + \boldsymbol{N}\boldsymbol{c}^{-1}, \tag{5.2}$$

where $\boldsymbol{N}$ is antisymmetric. By plugging (5.2) in the Oldroyd-B constitutive relation, we obtain

$$\frac{\partial \boldsymbol{c}}{\partial t} + (\mathbf{u}\cdot\nabla)\boldsymbol{c} - (\boldsymbol{R}\boldsymbol{c} - \boldsymbol{c}\boldsymbol{R}) - 2\boldsymbol{B}\boldsymbol{c} = \frac{1}{\mathrm{Wi}}(\boldsymbol{\delta} - \boldsymbol{c}). \tag{5.3}$$

Because of the symmetric positive-definite (SPD) nature of the conformation tensor, we can have the factorization $\boldsymbol{c} = \boldsymbol{U}\boldsymbol{\Lambda}\boldsymbol{U}^T$, where $\boldsymbol{U}$ is an orthogonal matrix that consists of the eigenvectors of $\boldsymbol{c}$ and $\boldsymbol{\Lambda}$ is a diagonal matrix made with the corresponding eigenvalues of $\boldsymbol{c}$. Therefore, we obtain $\boldsymbol{\Psi} = \boldsymbol{U}(\ln\boldsymbol{\Lambda})\boldsymbol{U}^T$. Then, we can write the Oldroyd-B constitutive relation in terms of $\boldsymbol{\Psi}$ and solve it numerically:

$$\frac{\partial \boldsymbol{\Psi}}{\partial t} + (\mathbf{u}\cdot\nabla)\boldsymbol{\Psi} - (\boldsymbol{R}\boldsymbol{\Psi} - \boldsymbol{\Psi}\boldsymbol{R}) - 2\boldsymbol{B}\boldsymbol{\Psi} = \frac{1}{\mathrm{Wi}}\exp(-\boldsymbol{\Psi})(\boldsymbol{\delta} - \exp(\boldsymbol{\Psi})). \tag{5.4}$$

Note that the positivity of $\boldsymbol{c}$ is guaranteed automatically in this way.

Fattal and Kupferman [2004] reported numerical results on the lid-driven cavity benchmark for a finitely extensible Chilcott–Rallison (FENE-CR) fluid (Chilcott and Rallison [1988]) with a Weissenberg number of up to 5.0. Fattal and Kupferman [2005] made a break-through in HWNP with this idea on the Oldroyd-B model for the lid-driven cavity benchmark using finite difference methods. Recently, this method has been further investigated by Pan, Hao and Glowinski [2009] based on the finite element method and an operator-splitting Lie's scheme. Hulsen, Fattal and Kupferman [2005] applied the log-conformation formulation combined with the DEVSS/DG to the Oldroyd-B as well as the Giesekus model for the flow-past-cylinder benchmark in the finite element context. Coronado, Arora, Behr and Pasquali [2007], on the other hand, gave an alternative log-conformation formulation and applied the DEVSS-TG/SUPG method (Pasquali and Scriven [2002]) for the flow-past-cylinder benchmark. Their reported numerical results are for Weissenberg numbers of up to 1.8 (Hulsen, Fattal and Kupferman [2005])

and 1.05 (Coronado, Arora, Behr and Pasquali [2007]). Recently, Afonso, Oliveira, Pinho and Alves [2009] applied a finite volume method on the log-conformation and reported computational results for the flow-past-cylinder benchmark up to a Weissenberg number of 2.5; but mesh convergence was not confirmed for Weissenberg numbers larger than around 0.9.

The stability of the algorithm in Fattal and Kupferman [2004] has been analyzed by Boyaval, Lelievre and Mangoubi [2009]. The key ingredients used in the analysis were the divergence-free condition and the positivity of the conformation tensor. We note that the log-formulation of the conformation tensor preserves positivity in the discrete sense naturally. In fact, preserving the positivity of the conformation tensor is regarded as one of the main issues in developing stable numerical schemes for viscoelastic flows. We next discuss several attempts to address this issue.

5.3. *Positivity-preserving schemes*

The HWNP has been closely investigated in correlation with the loss of the positivity-preserving property of the conformation tensor $\boldsymbol{c}$ on the discrete level (Beris and Edwards [1994], Dupret, Marchal and Crochet [1985], Hulsen [1988], Joseph and Saut [1986], Owens and Phillips [2002]). Although there have been many attempts to construct positivity-preserving schemes, only a handful of schemes are available that preserve the positive-definite character of the conformation tensor on the discrete level. These include the log-conformation schemes discussed above. Another notable example is given by Lozinski and Owens [2003]. Using the fact that the conformation tensor $\boldsymbol{c}$ is positive, they wrote the conformation tensor $\boldsymbol{c}$ as $\boldsymbol{c} = \boldsymbol{C}\boldsymbol{C}^T$ and defined the matrix $\boldsymbol{C}$ by the solution to some semidiscrete equation. More precisely, let $\mathbf{u}^n$ and $\boldsymbol{c}^n = \boldsymbol{C}^n(\boldsymbol{C}^n)^T$ be the nth time step approximate solution to the velocity field $\mathbf{u}$ and the conformation tensor $\boldsymbol{c}$, respectively. Then, $\boldsymbol{C}^n$ is defined as the solution to the equation given as follows:

$$\boldsymbol{C}^n + k\Big(\frac{1}{2\mathrm{Wi}}\boldsymbol{C}^n + (\mathbf{u}^n \cdot \nabla)\boldsymbol{C}^n - \nabla\mathbf{u}^n\boldsymbol{C}^n\Big) = \sqrt{\boldsymbol{c}^{n-1} + \frac{\eta_p k}{\mathrm{Wi}^2}\boldsymbol{\delta}}, \tag{5.5}$$

where k is the time step size. It is further shown that this semidiscretization is consistent in Lozinski and Owens [2003]. This approach has been further explored by Hao, Pan, Glowinski and Joseph [2009] as well.

Vaithianathan, Robert, Brasseur and Collins [2006, 2007] have developed a positivity-preserving algorithm that takes into account that the conformation tensor $\boldsymbol{c}$ can be decomposed as $\boldsymbol{c} = \boldsymbol{U}\boldsymbol{\Lambda}\boldsymbol{U}^T$, where $\boldsymbol{U}$ is the orthogonal matrix that consists of eigenvectors of $\boldsymbol{c}$ and $\boldsymbol{\Lambda}$ is the diagonal matrix consisting of the eigenvalues of $\boldsymbol{c}$. They wrote equations for both $\boldsymbol{\Lambda}$ and $\boldsymbol{U}$. These are evolved by solving equations that define these unknowns, which have been successfully applied for the turbulent flow of a viscoelastic polymer solution (Vaithianathan, Robert, Brasseur and Collins [2006, 2007]).

Lee and Xu's [2006] made an attempt to tackle the high Weissenberg number problems by preserving the positivity of the conformation tensors on the fully discrete level. The idea relies on the link between the constitutive equations and the symmetric matrix Riccati differential equations (Abou-Kandil, Freiling, Ionescu and Jank [2003], Reid [1972]). We will demonstrate why this is crucial in the stability of the solutions and prove that the discrete solution exists in time without break-down in Section 8. More importantly, we will

show how this approach can be generalized so that the proposed method will be able to handle most existing macroscopic constitutive equations in a unified and efficient way.

Lee and Xu's [2006] method is closely related to the method proposed by Petera [2002], which is based on a conformation tensor formulation of the constitutive laws and the method of characteristics for the upper convected time derivative directly. Petera [2002] developed an Eulerian–Lagrangian discretization based on the direct discretization of the generalized Lie derivative introduced by Hughes and Winget in their pioneering work (Fortin and Esselaoui [1987], Hughes and Winget [1980]). However, this method does not preserve the strong divergence-free condition. While the method by Petera [2002] can be shown to preserve the positivity of the conformation tensor, due to the lack of the strong divergence-free condition in his scheme, stability could not be proven; the relevant energy estimates were missing as well. Moreover, the fact that the conformation tensor formulations can be identified with the Riccati equations, as discussed in Section 3, was not noticed there. In particular, the techniques introduced by Fortin and Esselaoui [1987] have been further investigated by Kabanemi, Bertrand, Tanguy and Ait-Kadi [1994].

5.4. *Constitutive equations with diffusion*

Other approaches attempt to stabilize the viscoelastic models by adding a small diffusion term to the constitutive equations. Considering the fact that the difficulty of simulating and proving the global-in-time solutions to the general complex fluids lies in the hyperbolic nature of the constitutive equations, this is a natural choice. Not only does this addition stabilize the equation, it also eases the proof of the global-in-time existence of solutions (see Lin, Liu and Zhang [2005], for example.) Another existence proof can be found in El-Kareh and Leal [1989]. Furthermore, Sureshkumar and Beris [1995] investigated this approach for the Poiseuille flow of the Oldroyd-B model and concluded that a small stress diffusivity can be introduced so that enhanced stability can be achieved without altering the flow rheology.

The main issue, which is still open here, is how to impose the boundary conditions upon adding the diffusivity of the stress fields to the constitutive equations (Beris and Edwards [1994]). The pure Neumann boundary or the Robin boundary conditions are often given (see Adams, Fielding and Olmsted [2008], Black and Graham [2001]). It is, however, impossible to know how macromolecules react near the boundary in general and the construction of the right boundary conditions still remains elusive. In fact, the molecular derivation of the Oldroyd-B model has the diffusion terms although the diffusivity constant is small, and it has been shown that, generally, the multiscale approach is more stable (Bajaj, Bhat, Prakash and Pasquali [2006]). The addition of dissipation, therefore, may help achieve the stability of the numerical calculations. This technique has been widely used for turbulent drag reduction (Sureshkumar and Beris [1997]). Experiments in Sureshkumar and Beris [1995] showed that adding the diffusion term in the constitutive equations has definite positive effects without altering the flow pattern significantly.

6. A family of Eulerian–Lagrangian finite element methods

In this section, we present our numerical methods to solve the viscoelastic flow models introduced in Section 3. Typically, the viscoelastic fluids are described by the time-dependent

models, and even steady-state computations are generally performed using time marching (Alves, Oliveira and Pinho [2003]) for the corresponding time-dependent problem. Therefore, our interest lies in developing time-dependent non-Newtonian models and their time and space discretization. Our aim here is to introduce, in a systematic way, a class of positivity-preserving discretizations of the Riccati formulation of the constitutive equations in terms of the conformation tensor. In particular, we will demonstrate that our schemes possess the important stability property, and we refer to a recent work by Boyaval, Lelievre and Mangoubi [2009], where similar stability results have been presented as well.

6.1. Temporal discretization

In the Lagrangian frame, it has been established that the general macroscopic constitutive equation can be cast into (3.18). Therefore, it is natural to employ the Lagrangian approach, and there are two main ways to use this approach.

The first idea, the pure Lagrangian approach or the method of characteristics, is to follow the particle trajectories in time and to use the initial positions of the particles as nodes at which the solutions are evaluated. This approach has an inherent disadvantage in that grid points can be severely distorted, and therefore, the accuracy of long-time calculations can easily be degraded. Further, the relocation of particle positions is unavoidable, in which case it is necessary to interpolate the solutions at the new positions. And, this in turn introduces additional numerical error (Baaijens [1993]).

In order to avoid mesh distortion, we can view the fixed discretization at any time level as the particle positions and consider the characteristic foot (or departure foot) as the previous position of this given particle. This method, known as the Eulerian–Lagrangian method (ELM) or the semi-Lagrangian method (SLM), was introduced to the finite element community in the early 1980s; see Douglas and Russell [1982] and Pironneau [1982].

6.1.1. Eulerian–Lagrangian method for the momentum equation

The ELM begins by establishing the characteristic foot of any given particle at the current time step. Note that similar approaches have been applied to the computation of viscoelastic flows in Bonito, Picasso and Laso [2006] and Phillips and Williams [1999] as well.

Let x be the position of any material particle at the current time t; let x also be used to refer to the particle itself. Suppose that the particle x moves with the velocity $\mathbf{u}(\phi_{t,s}(x), s)$ at time s. The characteristic foot (or the departure foot) $y = \phi_{t,s}(x)$ of the particle x at any previous time $s \le t$ can be found by solving the following flow map equation:

$$\frac{\partial}{\partial s}\phi_{t,s}(x) = \mathbf{u}(\phi_{t,s}(x), s), \quad \phi_{t,t}(x) = x. \tag{6.1}$$

A straightforward approximation scheme for (6.1) is the first-order forward Euler method:

$$\frac{x - y}{k} = \mathbf{u}(y, s) + O(k), \tag{6.2}$$

where k is the time step size $k = t - s$. We denote the approximate solution to Eqn (6.2) by $\widetilde{y}$, which satisfies the equation

$$\widetilde{y} = x - k\mathbf{u}(\widetilde{y}, s). \tag{6.3}$$

We note that the characteristic foot $\widetilde{y}$ is defined implicitly. Hence, we must apply certain nonlinear iterations to obtain the solution to Eqn (6.3).

Unfortunately, the explicit Euler scheme does not preserve volume, which is crucial for the stability of numerical simulations and the convergence of nonlinear iterative methods; see Section 8 for more detail. Feng and Shang [1995] discussed volume-preserving numerical schemes for the ordinary differential equation (6.1) and noted that the simplest one replaces $\mathbf{u}(\widetilde{y}, s)$ in (6.3) with $\mathbf{u}\big((\widetilde{y}+x)/2, s\big)$, i.e.,

$$\widetilde{y} = x - k\mathbf{u}\Big(\frac{\widetilde{y}+x}{2}, s\Big). \tag{6.4}$$

Next, we offer a simple discussion to demonstrate why this scheme is volume-preserving.

Lemma 6.1 (First-Order Volume-Preserving Scheme). *Let* $\Omega \subset \mathbb{R}^2$ *Suppose* $\mathbf{u}(s) \in (H^1(\Omega))^d$ *and* $\nabla \cdot \mathbf{u}(s) = 0$. *If the time step size* k *is small enough, then the scheme (6.4) is well defined and volume preserving, i.e.,* $\det(\nabla\widetilde{y}) = 1$.

Proof. First, if k is small enough, Eqn (6.4) is solvable, and the scheme is well defined. Now let $\boldsymbol{J} := \nabla\widetilde{y}$ be the Jocobian matrix. Taking derivative with respect to x on both sides of (6.4), we can obtain

$$\boldsymbol{J} = \boldsymbol{\delta} - \frac{k}{2}\nabla\mathbf{u}\Big(\frac{\widetilde{y}+x}{2}, s\Big)(\boldsymbol{J}+\boldsymbol{\delta}).$$

This immediately implies that

$$\Big[\boldsymbol{\delta} + \frac{k}{2}\nabla\mathbf{u}\Big(\frac{\widetilde{y}+x}{2}, s\Big)\Big]\boldsymbol{J} = \boldsymbol{\delta} - \frac{k}{2}\nabla\mathbf{u}\Big(\frac{\widetilde{y}+x}{2}, s\Big).$$

Hence, if k is small enough, $\boldsymbol{\delta} + \frac{k}{2}\nabla\mathbf{u}\Big(\frac{\widetilde{y}+x}{2}, s\Big)$ is invertible, and we can solve for $\boldsymbol{J}$. So the determinate of the Jacobian matrix is

$$\det\boldsymbol{J} = \det\Big[\boldsymbol{\delta} + \frac{k}{2}\nabla\mathbf{u}\Big(\frac{\widetilde{y}+x}{2}, s\Big)\Big]^{-1}\det\Big[\boldsymbol{\delta} - \frac{k}{2}\nabla\mathbf{u}\Big(\frac{\widetilde{y}+x}{2}, s\Big)\Big].$$

To show $\det\boldsymbol{J} = 1$, we assume that

$$\frac{k}{2}\nabla\mathbf{u}\Big(\frac{\widetilde{y}+x}{2}, s\Big) = \begin{pmatrix} a_{11} & a_{12} \\ a_{21} & a_{22} \end{pmatrix} \quad \text{and} \quad a_{11} + a_{22} = 0.$$

Therefore, by direct calculation, we obtain

$$\det\boldsymbol{J} = \frac{1 - a_{11} - a_{22} + a_{11}a_{22} - a_{12}a_{21}}{1 + a_{11} + a_{22} + a_{11}a_{22} - a_{12}a_{21}} = 1,$$

which completes the proof. □

Remark 6.1 (Alternative Volume-Preserving Schemes). The scheme (6.4) is only of first order. An alternative is this second-order scheme:

$$\widetilde{y} = x - \frac{k}{2}\Big(\mathbf{u}\Big(\frac{\widetilde{y}+x}{2}, s\Big) + \mathbf{u}\Big(\frac{\widetilde{y}+x}{2}, t\Big)\Big). \tag{6.5}$$

The aforementioned two schemes (6.4) and (6.5) preserve volume in $\mathbb{R}^2$. For three-dimensional problems, constructing volume-preserving schemes is possible, but more complicated; see FENG and SHANG [1995] for details.

We will now apply this idea to discretizing the momentum equation of the Oldroyd-B model. More specifically, we will assume that the solution at time level $s = t^{\text{old}}$ is known; that is, $(\mathbf{u}^{\text{old}}, p^{\text{old}}, \boldsymbol{T}^{\text{old}})$ is given, and for any given mesh points at time level $t = t^{\text{new}}$, we let $\widetilde{y}$ be solutions to the discrete flow map equation (6.3). Namely, $\widetilde{y}$ is an approximation of the departure foot $y = \phi_{t^{\text{new}},\, t^{\text{old}}}(x)$. In the Lagrangian view, the momentum equation (3.1) can be viewed as an ODE; therefore, it can be discretized by using the flow map solutions as follows:

$$\mathsf{Re}\left(\frac{\mathbf{u}^{\text{new}} - \mathbf{u}^{\text{old}} \circ \widetilde{y}}{k}\right) = \eta_s \Delta \mathbf{u}^{\text{new}} - \nabla p^{\text{new}} + \nabla \cdot \boldsymbol{T}^{\text{new}}.$$

Therefore, we arrive at the following semidiscrete equation (continuous in space variable):

$$\frac{\mathsf{Re}}{k}\mathbf{u}^{\text{new}} - \eta_s \Delta \mathbf{u}^{\text{new}} + \nabla p^{\text{new}} - \nabla \cdot \boldsymbol{T}^{\text{new}} = \frac{\mathsf{Re}}{k}\mathbf{u}^{\text{old}} \circ \widetilde{y}. \tag{6.6}$$

6.1.2. *Eulerian–Lagrangian method for constitutive equations*

The particle-following approach (6.6) can be naturally applied to approximate generalized Lie derivatives as well. We now explain it using the model equation (3.18) with positive constant parameters α and β as an example.

Approximations based on the generalized Lie derivative First, we consider the numerical discretization of the generalized Lie derivative $\mathcal{L}_{u,\boldsymbol{R}}\boldsymbol{\zeta}$ at time t^{new}. By Definition 2.1, we can employ the first-order difference approximation for the time derivative to obtain

$$\begin{aligned}&\frac{\boldsymbol{E}(s,t)\boldsymbol{\zeta}(s,t)\boldsymbol{E}(s,t)^T - \boldsymbol{E}(s-k,t)\boldsymbol{\zeta}(s-k,t)\boldsymbol{E}(s-k,t)^T}{k}\Big|_{s=t}\\ &\quad = \frac{\boldsymbol{\zeta}(t,t) - \boldsymbol{E}(t-k,t)\boldsymbol{\zeta}(t-k,t)\boldsymbol{E}(t-k,t)^T}{k}.\end{aligned} \tag{6.7}$$

Let $\widetilde{\boldsymbol{E}}$ be an approximate solution to the ODE for the transition matrix, namely,

$$\frac{\partial \boldsymbol{E}(s,t)}{\partial t} = \boldsymbol{R}(s,t)\boldsymbol{E}(s,t) \quad \text{and} \quad \boldsymbol{E}(s,s) = \boldsymbol{\delta}. \tag{6.8}$$

For example, we can apply the explicit Euler method:

$$\frac{\widetilde{\boldsymbol{E}} - \boldsymbol{\delta}}{k} = \boldsymbol{R}(t^{\text{old}})\boldsymbol{\delta} \Longrightarrow \widetilde{\boldsymbol{E}} = \boldsymbol{\delta} + k\boldsymbol{R}(t^{\text{old}}). \tag{6.9}$$

We can also apply the implicit Euler method:

$$\frac{\widetilde{\boldsymbol{E}} - \boldsymbol{\delta}}{k} = \boldsymbol{R}(t^{\text{new}})\widetilde{\boldsymbol{E}} \Longrightarrow \widetilde{\boldsymbol{E}} = \big(\boldsymbol{\delta} - k\boldsymbol{R}(t^{\text{new}})\big)^{-1}. \tag{6.10}$$

Using either (6.9) or (6.10) for approximating the transition matrix $\widetilde{\boldsymbol{E}}$ and the approximate solution $\widetilde{y}$ to the flow map equation, we derive a numerical discretization of the generalized Lie derivative as follows:

$$\mathcal{L}_{u,\boldsymbol{R}}\zeta(t^{\text{new}}) \approx \frac{\boldsymbol{\zeta}^{\text{new}} - \widetilde{\boldsymbol{E}}(\boldsymbol{\zeta}^{\text{old}} \circ \widetilde{y})\widetilde{\boldsymbol{E}}^T}{k}. \tag{6.11}$$

This approximation can be easily shown to satisfy the desired property that the conformation tensor is positive definite in the semidiscrete level when applied to approximate the general Riccati form of the constitutive law (3.18).

LEMMA 6.2 (Positivity-Preserving Semidiscretization). *Consider the semidiscrete scheme (6.11) for the model equation (3.18) with positive parameters α and β, namely,*

$$\frac{\boldsymbol{c}^{\text{new}} - \widetilde{\boldsymbol{E}}(\boldsymbol{c}^{\text{old}} \circ \widetilde{y})\widetilde{\boldsymbol{E}}^T}{k} + \alpha\boldsymbol{c}^{\text{new}} = \beta\boldsymbol{\delta}. \tag{6.12}$$

If $\boldsymbol{c}^{\text{old}}$ is positive definite, then the numerical scheme preserves positivity, namely, $\boldsymbol{c}^{\text{new}}$ is still positive definite.

PROOF. We can solve the Eqn (6.12) in terms of $\boldsymbol{c}^{\text{new}}$ to obtain

$$(1 + k\alpha)\boldsymbol{c}^{\text{new}} = \widetilde{\boldsymbol{E}}(\boldsymbol{c}^{\text{old}} \circ \widetilde{y})\widetilde{\boldsymbol{E}}^T + k\beta\boldsymbol{\delta}. \tag{6.13}$$

As an immediate consequence, if $\boldsymbol{c}^{\text{old}}$ is positive definite, then so is $\boldsymbol{c}^{\text{new}}$. □

Approximations for the Riccati form of constitutive laws However, the above discretization of the generalized Lie derivative is not the only way to obtain positive-definite discrete conformation tensors. We can simply apply the discretization of the material derivative to obtain the following semidiscrete systems:

$$\frac{\boldsymbol{c}^{\text{new}} - \boldsymbol{c}^{\text{old}} \circ \widetilde{y}}{k} - \boldsymbol{R}^{\text{new}}\boldsymbol{c}^{\text{new}} - \boldsymbol{c}^{\text{new}}(\boldsymbol{R}^{\text{new}})^T + \alpha\boldsymbol{c}^{\text{new}} = \beta\boldsymbol{\delta}. \tag{6.14}$$

Known as the Lyapunov equation, this equation can be reformulated as a symmetric algebraic Riccati equation by a simple change of variable:

$$\left(\frac{\alpha k + 1}{2k}\boldsymbol{\delta} - \boldsymbol{R}^{\text{new}}\right)\boldsymbol{c}^{\text{new}} + \boldsymbol{c}^{\text{new}}\left(\frac{\alpha k + 1}{2k}\boldsymbol{\delta} - \boldsymbol{R}^{\text{new}}\right)^T = \frac{\boldsymbol{c}^{\text{old}} \circ \widetilde{y}}{k} + \beta\boldsymbol{\delta}. \tag{6.15}$$

In fact, the solution $\boldsymbol{c}^{\text{new}}$ is positive definite if $\boldsymbol{c}^{\text{old}} \circ \widetilde{y}$ is positive definite.

Approximations based on the explicit solution We can also design numerical schemes based on the explicit solution of the Riccati form of the constitutive equations. In general, the numerical schemes based on the analytic solution (3.19) require approximations of $\boldsymbol{E}(s, t)$, (3.22), and the time integral in (3.19); see Lemma 3.1. Approximations of $\boldsymbol{E}(s, t)$ do not affect the approximated conformation tensor's positivity property. The integral expression in (3.19) should be computed by using numerical quadratures with positive weights in order

to maintain the positivity property, which is the approach taken by Dieci [1994] and Dieci and Eirola [1994, 1996].

There are many possible methods based on explicit integral expression (3.19) of the solution; an extensive list of schemes can be found in Lee and Xu's [2006]. Here, we present only one such example: if α and β are both constants, the explicit form of the solution can be approximated by the left-point Euler method:

$$\boldsymbol{c}^{\text{new}} = \exp(-k\alpha)\widetilde{\boldsymbol{E}}(\boldsymbol{c}^{\text{old}} \circ \widetilde{y})\,\widetilde{\boldsymbol{E}}^{T} + k\beta\boldsymbol{\delta}. \tag{6.16}$$

If we use the first-order Taylor expansion for the exponential function and drop higher-order terms with respect to k on the right-hand side, then we get the exact same scheme as (6.12).

6.2. *Spatial discretization*

It is now clear that the Eulerian–Lagrangian framework provides semidiscrete equations, which preserves the positivity of the conformation tensor. The main goal of this section is to introduce spatial discretizations so that positivity can be realized in the fully discrete sense as well. It is worth noting that the Eulerian–Lagrangian approach follows the particle trajectory and the interpolated solution may not be positive even if the solution is positive at mesh points. This will restrict the choice of the approximation spaces, in particular the approximate stress field. In this section, we introduce various approximation spaces for which the positivity of the conformation tensors can be preserved.

6.2.1. *Stokes-like saddle point problems*

We begin by introducing the equations that will be discretized in space. After applying the ELM to the model problem (3.1), (3.2), and (3.18), we obtain the following semidiscrete problem: find $(\mathbf{u}^{\text{new}}, p^{\text{new}}, \boldsymbol{c}^{\text{new}})$ such that

$$\frac{\mathsf{Re}}{k}\mathbf{u}^{\text{new}} - \eta_s\Delta\mathbf{u}^{\text{new}} + \nabla p^{\text{new}} = \frac{\mathsf{Re}}{k}\mathbf{u}^{\text{old}} \circ \widetilde{y} + \nabla\cdot\boldsymbol{c}^{\text{new}} \tag{6.17}$$

$$\nabla\cdot\mathbf{u}^{\text{new}} = 0 \tag{6.18}$$

$$(1 + k\alpha)\boldsymbol{c}^{\text{new}} = \widetilde{\boldsymbol{E}}(\boldsymbol{c}^{\text{old}} \circ \widetilde{y})\widetilde{\boldsymbol{E}}^{T} + \beta\boldsymbol{\delta}. \tag{6.19}$$

We note that Eqn (6.17) is nonlinear and coupled together through the conformation tensor with (6.19); the nonlinearity also lies in the computation of $\widetilde{y}$ and $\widetilde{\boldsymbol{E}}$. The finite element spaces for the unknowns $\mathbf{u}$, p, and $\boldsymbol{c}$ should be constructed carefully based on the stability conditions to keep the solution from blowing up as the mesh size reduces.

In this section, we identify the ingredients necessary to achieving this goal by considering the momentum equation and continuity equation with the conformation tensor being given explicitly. We consider the most straightforward linearization method here: the conformation tensor $\boldsymbol{c}$ explicitly given at each iteration. In each nonlinear iteration, Eqns (6.17) and (6.18) can be written as the following system of equations up to a simple rescaling:

$$\begin{cases} \rho^2\mathbf{u} - \kappa^2\Delta\mathbf{u} + \nabla p = \mathbf{g} \\ \nabla\cdot\mathbf{u} = 0, \end{cases} \tag{6.20}$$

where $\mathbf{g}$ depends on $\mathbf{u}$ and $\rho^2, \kappa^2 \lesssim 1$.

The main goal now is to identify stable finite element pairs for the velocity and pressure so that accuracy is independent of all relevant parameters ρ^2 and κ^2. We begin by casting Eqn (6.20) into a weak formulation as follows: find $(\mathbf{u}, p) \in (H_0^1(\Omega))^d \times L_0^2(\Omega)$ such that

$$\begin{cases} a_p(\mathbf{u}, \mathbf{v}) + b(\mathbf{v}, p) = \langle \mathbf{g}, \mathbf{v} \rangle & \forall \mathbf{v} \in (H_0^1(\Omega))^d \\ b(\mathbf{u}, q) = 0 & \forall q \in L_0^2(\Omega), \end{cases} \tag{6.21}$$

where the bilinear forms $a_p(\cdot, \cdot) : (H_0^1)^d \times (H_0^1)^d \mapsto \mathbb{R}$ and $b(\cdot, \cdot) : (H_0^1)^d \times L_0^2 \mapsto \mathbb{R}$ are defined as

$$a_p(\mathbf{u}, \mathbf{v}) := \rho^2(\mathbf{u}, \mathbf{v}) + \kappa^2(\nabla \mathbf{u} : \nabla \mathbf{v}) \quad \text{and} \quad b(\mathbf{v}, p) := -\int_\Omega (\nabla \cdot \mathbf{v})\, p \, \mathrm{d}x.$$

Here, we use the standard notation that $(\cdot : \cdot)$ acting on two matrix-valued functions $\boldsymbol{A} = (a_{i,j}) \in \mathbb{M}$ and $\boldsymbol{B} = (b_{i,j}) \in \mathbb{M}$ denotes

$$(\boldsymbol{A} : \boldsymbol{B}) := \int_\Omega \mathrm{tr}(\boldsymbol{A}\boldsymbol{B}) \, \mathrm{d}\boldsymbol{x} = \int_\Omega \sum_{i,j=1}^{d} a_{i,j} b_{i,j} \, \mathrm{d}\boldsymbol{x}, \tag{6.22}$$

where $\mathrm{tr} : \mathbb{M} \mapsto \mathbb{R}$ is the standard trace operator of a matrix.

Apparently, the bilinear form $a_p(\cdot, \cdot)$ induces a norm

$$\|\mathbf{u}\|_{a_p}^2 := a_p(\mathbf{u}, \mathbf{u}) = \rho^2 \|\mathbf{u}\|_0^2 + \kappa^2 |\mathbf{u}|_1^2.$$

We now introduce the energy norm $|||\cdot|||$ on $(H_0^1(\Omega))^d$ as follows:

$$|||\mathbf{u}|||^2 := \|\mathbf{u}\|_{a_p}^2 + \|\nabla \cdot \mathbf{u}\|_0^2 \qquad \forall \mathbf{u} \in (H_0^1(\Omega))^d.$$

It is then clear that the bilinear forms $a_p(\cdot, \cdot)$ and $b(\cdot, \cdot)$ are continuous, i.e.,

$$\begin{aligned} a_p(\mathbf{u}, \mathbf{v}) &\lesssim |||\mathbf{u}|||\ |||\mathbf{v}||| \qquad \forall \mathbf{u}, \mathbf{v} \in (H_0^1)^d \\ b(\mathbf{v}, q) &\lesssim |||\mathbf{v}|||\ \|q\|_0 \qquad \forall \mathbf{v} \in (H_0^1)^d, q \in L_0^2. \end{aligned}$$

We also note that $|||\mathbf{u}||| = \|\mathbf{u}\|_{a_p}$ for any $\mathbf{u} \in \boldsymbol{\mathcal{N}} := \{\mathbf{v} \in (H_0^1)^d : \nabla \cdot \mathbf{v} = 0\}$. Therefore, $a_p(\cdot, \cdot)$ is also elliptic on $\boldsymbol{\mathcal{N}}$.

Furthermore, using the following inf-sup condition (or the Brezzi condition) that

$$\sup_{\mathbf{v} \in (H_0^1)^d} \frac{b(\mathbf{v}, q)}{\|\mathbf{v}\|_1} \gtrsim \|q\|_0 \qquad \forall q \in L_0^2, \tag{6.23}$$

and the fact that $\|\nabla \cdot \mathbf{u}\|_0 \leq \|\mathbf{u}\|_1$, we can easily obtain that for $\rho^2, \kappa^2 \lesssim 1$,

$$\sup_{\mathbf{v} \in (H_0^1)^2} \frac{b(\mathbf{v}, q)}{|||\mathbf{v}|||} \gtrsim \sup_{\mathbf{v} \in (H_0^1)^2} \frac{b(\mathbf{v}, q)}{\|\mathbf{v}\|_1} \gtrsim \|q\|_0 \qquad \forall q \in L_0^2. \tag{6.24}$$

This means that the Eqn (6.21) is uniformly stable with respect to the norm $|||\cdot|||$ for the velocity and $\|\cdot\|_0$ for the pressure.

6.2.2. Stable discretizations of the generalized Stokes equation

Similar considerations can be directly transferred to the discrete case as well. We assume that the domain $\Omega \subset \mathbb{R}^d$ has been partitioned into triangular/tetrahedral elements $\mathcal{T}_h = \{E\}$ and that the conforming and quasi-uniform partition $\mathcal{T}_h$ satisfies

$$\overline{\Omega} = \bigcup_{E \in \mathcal{T}_h} \overline{E}. \tag{6.25}$$

Based on the partitions $\mathcal{T}_h$, we will choose appropriate approximation spaces $\mathbf{V}_h$ and W_h for the primitive variables $\mathbf{u}$ and p, respectively.

Consider a discrete weak formulation that is formulated by making the appropriate choice of space $\mathbf{V}_h \subset (H_0^1(\Omega))^d$ for the velocity and $W_h \subset L_0^2(\Omega)$ for the pressure: find $(\mathbf{u}_h, p_h) \in \mathbf{V}_h \times W_h$ such that

$$\begin{cases} a_p(\mathbf{u}_h, \mathbf{v}_h) + b(\mathbf{v}_h, p_h) = \langle \mathbf{g}, \mathbf{v}_h \rangle & \forall \mathbf{v}_h \in \mathbf{V}_h \\ b(\mathbf{u}_h, q_h) = 0 & \forall q_h \in W_h. \end{cases} \tag{6.26}$$

As demonstrated by Xie, Xu and Xue [2008], the uniform well-posedness and error analysis for the finite element pairs $\mathbf{V}_h \times W_h$ can be achieved if we can show that the following two conditions are satisfied from the well-known (Brezzi theory Brezzi [1974], Brezzi and Fortin [1991]), namely,

$$\sup_{\mathbf{v}_h \in \mathbf{V}_h} \frac{b(\mathbf{v}_h, q_h)}{\|\mathbf{v}_h\|_1} \gtrsim \|q_h\|_0 \qquad \forall q_h \in W_h, \tag{6.27}$$

and

$$\nabla \cdot \mathbf{V}_h \subseteq W_h. \tag{6.28}$$

We define $a(\mathbf{u}, \mathbf{v}) := a_p(\mathbf{u}, \mathbf{v}) + a_s(\mathbf{u}, \mathbf{v})$ with $a_s(\mathbf{u}, \mathbf{v}) := (\nabla \cdot \mathbf{u}, \nabla \cdot \mathbf{v})$. Under the two afore stated conditions (6.27) and (6.28), we can immediately see that

$$\sup_{\mathbf{v}_h \in \mathbf{V}_h} \frac{b(\mathbf{v}_h, q_h)}{|||\mathbf{v}_h|||} \gtrsim \|q_h\|_0 \qquad \forall q_h \in W_h \tag{6.29}$$

and

$$a(\mathbf{u}_h, \mathbf{u}_h) \gtrsim |||\mathbf{u}_h|||^2 \qquad \forall \mathbf{u}_h \in \boldsymbol{\mathcal{N}}_h, \tag{6.30}$$

where $\boldsymbol{\mathcal{N}}_h := \{\mathbf{v}_h \in \mathbf{V}_h : \nabla \cdot \mathbf{v}_h = 0\}$.

Now, we give some examples of conforming finite element methods that satisfy both conditions, (6.27) and (6.28).

Example 6.1 (Scott–Vogelius Finite Elements). The $P_0^4 - P_{-1}^3$ Scott–Vogelius element (Scott and Vogelius [1985a,b]) is important in fluid mechanics computation. It uses the piecewise continuous polynomials on triangles of a degree up to 4 to approximate the velocity field and uses the piecewise discontinuous polynomials of a degree up to 3 for the pressure. In $\mathbb{R}^2$, on each triangle, the P_0^4 space has 15 degrees of freedom (DOFs) determined

by values at three vertices, three quartering points on each edge, and three interior points inside each triangle. The P^3_{-1} space has 10 DOFs on each triangle, all of which are given inside the triangle independently. This element is stable in the sense that it satisfies the inf-sup condition, if the triangulation is singular-point free (a vertex is called singular if all edges meeting at the vertex fall into two crossing straight lines). This kind of element is of key importance because it can preserve the incompressible condition, i.e., the discrete velocity is divergence-free pointwise.

Example 6.2 (Austin–Manteuffel–McCormick Finite Elements). The tensor-product finite element in two-dimensional domains given by Austin, Manteuffel and McCormick [2004] can easily be extended into three-dimensional domains. In each reference triangle, for the horizontal component of the velocity fields, the product of the cubic Hermite polynomial in the x_1 variable and the quadratic polynomial in the x_2 variable are used. For the vertical component of the velocity fields, the product of the quadratic polynomial in the x_1 variable and the cubic Hermite polynomial in the x_2 variable are used. For the pressure, the product of the quadratic polynomial in the x_1 and x_2 variable is used. This element has been shown to be uniformly stable by Lee, Wu and Chen [2009].

6.2.3. *Approximation Space for Stress*

Our guiding principle in choosing the approximation space for the stress fields is to preserve the positivity of the conformation tensor. The main bottleneck in this process is to evaluate the conformation tensor at any points, which may not necessarily be the mesh points. This can be reinterpreted as constructing an interpolation operator $\Pi_h^S : \mathbb{M} \mapsto \mathbb{M}$, which preserves positivity in the following sense:

$$\boldsymbol{\sigma} > 0 \quad \Longrightarrow \quad \Pi_h^S(\boldsymbol{\sigma}) > 0, \quad \forall \boldsymbol{\sigma} \in \mathbb{M}, \tag{6.31}$$

where $\boldsymbol{\sigma} > 0$ means $\boldsymbol{\sigma}$ is positive definite.

For this purpose, we first consider the scalar positivity-preserving interpolations. We start with two simple examples:

Example 6.3 (Piecewise Constant Interpolation). The simplest finite element space that preserves the positivity of the scalar functions is, of course, the space of the piecewise constant functions. In this case, the existence of the positivity-preserving interpolation operator Π_h is obvious. For example, we can take, on each element $E \in \mathcal{T}_h$,

$$\Pi_h(g)(x) := \frac{1}{|E|} \int_E g \, \mathrm{d}x \qquad \forall x \in E, \tag{6.32}$$

where $|E|$ is the area of E. It is easy to see that

$$\|\Pi_h(g)\|_\infty = \max_E \frac{1}{|E|} \int_E g \le \max_E |E|^{-1/2} \|g\|_0 \tag{6.33}$$

and

$$\|\Pi_h(g)\|_{L^1} = \sum_E \int_E |\Pi_h(g)| \le \sum_E \int_E |g| = \|g\|_{L^1}. \tag{6.34}$$

Notice that these two inequalities are sharp. To see this, we can take a function g that is 1 on an element E and 0 elsewhere.

EXAMPLE 6.4 (Piecewise Linear Interpolation). The other choices can be given by continuous or discontinuous piecewise linear finite element spaces. For cases in which we choose a globally continuous piecewise linear finite element space, the standard pointwise nodal value interpolant would be positivity preserving. In case the solution is not smooth or the point values of g are not well defined, we can define the nodal value of $\Pi_h(g)(x_i)$ as the local mean value as follows:

$$\Pi_h(g)(x_i) := \frac{1}{|B_i|} \int_{B_i} g \, dx, \tag{6.35}$$

where $B_i = B(x_i, r_i(x_i))$ and where the ball centered at x_i and with radius $r_i(x_i)$ with $r_i(x_i)$ small enough so that B_i is contained in the union of closed elements containing x_i. This interpolation can be shown to be of second-order accuracy (NOCHETTO and WAHLBIN [2002]). For a case in which we choose a discontinuous piecewise linear finite element space, the construction of positivity-preserving operator Π_h for the above continuous piecewise linear element can be applied similarly.

REMARK 6.2 (High-Order Interpolations). We note that it is well known that the positivity-preserving interpolant cannot be made for a polynomial of degree 2 or higher. To summarize, we can choose the approximation space $\boldsymbol{S}_h$ for the conformation tensor as either piecewise constant or piecewise linear polynomial spaces in case the positivity preserving is the main restriction and, therefore, the accuracy of the approximations for such choices is either first-order or second-order.

Now, we introduce a lemma that though simple, is useful, as it allows us to construct positivity-preserving interpolation operators for tensors based on simple scalar interpolations.

LEMMA 6.3 (Positivity-Preserving Interpolations). *Let Π_h be a positivity-preserving interpolation operator for scalar functions, that is, if $g > 0$ on Ω, then $\Pi_h(g) > 0$ on Ω. Then, the interpolation operator Π_h induces Π_h^S such that*

$$\Pi_h^S(\boldsymbol{\sigma}) = (\Pi_h(\boldsymbol{\sigma}_{i,j}))_{i,j=1,\ldots,d}. \tag{6.36}$$

And Π_h^S is a positivity-preserving interpolation in $\mathbb{M}$.

PROOF. We note that the operator Π_h defined on scalar functions preserves the positivity in the sense that $g > 0$ implies $\Pi_h(g) > 0$. We choose any positive-definite tensor $\boldsymbol{\sigma} = (\sigma_{i,j})_{i,j=1,\ldots,d} \in \mathbb{M}$ and any nonzero vector $\xi = (\xi_i)_{i=1,\ldots,d} \in \mathbb{R}^d$ and observe that

$$0 < \xi^T \boldsymbol{\sigma} \xi = \sum_{i,j=1}^{d} \xi_i \sigma_{i,j} \xi_j \quad \Longrightarrow \quad 0 < \Pi_h\left(\xi^T \boldsymbol{\sigma} \xi\right).$$

We exploit the fact that the operator Π_h is linear to see that

$$\Pi_h\left(\xi^T \boldsymbol{\sigma} \xi\right) = \sum_{i,j=1}^{d} \xi_i \Pi_h(\sigma_{i,j}) \xi_j. \tag{6.37}$$

Therefore, the operator Π_h^S is positivity preserving. □

The following simple lemma is useful for deriving the discrete analog of the bridging identity (4.3) that has been crucially used to obtain the energy estimate in the continuous level.

LEMMA 6.4 (Bridging Lemma). *For matrix-valued functions* $\boldsymbol{A}$ *and* $\boldsymbol{B} : \mathbb{R}^d \to \mathbb{M}$*, the following identities hold true:*

$$\left(\Pi_h^S(\boldsymbol{A}) : \boldsymbol{B}\right) = \left(\Pi_h^S(\boldsymbol{A}) : \Pi_h^S(\boldsymbol{B})\right) = \left(\boldsymbol{A} : \Pi_h^S(\boldsymbol{B})\right). \tag{6.38}$$

PROOF. These equalities can be obtained by noticing that Π_h^S is an L^2 projection to the space of constant matrices. We show a more direct proof here. It is enough to show that for any scalar functions f and g, we have

$$\int_\Omega f\, \Pi_h(g)\, \mathrm{d}x = \int_\Omega \Pi_h(f)\, \Pi_h(g)\, \mathrm{d}x = \int_\Omega \Pi_h(f)\, g\, \mathrm{d}x. \tag{6.39}$$

And it can be shown from the following relation:

$$\begin{aligned}\int_\Omega f\, \Pi_h(g)\, \mathrm{d}x &= \int_\Omega f \sum_E \left(\frac{1}{|E|}\int_E g\, \mathrm{d}x\right) \varphi_E\, \mathrm{d}y = \sum_E \left(\int_\Omega f\, \varphi_E\, \mathrm{d}y\right)\left(\frac{1}{|E|}\int_E g\, \mathrm{d}x\right) \\ &= \sum_E \int_\Omega \left(\frac{1}{|E|}\int_E f\, \mathrm{d}y\right) \varphi_E\, \mathrm{d}z \left(\frac{1}{|E|}\int_E g\, \mathrm{d}x\right) = \int_\Omega \Pi_h(f)\, \Pi_h(g)\, \mathrm{d}x.\end{aligned}$$

The second equality follows using the same argument. □

REMARK 6.3 (Connecting the Momentum Balance with the Constitutive Laws). Lemma 6.4 can be used to establish the discrete analog of the important bridging identity (4.3) in the continuous level, namely,

$$\left(\Pi_h^S(\nabla \mathbf{u}) : \boldsymbol{c}\right) = \left(\Pi_h^S(\nabla \mathbf{u}) : \Pi_h^S(\boldsymbol{c})\right) = \left(\nabla \mathbf{u} : \Pi_h^S(\boldsymbol{c})\right). \tag{6.40}$$

We will apply this to obtain the discrete energy estimate in Section 8.

6.3. *Full discretizations*

In this section, we will conclude our discussion on discretization by combining time and space discretizations. We choose the approximation spaces $\mathbf{V}_h \times W_h \in (H_0^1(\Omega))^d \times L_0^2(\Omega)$

so that they satisfy both the inf-sup condition and the strong divergence-free condition. In addition, we choose $\boldsymbol{S}_h$ to be a symmetric tensor space whose entries belong to the piecewise polynomial spaces with a degree less than or equal to one.

The weak formulation of the semidiscrete system of Eqns (6.17)–(6.19) can be written as follows: given $\mathbf{u}_h^{\text{old}}$, p_h^{old}, and $\boldsymbol{c}_h^{\text{old}}$, find $(\mathbf{u}_h^{\text{new}}, p_h^{\text{new}}, \boldsymbol{c}_h^{\text{new}}) \in \mathbf{V}_h \times W_h \times \boldsymbol{S}_h$ such that for any $(\mathbf{v}_h, q_h, \boldsymbol{\sigma}_h) \in \mathbf{V}_h \times W_h \times \boldsymbol{S}_h$,

$$\begin{aligned} \mathrm{Re}\left(\frac{\mathbf{u}_h^{\text{new}}}{k}, \mathbf{v}_h\right) + \eta_s\left(\mathcal{D}(\mathbf{u}_h^{\text{new}}) : \mathcal{D}(\mathbf{v}_h)\right) - \left(p_h^{\text{new}}, \nabla\cdot\mathbf{v}_h\right) \\ = \mathrm{Re}\left(\frac{\Pi_h^V(\mathbf{u}_h^{\text{old}}\circ\widetilde{y})}{k}, \mathbf{v}_h\right) - \left(\boldsymbol{c}_h^{\text{new}} : \mathcal{D}(\mathbf{v}_h)\right), \end{aligned} \tag{6.41}$$

$$\left(\nabla\cdot\mathbf{u}_h^{\text{new}}, q_h\right) = 0, \tag{6.42}$$

$$(1+k\alpha)\left(\boldsymbol{c}_h^{\text{new}} : \boldsymbol{\sigma}_h\right) = \left(\widetilde{\boldsymbol{E}}_h\Pi_h^S(\boldsymbol{c}_h^{\text{old}}\circ\widetilde{y})\widetilde{\boldsymbol{E}}_h^T : \boldsymbol{\sigma}_h\right) + \beta\left(\boldsymbol{\delta} : \boldsymbol{\sigma}_h\right). \tag{6.43}$$

Based on the various approximations for the constitutive equation in Section 6.1.2, we can devise many approximations for the constitutive equation (3.18). There are a number of approaches to handling the constitutive laws. The weak formulation (6.43) leads us to the following discrete equation:

$$\boldsymbol{A}C_h = F_h, \tag{6.44}$$

where $\boldsymbol{A} = (a_{i,j}) \in \mathbb{M}$, and $a_{i,j} = \int_\Omega (1+k\alpha)\boldsymbol{\varphi}_j\boldsymbol{\varphi}_i\,\mathrm{d}x$ and $\{\boldsymbol{\varphi}_i\}_i$ are the basis functions for each entry of the stress approximation fields, the entries of C_h are the components of the expression of the tensor $\boldsymbol{c}_h^{\text{new}}$ in terms of the finite element basis, and F_h is the force terms due to the right-hand side in Eqn (6.43).

Remark 6.4 (Discretization Based on the Algebraic Riccati Form). Note that the discretization of the material derivative in the constitutive equation (6.14) leads to the following discrete constitutive equation:

$$\frac{\boldsymbol{c}_h^{\text{new}} - \Pi_h^S(\boldsymbol{c}_h^{\text{old}}\circ\widetilde{y})}{k} - \boldsymbol{R}_h\boldsymbol{c}_h^{\text{new}} - \boldsymbol{c}_h^{\text{new}}\boldsymbol{R}_h^T + \alpha\boldsymbol{c}_h^{\text{new}} = \beta\boldsymbol{\delta}. \tag{6.45}$$

The equation can be recast into the well-known algebraic Riccati equation called the Lyapunov equation given as follows:

$$\left(\frac{\alpha k+1}{2k} - \boldsymbol{R}_h\right)\boldsymbol{c}_h^{\text{new}} + \boldsymbol{c}_h^{\text{new}}\left(\frac{\alpha k+1}{2k} - \boldsymbol{R}_h\right)^T = \frac{\Pi_h^S(\boldsymbol{c}_h^{\text{old}}\circ\widetilde{y})}{k} + \beta\boldsymbol{\delta}. \tag{6.46}$$

Example 6.5 (A Fully Discrete Scheme for the Oldroyd-B Model). We would like to give a fully discrete scheme for the Oldroyd-B model, (3.1), (3.2), and (3.11), which we will discuss in later sections; for various other schemes, we refer interested readers to Lee and Xu's [2006].

ALGORITHM 1 Full Discretization–One Time Step

Step 0: Given $\mathbf{u}_h^n$ and $\boldsymbol{c}_h^n$.

Step 1: For any particle x, compute the departure feet

$$\widetilde{y}^n = x - k\,\mathbf{u}_h^n\left(\frac{\widetilde{y}^n + x}{2}\right).$$

Step 2: Solve the following nonlinear system:

$$\begin{cases} \mathrm{Re}\,\mathbf{u}_h^{n+1} - k\Delta_h\mathbf{u}_h^{n+1} + k\nabla_h p_h^{n+1} = k\nabla_h\cdot\boldsymbol{c}_h^{n+1} + \mathrm{Re}\,\Pi_h^V(\mathbf{u}_h^n\circ\widetilde{y}^n), \\ \nabla\cdot\mathbf{u}_h^{n+1} = 0, \\ (1+k\alpha)\boldsymbol{c}_h^{n+1} = \boldsymbol{F}_h^{n+1}\Pi_h^S(\boldsymbol{c}_h^n\circ\widetilde{y}^n)(\boldsymbol{F}_h^{n+1})^T + k\beta\boldsymbol{\delta}, \end{cases}$$

where $\boldsymbol{F}_h^{n+1} := \left(\boldsymbol{\delta} - k\Pi_h^S(\nabla\mathbf{u}_h^{n+1})\right)^{-1}$.

7. Fast and robust solvers for Stokes-type systems

As discussed in Section 6, by applying the Eulerian–Lagrangian method (ELM) to the non-Newtonian models, we reduce the task of solving nonlinear systems of equations to solving symmetric linear systems of Stokes type at each iteration. Therefore, the optimal solution methods and multilevel preconditioners for non-Newtonian fluids can be devised, if we can solve the following Stokes-type equation defined in Ω:

$$\rho^2\,\mathbf{u} - \kappa^2\Delta\mathbf{u} + \nabla p = \mathbf{g} \quad \text{and} \quad \nabla\cdot\mathbf{u} = 0, \tag{7.1}$$

where $\mathbf{g}$ is a function that depends on the conformation tensor from the constitutive equation of the underlying model. We note that ρ^2 and κ^2 in Eqn (7.1) are material-dependent parameters. (The uniformly stable finite elements with respect to the parameters ρ and κ were discussed in Section 6.)

7.1. Discrete Stokes-type system

The purpose of this section is to consider the fast solution techniques for such parameter-dependent problems as the Stokes-type equation given in (7.1). We begin by writing the discrete weak formulation of the Stokes-type equation (7.1) given as follows: find $(\mathbf{u}_h, p_h) \in \mathbf{V}_h \times W_h$ such that

$$\begin{cases} a_p(\mathbf{u}_h, \mathbf{v}_h) + b(\mathbf{v}_h, p_h) = \langle \mathbf{g}, \mathbf{v}_h\rangle & \forall \mathbf{v}_h \in \mathbf{V}_h \\ b(\mathbf{u}_h, q_h) = 0 & \forall q_h \in W_h, \end{cases} \tag{7.2}$$

where the bilinear forms are defined as

$$a_p(\mathbf{u}_h, \mathbf{v}_h) := \rho^2(\mathbf{u}_h, \mathbf{v}_h) + \kappa^2(\nabla\mathbf{u}_h : \nabla\mathbf{v}_h) \quad \text{and} \quad b(\mathbf{v}_h, p_h) := -\int_\Omega \nabla\cdot\mathbf{v}_h\, p_h\,\mathrm{d}x.$$

Throughout this section, for convenience of the presentation, we will consider the operator form of Eqn (7.2) given as follows:

$$\begin{pmatrix} \mathcal{A}_p & \mathcal{B}^* \\ \mathcal{B} & 0 \end{pmatrix} \begin{pmatrix} \mathbf{u}_h \\ p_h \end{pmatrix} = \begin{pmatrix} \mathbf{g} \\ 0 \end{pmatrix}, \tag{7.3}$$

where $\mathcal{A}_p = \rho^2 I - \kappa^2 \Delta_h$, $\mathcal{B} = -\nabla\cdot$, and $\mathcal{B}^* = \nabla_h$.

Our goal here is to discuss two types of iterative methods for solving the discrete version of Eqn (7.1): one is the augmented Lagrangian method, and the other is the preconditioned minimal residual (MinRes) method. For a comparison of the computational costs of solving techniques for Stokes-type systems, we refer to the recent work of Larin and Reusken [2008] and references therein; see Xu [2009, 2010] as well.

7.2. *Augmented Lagrangian method*

Augmented Lagrangian methods for Stokes problems have been introduced by Fortin and Glowinski in Fortin and Glowinski [1982] and Fortin and Glowinski [1983]. They have been further discussed in Glowinski and Le Tallec [1989] and Glowinski [2003]. In this section, we discuss the augmented Lagrangian Uzawa method that can be shown to be fast and robust with respect to parameters ρ, κ as well as the mesh size h.

We assume that the mixed finite elements employed here satisfy the uniform accuracy for the aforementioned Stokes-type equation (7.1). Namely, the pair of finite element spaces $\mathbf{V}_h$ and W_h for velocity fields and pressure satisfy the classical inf-sup conditions and the strong divergence-free condition, namely, $\nabla \cdot \mathbf{V}_h \subseteq W_h$ as discussed in Xie, Xu and Xue [2008]. For conforming finite elements, it is well known that the Scott–Vogelius elements Scott and Vogelius [1985a,b] enjoy the optimal approximation property for the problem (7.1). And it has recently been established that finite elements introduced by Austin, Manteuffel and McCormick [2004] have such a property as well Lee [2009]; see Example 6.1 and Example 6.2.

The Augmented Lagrangian iterative method for the operator form of Stokes-type equation (7.3) can be viewed as the Uzawa method for the following penalized problem:

$$\begin{pmatrix} \mathcal{A}_p + \mu^2 \mathcal{B}^* \mathcal{B} & \mathcal{B}^* \\ \mathcal{B} & 0 \end{pmatrix} \begin{pmatrix} \mathbf{u}_h \\ p_h \end{pmatrix} = \begin{pmatrix} \mathbf{g} \\ 0 \end{pmatrix}, \tag{7.4}$$

where $\mu^2 \geq 0$ is an arbitrary parameter. Note that due to the fact that the strong divergence-free condition holds for the finite element pair, the formulations (7.3) and (7.4) are equivalent. The optimal choice of damping parameter for the Uzawa method has been discussed by Nochetto and Pyo [2004].

An application of the Uzawa method with damping parameter μ^2 reads as follows: given $(\mathbf{u}_h^i, p_h^i)$, the new iterate $(\mathbf{u}_h^{i+1}, p_h^{i+1})$ is obtained by solving the following equations in an alternating way:

$$(\mathcal{A}_p + \mu^2 \mathcal{B}^* \mathcal{B}) \mathbf{u}_h^{i+1} = \mathbf{g} - B^* p_h^i \tag{7.5}$$

$$p_h^{i+1} = p_h^i + \mu^2 B \mathbf{u}_h^{i+1}. \tag{7.6}$$

The contraction factor of the Uzawa iterations (7.5) can be shown to be $O(\mu^{-2})$ when $\mu^2 \gg 1$ (Lee, Wu, Xu and Zikatanov [2007]). Therefore, if μ^2 is big enough, the Uzawa iteration converges very fast. However, as discussed in Lee, Wu and Chen [2009], the trade-off for achieving such a fast convergence is the inversion of a nearly singular operator $\mathcal{A}_p + \mu^2 \mathcal{B}^* \mathcal{B}$.

It should be noted here that while the construction of robust multilevel methods for the operator $\mathcal{A}_p + \mu^2 \mathcal{B}^* \mathcal{B}$ is well-known, theoretical analysis on this point is missing from the literature. In fact, Austin, Manteuffel and McCormick [2004] posed the theoretical justification of their numerical experiments on the multilevel method for the operator $\mathcal{A}_p + \mu^2 \mathcal{B}^* \mathcal{B}$ as an open problem. Recent papers by Lee [2009] and Lee, Wu and Chen [2009], however, have addressed this question. In this article, we will not attempt to reproduce this work. Instead, we focus on algorithmic details for the robust multigrid methods for the operator $\mathcal{A}_p + \mu^2 \mathcal{B}^* \mathcal{B}$ in terms of μ^2 as well as the mesh size, thereby introducing fast and robust solvers for Stokes-type equations.

We now present the robust multigrid algorithm for $\mathcal{A}_p + \mu^2 \mathcal{B}^* \mathcal{B}$ in an abstract framework. Let $\mathbf{V}$ be a real Hilbert space with the inner product $a(\cdot, \cdot)$ and the induced norm $\|\cdot\|_a = a(\cdot, \cdot)^{1/2}$. We begin by constructing *multilevel* finite element spaces on which our multigrid method is based. We assume that Ω has been triangulated by nested triangulations $\mathcal{T}_1 \subset \mathcal{T}_2 \subset \cdots \subset \mathcal{T}_L$, where $\mathcal{T}_L$ forms the finest triangulation of Ω. For each $1 \le l \le L$, we let $\{x_l^i\}_i$ be vertices of the triangulation $\mathcal{T}_l$ and denote $\mathcal{T}_l^i$ by the set of triangles in $\mathcal{T}_l$ meeting at the vertex x_l^i. We define the local patch as follows:

$$\Omega_l^i = \bigcup_{E \in \mathcal{T}_l^i} E. \tag{7.7}$$

These patches form an overlapping covering of Ω for each k. We then build the finite element spaces on Ω_l^i as follows:

$$\mathbf{V}_l^i = \{\mathbf{v}_l \in \mathbf{V}_l : \operatorname{supp}(\mathbf{v}_l) \subset \overline{\Omega}_l^i\}. \tag{7.8}$$

Correspondingly, we also define W_l^i, the subspace of W_l, which is supported on Ω_l^i. It is then clear that

$$\mathbf{V} = \sum_{l=1}^{L} \mathbf{V}_l = \sum_{l=1}^{L} \sum_{i=1}^{N_l} \mathbf{V}_l^i,$$

where N_l is the number of vertices for the triangulation $\mathcal{T}_l$.

We further introduce additional notation that the space $\boldsymbol{\mathcal{N}}_l^i$ for $1 \le l \le J$ and $1 \le i \le N_l$,

$$\begin{aligned} \boldsymbol{\mathcal{N}}_l^i &= \left\{\mathbf{u} \in \mathbf{V}_l^i : (\nabla \cdot \mathbf{u}, q) = 0, \quad \forall q \in \nabla \cdot \mathbf{V}_l^i\right\} \\ &= \left\{\mathbf{u} \in \mathbf{V}_l : (\nabla \cdot \mathbf{u}, \nabla \cdot \mathbf{v}) = 0, \quad \forall \mathbf{v} \in \mathbf{V}_l\right\}. \end{aligned}$$

The robust multigrid method will be constructed by the successive subspace correction (SSC) method with local exact solvers in each subspace $\mathbf{V}_l^i$. In this setting, it is easy to

demonstrate that the finite element spaces $\mathbf{V}_l$ and W_l generated based on the triangulations $\mathcal{T}_l$ are nested, especially for Scott–Vogelius finite elements and Austin–Mantueffel and McCormick finite elements, namely, we have

$$\mathbf{V}_1 \subset \cdots \mathbf{V}_l \subset \cdots \mathbf{V}_J, \quad \text{and} \quad W_1 \subset \cdots W_l \subset \cdots W_J. \tag{7.9}$$

Furthermore, in this setting, the following assumptions hold true:

$$\text{A1:} \quad \mathbf{V} = \sum_{l=1}^{L} \sum_{i=1}^{N_l} \mathbf{V}_l^i \quad \text{and} \quad \text{A2:} \quad \boldsymbol{\mathcal{N}} = \sum_{l=1}^{L} \sum_{i=1}^{N_l} \left(\mathbf{V}_l^i \cap \boldsymbol{\mathcal{N}}\right).$$

Under these assumptions, we can establish that the following subspace correction algorithm possesses the optimal convergence property; see Lee [2009] and Lee, Wu and Chen [2009].

Algorithm 2 Successive Subspace Correction Method

Give the initial guess $\mathbf{u}^0 \in \mathbf{V}$ and let $m = 0$.
while The residual is bigger than the given tolerance **do**
  $\mathbf{u}_0^m = \mathbf{u}^m$;
  for $l = 1, \ldots, L$ **do**
    for $i = 1, \ldots, N_l$ **do**
      Find $\mathbf{e}_i \in \mathbf{V}_l^i$, s.t. $a(\mathbf{e}_i, \mathbf{v}_i) = \mathbf{g}(\mathbf{v}_i) - a(\mathbf{u}_{i-1}^m, \mathbf{v}_i), \quad \forall \mathbf{v}_i \in \mathbf{V}_l^i$;
      $\mathbf{u}_i^m = \mathbf{u}_{i-1}^m + \mathbf{e}_i$;
    end for
  end for
  $\mathbf{u}^{m+1} = \mathbf{u}_L^m$;
  $m = m + 1$;
end while

7.3. Preconditioned MinRes method

In this section, we will introduce another algorithm; for this one, it is not necessary to assume the strong divergence-free condition. For instance, we can employ the well-known Taylor–Hood finite elements (Taylor and Hood [1973]) to approximate velocity/pressure fields. To solve the discrete saddle point problem, we can use the preconditioned minimal residual (MinRes) method by Paige and Saunders [1975]. Like the conjugate gradient method, the efficiency of MinRes depends heavily on the construction of preconditioners, which should be spectrally equivalent to the inverse of the original operator.

The time-dependent Stokes system has the coefficient matrix in the following form

$$\mathcal{A} = \begin{pmatrix} \mathcal{A}_p & \mathcal{B}^* \\ \mathcal{B} & 0 \end{pmatrix}. \tag{7.10}$$

For this system, we apply the MinRes method with the block diagonal preconditioners by Rusten and Winther [1992] and Bramble and Pasciak [1997], namely,

$$\mathcal{P} = \begin{pmatrix} \mathcal{P}_A & 0 \\ 0 & \mathcal{P}_S \end{pmatrix},$$

where $\mathcal{P}_L$ is a multigrid preconditioner for the Laplace-like matrix $\mathcal{A}_p$ and $\mathcal{P}_S$ is a preconditioner corresponding to the Schur complement. The matrix $\mathcal{A}_p$ has a block-diagonal form with each diagonal block corresponding to a scalar reaction-diffusion problem. And the Schur complement preconditioner can be chosen to be

$$\mathcal{P}_S = \max(\kappa^2, \rho^2 h^2) M^{-1} + \rho^2 (-\Delta_N)^{-1},$$

where M is the mass matrix for the pressure space and $-\Delta_N$ is the auxiliary Laplace operator with the Neumann boundary condition. This preconditioner is shown to be uniform with respect to ρ, κ, and h; see Bramble and Pasciak [1997] and Olshanskii, Peters and Reusken [2006]. Since fast solvers, like multigrid method (Bramble [1993], Brandt [1977], Hackbusch [1985]), for scalar reaction-diffusion problems are available (see Xu [2010]), we can solve the Stokes-type system efficiently.

8. Stability analysis and existence of discrete solutions

In this section, we show that our discretization schemes as discussed in Section 6 are stable. The stability will then be used to establish the existence of the discrete solutions in time evolution. For simplicity and clarity in presenting the main ideas of the proof, we only discuss the Oldroyd-B model:

$$\begin{cases} \mathrm{Re}\left(\frac{\partial \mathbf{u}}{\partial t} + \mathbf{u}\cdot\nabla\mathbf{u}\right) = \eta_s \Delta \mathbf{u} - \nabla p + \nabla\cdot\boldsymbol{c}, & \text{in } \Omega\times\mathbb{R}^+, \\ \nabla\cdot\mathbf{u} = 0, & \text{in } \Omega\times\mathbb{R}^+, \\ \alpha\boldsymbol{c} + \mathcal{L}_{\mathbf{u},\nabla\mathbf{u}}\boldsymbol{c} = \beta\boldsymbol{\delta}, & \text{in } \Omega\times\mathbb{R}^+, \\ \mathbf{u}(x,t) = 0, & \text{in } \partial\Omega\times\mathbb{R}^+, \\ \mathbf{u}(x,0) = \mathbf{u}_0(x), & \text{in } \Omega, \\ \boldsymbol{c}(x,0) = \boldsymbol{c}_0(x), & \text{in } \Omega, \end{cases} \tag{8.1}$$

with $\alpha = 1/\mathrm{Wi}$ and $\beta = \eta_p/\mathrm{Wi}^2$, in a polygonal domain $\Omega \subset \mathbb{R}^2$ here. The extension of these stability and convergence results to more general cases is straightforward.

8.1. *Stability analysis for discrete solutions*

We first consider the discrete analog of the continuous energy estimate in Theorem 4.1. We are not aiming to presenting the stability analysis for all the schemes introduced in Section 6; instead, we focus on a particular scheme and demonstrate unambiguously the critical role played in the analysis by the positivity of the conformation tensor and the volume preservation of flow maps.

Let us now start to investigate the discrete scheme in Algorithm 1: given the solution $(\mathbf{u}_h^n, p_h^n, \boldsymbol{c}_h^n) \in \mathbf{V}_h \times W_h \times \boldsymbol{S}_h$ from the previous time level, find $(\mathbf{u}_h^{n+1}, p_h^{n+1}, \boldsymbol{c}_h^{n+1}) \in \mathbf{V}_h \times W_h \times \boldsymbol{S}_h$ by the following relation equations:

$$\begin{aligned}
&\mathsf{Re}\Big(\frac{\mathbf{u}_h^{n+1} - \Pi_h^V\left(\mathbf{u}_h^n \circ \widetilde{y}^n\right)}{k}, \mathbf{v}_h\Big) - (p_h^{n+1}, \nabla \cdot \mathbf{u}_h) + \eta_s \left(\mathcal{D}(\mathbf{u}_h^{n+1}) : \mathcal{D}(\mathbf{v}_h)\right) \\
&\quad = -\left(\boldsymbol{c}_h^{n+1} : \mathcal{D}(\mathbf{v}_h)\right) \qquad (8.2)\\
&(\nabla \cdot \mathbf{u}_h^{n+1}, q_h) = 0 \qquad (8.3)\\
&(1 + k\alpha)\left(\boldsymbol{c}_h^{n+1} : \boldsymbol{\sigma}_h\right) = \left(\widetilde{\boldsymbol{F}}_h^{n+1} \Pi_h^S(\boldsymbol{c}_h^n \circ \widetilde{y}^n)(\widetilde{\boldsymbol{F}}_h^{n+1})^T : \boldsymbol{\sigma}_h\right) + k\beta\left(\boldsymbol{\delta} : \boldsymbol{\sigma}_h\right), \qquad (8.4)
\end{aligned}$$

for all $(\mathbf{v}_h, q_h, \boldsymbol{\sigma}_h) \in \mathbf{V}_h \times W_h \times \boldsymbol{S}_h$.

Here, $\widetilde{\boldsymbol{F}}_h^{n+1} = \left(\boldsymbol{\delta} - k\Pi_h^S(\nabla \mathbf{u}_h^{n+1})\right)^{-1}$ is an approximation to the deformation tensor $\boldsymbol{F}$; see Section 6.3 for more details. And we use the interpolation operator $\Pi_h^S : L^2(\Omega) \mapsto L^2(\Omega)$ introduced in Section 6.1, i.e.,

$$\Pi_h^S(\boldsymbol{\sigma}) = \left(\Pi_h(\sigma_{i,j})\right)_{i,j=1,\ldots,d} \quad \text{with} \quad \Pi_h(g) := \sum_{E \in \mathcal{T}_h} \left(\frac{1}{|E|}\int_E g\,\mathrm{d}x\right)\phi_E(\cdot), \qquad (8.5)$$

where $\mathcal{T}_h = \{E\}$ is a quasi-uniform triangular partition of the physical domain Ω with characteristic mesh size h, and ϕ_E is a characteristic function that is one on $\overline{E}$ and zero elsewhere.

As discussed in Section 6.2.2, we assume that the pair of spaces $\mathbf{V}_h$ and W_h satisfy the inf-sup condition as well as

$$\nabla \cdot \mathbf{u}_h \in W_h \qquad \forall\, \mathbf{u}_h \in \mathbf{V}_h. \qquad (8.6)$$

The property (8.6) is crucial to constructing the volume-preserving flow map in both two- and three-dimensional domains as discussed in Feng and Shang [1995].

The flow map $\phi_{t,s} : \Omega \mapsto \Omega$ can be obtained so that the approximate flow map $\widetilde{y}$ satisfies the following identity:

$$\int_\Omega g \circ \widetilde{y}\,\mathrm{d}x = \int_\Omega g\,\mathrm{d}x \qquad \forall\, g \in L^1(\Omega). \qquad (8.7)$$

And (8.7) is the key to deriving uniform energy estimates for the solution to the discrete model equations (8.2)–(8.4). Recall that the discrete scheme (6.4) preserves volume in $\mathbb{R}^2$. We can easily show that this scheme satisfies (8.7) by simple change of variables.

Now, we are ready to present the discrete analog of the energy estimate.

Theorem 8.1 (Discrete Energy Estimate). *The discrete solution to (8.2)–(8.4) admits the following estimate: if* $\mathsf{Wi} < \infty$ *and* $n \geq 1$, *then*

$$\mathsf{Re}\|\mathbf{u}_h^n\|_0^2 + \|\boldsymbol{c}_h^n\|_{L^1} \leq c_1 \mathrm{e}^{-\mathsf{C}_1 t^n}\left(\mathsf{Re}\|\mathbf{u}_h^0\|_0^2 + \|\boldsymbol{c}_h^0\|_{L^1}\right) + c_2, \qquad (8.8)$$

$$2\eta_s \sum_{\ell=1}^{n} k\|\mathcal{D}(\mathbf{u}_h^\ell)\|_0^2 \leq \mathsf{Re}\,\|\mathbf{u}_h^0\|_0^2 + \|\boldsymbol{c}_h^0\|_{L^1} + c_2 t^n. \qquad (8.9)$$

Here, c_1 *and* c_2 *are generic constants.*

PROOF. From (8.4), we have the following relation:

$$(1+k\alpha)\,\boldsymbol{c}_h^{n+1} = \left(\boldsymbol{\delta} - k\Pi_h^S(\nabla \mathbf{u}_h^{n+1})\right)^{-1} \Pi_h^S(\boldsymbol{c}_h^n \circ \widetilde{\mathcal{Y}}^n) \left(\boldsymbol{\delta} - k\Pi_h^S(\nabla \mathbf{u}_h^{n+1})\right)^{-T} + k\beta\boldsymbol{\delta}. \tag{8.10}$$

We first multiply $\boldsymbol{\delta} - k\Pi_h^S(\nabla \mathbf{u}_h^{n+1})$ to the left and $\boldsymbol{\delta} - k\Pi_h^S(\nabla \mathbf{u}_h^{n+1})^T$ to the right of Eqn (8.10) to obtain that

$$\begin{aligned}(1+k\alpha)&\left(\boldsymbol{\delta} - k\Pi_h^S(\nabla \mathbf{u}_h^{n+1})\right)\boldsymbol{c}_h^{n+1}\left(\boldsymbol{\delta} - k\Pi_h^S(\nabla \mathbf{u}_h^{n+1})\right)^T \\ &= \Pi_h^S(\boldsymbol{c}_h^n \circ \widetilde{\mathcal{Y}}^n) + k\beta\left(\boldsymbol{\delta} - k\Pi_h^S(\nabla \mathbf{u}_h^{n+1})\right)\left(\boldsymbol{\delta} - k\Pi_h^S(\nabla \mathbf{u}_h^{n+1})\right)^T.\end{aligned} \tag{8.11}$$

Hence, by taking trace and then integration on both sides of the equation above, we get that

$$\begin{aligned}k(1+k\alpha)&\int_\Omega \operatorname{tr}\left(\Pi_h^S(\nabla \mathbf{u}_h^{n+1})\boldsymbol{c}_h^{n+1} + \boldsymbol{c}_h^{n+1}\Pi_h^S(\nabla \mathbf{u}_h^{n+1})^T\right)\mathrm{d}x \\ &= (1+k\alpha)\,\|\boldsymbol{c}_h^{n+1}\|_{L^1} - \|\boldsymbol{c}_h^n \circ \widetilde{\mathcal{Y}}^n\|_{L^1} - \mathrm{d}\beta|\Omega|k \\ &\quad + k^2\beta\int_\Omega \operatorname{tr}\left(\Pi_h^S(\nabla \mathbf{u}_h^{n+1}) + \Pi_h^S(\nabla \mathbf{u}_h^{n+1})^T\right)\mathrm{d}x \\ &\quad + k^2(1+k\alpha)\int_\Omega \operatorname{tr}\left(\Pi_h^S(\nabla \mathbf{u}_h^{n+1})\left(\boldsymbol{c}_h^{n+1} - \frac{k\beta}{1+k\alpha}\boldsymbol{\delta}\right)\Pi_h^S(\nabla \mathbf{u}_h^{n+1})^T\right)\mathrm{d}x.\end{aligned} \tag{8.12}$$

We note that from (8.10), the approximate conformation tensor $\boldsymbol{c}_h^{n+1}$ satisfies

$$(1+k\alpha)\boldsymbol{c}_h^{n+1} - k\beta\boldsymbol{\delta} \geq 0 \qquad \forall\, n \geq 1, \tag{8.13}$$

if the initial condition $\boldsymbol{c}_h^0 \geq 0$. Since $\boldsymbol{c}_h^{n+1}$ is symmetric, by Lemma 6.4 and the discrete divergence-free condition, we can easily see that

$$\begin{aligned}&\int_\Omega \operatorname{tr}\left(\Pi_h^S(\nabla \mathbf{u}_h^{n+1}) + \Pi_h^S(\nabla \mathbf{u}_h^{n+1})^T\right)\mathrm{d}x \\ &\quad = \int_\Omega \operatorname{tr}\left(\nabla \mathbf{u}_h^{n+1} + (\nabla \mathbf{u}_h^{n+1})^T\right)\mathrm{d}x = 2\int_\Omega \nabla\cdot\mathbf{u}_h^{n+1}\mathrm{d}x = 0\end{aligned} \tag{8.14}$$

and

$$\begin{aligned}\int_\Omega \operatorname{tr}\left(\Pi_h^S(\nabla \mathbf{u}_h^{n+1})\boldsymbol{c}_h^{n+1}\right)\mathrm{d}x &= \int_\Omega \operatorname{tr}\left(\boldsymbol{c}_h^{n+1}\Pi_h^S(\nabla \mathbf{u}_h^{n+1})^T\right)\mathrm{d}x \\ &= \left(\boldsymbol{c}_h^{n+1} : \Pi_h^S(\mathcal{D}(\mathbf{u}_h^{n+1}))\right) = \left(\boldsymbol{c}_h^{n+1} : \mathcal{D}(\mathbf{u}_h^{n+1})\right).\end{aligned} \tag{8.15}$$

Finally, based on the volume-preserving property of $\widetilde{y}^n$, we have $\|\boldsymbol{c}_h^n \circ \widetilde{y}^n\|_{L^1} = \|\boldsymbol{c}_h^n\|_{L^1}$. Taking the facts (8.13), (8.14), and (8.15) into account, we can derive the following inequality from (8.12):

$$\left(\boldsymbol{c}_h^{n+1} : \mathcal{D}(\mathbf{u}_h^{n+1})\right) \geq \frac{1}{2k}\|\boldsymbol{c}_h^{n+1}\|_{L^1} - \frac{1}{2k(1+k\alpha)}\|\boldsymbol{c}_h^n\|_{L^1} - \frac{\mathrm{d}\beta|\Omega|}{2(1+k\alpha)}. \tag{8.16}$$

We now consider the momentum equation (8.2). Using the energy method, together with the discrete divergence-free condition and (8.16), we can obtain

$$\begin{aligned}
&\frac{\mathsf{Re}}{k}\|\mathbf{u}_h^{n+1}\|_0^2 + \eta_s\|\mathcal{D}(\mathbf{u}_h^{n+1})\|_0^2 \\
&\quad= \frac{\mathsf{Re}}{k}\left(\Pi_h^V(\mathbf{u}_h^n \circ \widetilde{y}^n), \mathbf{u}_h^{n+1}\right) - \left(\boldsymbol{c}_h^{n+1} : \mathcal{D}(\mathbf{u}_h^{n+1})\right) \\
&\quad\leq \frac{\mathsf{Re}}{k}\left(\mathbf{u}_h^n \circ \widetilde{y}^n, \mathbf{u}_h^{n+1}\right) - \frac{1}{2k}\|\boldsymbol{c}_h^{n+1}\|_{L^1} + \frac{1}{2k(1+k\alpha)}\|\boldsymbol{c}_h^n\|_{L^1} + \frac{\mathrm{d}\beta|\Omega|}{2(1+k\alpha)}.
\end{aligned} \tag{8.17}$$

Applying the Cauchy–Schwarz inequality and the standard kick-back argument, we obtain the following relation:

$$\begin{aligned}
&\frac{\mathsf{Re}}{2k}\|\mathbf{u}_h^{n+1}\|_0^2 + \eta_s\|\mathcal{D}(\mathbf{u}_h^{n+1})\|_0^2 + \frac{1}{2k}\|\boldsymbol{c}_h^{n+1}\|_{L^1} \\
&\quad\leq \frac{\mathsf{Re}}{2k}\|\mathbf{u}_h^n\|_0^2 + \frac{1}{2k(1+k\alpha)}\|\boldsymbol{c}_h^n\|_{L^1} + \frac{\mathrm{d}\beta|\Omega|}{2(1+k\alpha)}.
\end{aligned} \tag{8.18}$$

We are now in the position to show the first estimate (8.8). Multiplying $2k$ to both sides of (8.18) and using Korn's inequality, we obtain that

$$\begin{aligned}
\kappa\|\mathbf{u}_h^{n+1}\|_0^2 + \|\boldsymbol{c}_h^{n+1}\|_{L^1} &\leq \mathsf{Re}\|\mathbf{u}_h^n\|_0^2 + \frac{1}{1+k\alpha}\|\boldsymbol{c}_h^n\|_{L^1} + \frac{k\mathrm{d}\beta|\Omega|}{1+k\alpha} \\
&\leq \exp\left(-\mathsf{C}_1 k\right)\left(\kappa\|\mathbf{u}_h^n\|_0^2 + \|\boldsymbol{c}_h^n\|_{L^1}\right) + \frac{k\mathrm{d}\beta|\Omega|}{1+k\alpha},
\end{aligned} \tag{8.19}$$

where $\kappa = \mathsf{Re} + 2k\eta_s\mathsf{C}_\Omega$ and C_Ω is a positive constant depending only on Ω. Here, $\mathsf{C}_1 > 0$ is chosen to be a constant such that

$$\max\left(\frac{\mathsf{Re}}{\mathsf{Re} + 2k\eta_s\mathsf{C}_\Omega}, \frac{1}{1+k\alpha}\right) \leq \exp\left(-\mathsf{C}_1 k\right), \quad 0 \leq k \leq 1. \tag{8.20}$$

Now, we use the induction argument to obtain:

$$\begin{aligned}
\kappa\|\mathbf{u}_h^n\|_0^2 + \|\boldsymbol{c}_h^n\|_{L^1} &\leq \exp(-\mathsf{C}_1 t^n)\left(\kappa\|\mathbf{u}_h^0\|_0^2 + \|\boldsymbol{c}_h^0\|_{L^1}\right) + \frac{k\mathrm{d}\beta|\Omega|}{1+k\alpha}\sum_{l=0}^{n}\exp(-\mathsf{C}_1 t^l) \\
&\leq \exp(-\mathsf{C}_1 t^n)\left(\kappa\|\mathbf{u}_h^0\|_0^2 + \|\boldsymbol{c}_h^0\|_{L^1}\right) + \mathsf{C}_2^n,
\end{aligned} \tag{8.21}$$

where

$$\mathsf{C}_2^n = k\mathrm{d}\beta|\Omega|\frac{1-\exp(-\mathsf{C}_1 t^n)}{1-\exp(-\mathsf{C}_1 k)}. \tag{8.22}$$

It is clear that we can choose generic constants c_1 and c_2 such that

$$\kappa\|\mathbf{u}_h^0\|_0^2 + \|\boldsymbol{c}_h^0\|_{L^1} \le c_1\left(\mathsf{Re}\|\mathbf{u}_h^0\|^2 + \|\boldsymbol{c}_h^0\|_{L^1}\right) \quad \text{and} \quad \mathsf{C}_2^n \le c_2. \tag{8.23}$$

We then obtain the desired result (8.8).

We now drive the other estimate (8.9). First, we multiply $2k$ to both sides of (8.18) and take summation for $l = 1, 2, \ldots, n$ for both sides to obtain:

$$\begin{aligned} 2\eta_s \sum_{l=1}^{n} k\|\mathcal{D}(\mathbf{u}_h^l)\|_0^2 &\le c_1\left(\mathsf{Re}\|\mathbf{u}_h^0\|_0^2 + \|\boldsymbol{c}_h^0\|_{L^1}\right) + \sum_{l=1}^{n} k\mathrm{d}\beta|\Omega|, \\ &\le c_1\left(\mathsf{Re}\|\mathbf{u}_h^0\|_0^2 + \|\boldsymbol{c}_h^0\|_{L^1}\right) + c_2 t^n. \end{aligned}$$

This completes the proof. □

We will now consider the limiting case in which $\mathsf{Wi} = \infty$; in this case, $\alpha = \beta = 0$.

COROLLARY 8.1. *Assume that* $\mathsf{Wi} = \infty$ *and* $\alpha = \beta = 0$. *Then, the following estimates hold true for any* $n \ge 1$*:*

$$\mathsf{Re}\|\mathbf{u}_h^n\|_0^2 + \|\boldsymbol{c}_h^n\|_{L^1} \le \mathsf{Re}\|\mathbf{u}_h^0\|_0^2 + \|\boldsymbol{c}_h^0\|_{L^1} \tag{8.24}$$

and

$$\eta_s \sum_{l=0}^{n} k\|\mathcal{D}(\mathbf{u}_h^l)\|_0^2 \le \mathsf{Re}\|\mathbf{u}_h^0\|_0^2 + \|\boldsymbol{c}_h^0\|_{L^1}. \tag{8.25}$$

PROOF. Note that in the limiting case, $\alpha = \beta = 0$ and $\boldsymbol{c}_h^n$ is itself a conformation tensor for $n \ge 0$. The result then immediately follows from two estimates (8.8) and (8.9) since $\mathsf{C}_1 = 0$ and $\mathsf{C}_2^n = 0$ for all $n \ge 0$. This completes the proof. □

REMARK 8.1 (Effects of Load). When there is a nonzero external force term $\boldsymbol{f}$ on the right-hand side of the momentum equation (8.2), it can be shown that the energy estimates in Theorem 8.1 are still valid as long as $\eta_s > 0$. In this case, the L^2 norm of $\boldsymbol{f}$ will enter into the constant c_2 in the inequality (8.8).

8.2. *Existence of the discrete solutions*

The discrete model equations (8.2)–(8.4) are fully nonlinear, and the well posedness of this model is not trivial. The main purpose of this section is to prove the existence of the discrete solution. We will show that the solution to the discrete problem exists for sufficiently small time step size k; furthermore, the discrete solution is unique. These will, in turn, confirm that the discrete problem, (8.2)–(8.4), is well defined. Theoretically, the restriction of k is only given by the mesh size h.

Let tol be the tolerance for the nonlinear iteration. We assume that $\mathbf{u}_h^n$, p_h^n, and $\boldsymbol{c}_h^n$ at the time level t^n are available. Then, we have the following algorithm for time marching:

The Algorithm 3 is a single-step time-marching algorithm. Once the initial condition $(\mathbf{u}_h^0, p_h^0, \boldsymbol{c}_h^0)$ is given, we can proceed to the evolution process. Note that the presence of $\boldsymbol{f}$ on the right-hand side of the Stokes-type equation is due to the Dirichlet boundary condition.

ALGORITHM 3 Nonlinear Iteration

Step 0: Given $\mathbf{u}_h^n$, p_h^n, and $\boldsymbol{c}_h^n$. Set

$$\mathbf{u}_h^{n,0} := \mathbf{u}_h^n, \quad p_h^{n,0} := p_h^n, \quad \text{and} \quad \boldsymbol{c}_h^{n,0} := \boldsymbol{c}_h^n.$$

Step 1: For any particle x, compute the departure feet

$$\widetilde{y}^n = x - k\,\mathbf{u}_h^{n,0}\Big(\frac{\widetilde{y}^n + x}{2}\Big).$$

Step 2: For $\ell = 0, 1, 2, \ldots$, do

(1) Solve the Stokes-type system

$$\begin{cases} \mathrm{Re}\,\mathbf{u}_h^{n,\ell+1} - k\Delta_h \mathbf{u}_h^{n,\ell+1} + k\nabla_h p_h^{n,\ell+1} \\ \qquad = \mathrm{Re}\,\Pi_h^V(\mathbf{u}_h^{n,0} \circ \widetilde{y}^n) + k\nabla_h \cdot \boldsymbol{c}_h^{n,\ell} + k\boldsymbol{f}, \\ \nabla \cdot \mathbf{u}_h^{n,\ell+1} = 0. \end{cases}$$

(2) Update the conformation tensor

$$(1 + k\alpha)\boldsymbol{c}_h^{n,\ell+1} = \boldsymbol{F}_h^{n,\ell+1}\Pi_h^S(\boldsymbol{c}_h^{n,0} \circ \widetilde{y}^n)(\boldsymbol{F}_h^{n,\ell+1})^T + k\beta\boldsymbol{\delta},$$

where $\boldsymbol{F}_h^{n,\ell+1} := \big(\boldsymbol{\delta} - k\Pi_h^S(\nabla \mathbf{u}_h^{n,\ell+1})\big)^{-1}$.

(3) If $\|\mathbf{u}_h^{n,\ell+1} - \mathbf{u}_h^{n,\ell}\|_1 \le \mathsf{tol}$ and $\|p_h^{n,\ell+1} - p_h^{n,\ell}\|_0 \le \mathsf{tol}$, then break.

Step 3: Update solution: $\mathbf{u}_h^{n+1} := \mathbf{u}_h^{n,\ell+1}$, $p_h^{n+1} := p_h^{n,\ell+1}$, and $\boldsymbol{c}_h^{n+1} := \boldsymbol{c}_h^{n,\ell+1}$.

REMARK 8.2 (Solving the Flow Map Equations). From the energy estimate (8.9), we know that $\|\mathbf{u}_h^n\|_1$ is bounded. Hence, if the time step size k is small enough, the nonlinear equation for the flow map in Step 1 of Algorithm 3 is solvable by the inverse function theorem. We will discuss iterative methods for solving the flow map equation in Section 9.

REMARK 8.3 (Feet Searching). We remark that one of the key ingredients for the Eulerian–Lagrangian method here used to solve the Riccati form of the constitutive equation is to find the function values at the departure feet, $\mathbf{u}_h^{n,0} \circ \widetilde{y}^n$ and $\boldsymbol{c}_h^{n,0} \circ \widetilde{y}^n$, as quickly and accurately as possible. In Algorithm 3, we did not provide referents for the points x. It can have different meanings in different discretization methods. But, of course, it is not practical to trace back through all points. We will explain the implementation details in Section 9.2.1. Usually, for the finite difference method, x is any grid point; for the finite element method, x is any quadrature point.

REMARK 8.4 (Parallel Computing for Solving Ricatti Equations). We note that the constitutive equations can be solved in a fully parallel way. This is because all the coefficients are defined locally by a $d \times d$ matrix equation in each of the nodes, all of which are completely independent.

The main goal in this section is to show that the Algorithm 3 is convergent in each time step under certain conditions on the time step size k. This has been discussed by Lee, Xu and Zhang [To appear]. Before introducing the main existence result, we would like to make a few comments:

(1) The discrete model, (8.2)–(8.4), is a highly coupled nonlinear system of equations. Therefore, we need to apply certain iterative methods that lead to the solution implicitly given in order to satisfy the discrete models. There are many such nonlinear iterative schemes, and we focus on one of them in Algorithm 3. Moreover, extending the existence proof to other methods is possible.
(2) This result can be achieved from the uniform stability estimate established in the previous section. In addition, we note that the notion we used here as the well posedness for the solution to the discrete models (8.2)–(8.4) should be distinguished from the one introduced by Kreiss [2001]. In particular, our result does not necessarily imply stability with respect to the perturbation of the data.
(3) Our analysis fully exploits the finite dimensionality of the solution space; therefore, technically, it will be difficult to extend this analysis to the existence analysis for the continuous level.

Our proof is based on the induction argument. Specially, we will assume that at time level t^n, the discrete solutions $\mathbf{u}_h^n$ and $\boldsymbol{c}_h^n$ are well defined and generate a sequence of iterates according to Algorithm 3 and show that the nonlinear iteration converges and defines $\mathbf{u}_h^{n+1}$ and $\boldsymbol{c}_h^{n+1}$. More precisely, we will show that the solutions at the time level t^{n+1} can be obtained uniquely by the Algorithm 3. We note that if $\mathbf{u}_h^n$ and $\boldsymbol{c}_h^n$ at the time level t^n satisfy the uniform bounds

$$\|\mathbf{u}_h^n\|_0 \lesssim 1 \quad \text{and} \quad \|\boldsymbol{c}_h^n\|_{L^1} \lesssim 1, \tag{8.26}$$

the fixed-point iteration (Algorithm 3) converges. We, therefore, conclude our proof by a simple recursive argument.

Remark 8.5 (Inverse Inequalities). We recall the well-known inverse inequalities (cf. Brenner and Scott [2002, chapter 4]) that

$$\|\mathbf{v}\|_\infty \lesssim h^{-1}\|\mathbf{v}\|_0 \quad \text{and} \quad \|\nabla \mathbf{v}\|_0 \lesssim h^{-1}\|\mathbf{v}\|_0, \qquad \forall\, \mathbf{v} \in \mathbf{V}_h. \tag{8.27}$$

Let us first establish that the sequence generated from Algorithm 3 is bounded uniformly.

Lemma 8.1 (Uniform Boundedness). *Suppose that $\boldsymbol{f} \in \left(L^2(\Omega)\right)^2$ For sufficiently small k, the sequence generated by Algorithm 3 is uniformly bounded in L^2 norm for the velocity and L^1 norm for the stress field, respectively.*

Proof. Using the strong divergence-free finite elements as in Section 6, we have $\nabla \cdot \mathbf{u}_h^{n,\ell} = 0$, for $\ell = 0, 1, 2, \ldots,$ By Lemma 6.1, it holds that $\det(\nabla \widehat{y}^n) = 1$. Employing the energy

method and the inverse inequality (8.27), we derive that

$$\begin{aligned}\mathrm{Re}\,\|\mathbf{u}_h^{n,\ell+1}\|_0^2 + k\|\nabla\mathbf{u}_h^{n,\ell+1}\|_0^2 \le{}& \frac{\mathrm{Re}}{2}\|\mathbf{u}_h^{n,0}\|_0^2 + \frac{\mathrm{Re}}{2}\|\mathbf{u}_h^{n,\ell+1}\|_0^2 + k\|\boldsymbol{f}\|_0\|\mathbf{u}_h^{n,\ell+1}\|_0\\ &+ k\|\boldsymbol{c}_h^{n,\ell}\|_{L^1}\|\nabla\mathbf{u}_h^{n,\ell+1}\|_\infty.\end{aligned}$$

Therefore, using the Cauchy–Schwarz inequality, we obtain

$$\begin{aligned}\mathrm{Re}\,\|\mathbf{u}_h^{n,\ell+1}\|_0^2 + k\|\nabla\mathbf{u}_h^{n,\ell+1}\|_0^2 \le{}& \frac{\mathrm{Re}}{2}\|\mathbf{u}_h^{n,0}\|_0^2 + \frac{\mathrm{Re}}{2}\|\mathbf{u}_h^{n,\ell+1}\|_0^2\\ &+ k\Big(\frac{\nu^{-2}}{2}\|\boldsymbol{f}\|_0^2 + \frac{\nu^2}{2}\|\mathbf{u}_h^{n,\ell+1}\|_0^2\Big) + k\Big(\frac{C_1h^{-2}}{2}\|\boldsymbol{c}_h^{n,\ell}\|_{L^1}^2 + \frac{1}{2}\|\nabla\mathbf{u}_h^{n,\ell+1}\|_0^2\Big),\end{aligned}$$

where ν is chosen such that $|\mathbf{u}_h^{n,\ell+1}|_1^2 \ge \nu^2\|\mathbf{u}_h^{n,\ell+1}\|_0^2$. We can then get, for all $\ell = 0, 1, 2, \ldots$, that

$$\mathrm{Re}\,\|\mathbf{u}_h^{n,\ell+1}\|_0^2 \le \mathrm{Re}\,\|\mathbf{u}_h^{n,0}\|_0^2 + C_1kh^{-2}\|\boldsymbol{c}_h^{n,\ell}\|_{L^1}^2 + C_0k\|\boldsymbol{f}\|_0^2, \tag{8.28}$$

where C_0 and C_1 are generic constants independent of k and h. Without loss of generality, we can assume that both C_0 and C_1 are greater than 1.

The equation (3) in Step 1 for updating the conformation tensor reveals the following inequality

$$\|\boldsymbol{c}_h^{n,\ell+1}\|_{L^1} \le \|\boldsymbol{F}_h^{n,\ell+1}\|_\infty^2\|\boldsymbol{c}_h^{n,0}\|_{L^1} + d|\Omega|\beta k. \tag{8.29}$$

Combining the last two inequalities, (8.28) and (8.29), we obtain

$$\begin{aligned}\mathrm{Re}\,\|\mathbf{u}_h^{n,\ell+1}\|_0^2 \le{}& \mathrm{Re}\,\|\mathbf{u}_h^{n,0}\|_0^2 + 2C_1kh^{-2}\|\boldsymbol{F}_h^{n,\ell}\|_\infty^4\|\boldsymbol{c}_h^{n,0}\|_{L^1}^2\\ &+ C_0k\|\boldsymbol{f}\|_0^2 + 2C_1d^2|\Omega|^2\beta^2k^2.\end{aligned} \tag{8.30}$$

Now, we define

$$\overline{C} := \big(\mathrm{Re}\,\|\mathbf{u}_h^{n,0}\|_0^2 + 4C_1\|\boldsymbol{c}_h^{n,0}\|_{L^1}^2 + C_0\|\boldsymbol{f}\|_0^2 + 2C_1d^2|\Omega|^2\beta^2\big)^{\frac{1}{2}}.$$

And we will show that, if k is small enough, $\overline{C}$ is a uniform upper bound for $\|\mathbf{u}_h^{n,\ell}\|_0$ and $\|\boldsymbol{c}_h^{n,\ell}\|_{L^1}$. This is apparently true for $\ell = 0$. Now, suppose that this is also true for ℓ, and we can now prove that it is true for $\ell+1$ with a fixed time step size k.

Using the inequality (6.33) and the inverse inequality, we have

$$\|\Pi_h^S(\nabla\mathbf{u}_h^{n,\ell})\|_\infty \le h^{-1}\|\nabla\mathbf{u}_h^{n,\ell}\|_0 \le C_2h^{-2}\|\mathbf{u}_h^{n,\ell}\|_0 \le \overline{C}C_2h^{-2}.$$

Hence, we can choose $2\overline{C}C_2k \le h^2$, which implies that $\boldsymbol{\delta} - k\Pi_h^S(\nabla\mathbf{u}_h^{n,\ell})$ is invertible and that $\boldsymbol{F}_h^{n,\ell}$ is well defined. Furthermore, we also have that

$$\|\boldsymbol{F}_h^{n,\ell}\|_\infty \le \frac{1}{1 - kh^{-1}\|\nabla\mathbf{u}_h^{n,\ell}\|_0} \le \frac{1}{1 - \overline{C}C_2kh^{-2}} \le 2.$$

Plugging the inequality above to (8.30), we obtain

$$\mathrm{Re}\,\|\mathbf{u}_h^{n,\ell+1}\|_0^2 \le \mathrm{Re}\,\|\mathbf{u}_h^{n,0}\|_0^2 + 32C_1 kh^{-2}\|\boldsymbol{c}_h^{n,0}\|_{L^1}^2 + C_0 k\|\boldsymbol{f}\|_0^2 + 2C_1 d^2|\Omega|^2\beta^2 k^2 \le \overline{C}^2,$$

if $k \le \min(1, h^2/8)$. And then (8.29) immediately gives that $\|\boldsymbol{c}_h^{n,\ell+1}\|_{L^1}$ is bounded uniformly, which completes the proof. □

Remark 8.6 (Condition on Time Step Size). From the proof, we can see that there is an upper bound for the time step size:

$$k \le \min\left(1, \frac{h^2}{8}, \frac{h^2}{2\overline{C}C_2}\right),$$

which depends on neither nonlinear iteration step ℓ nor time level n. Furthermore, this still holds for the infinite Weissenberg number case where $\alpha = \beta = 0$.

We would like to remark that the Lemma 8.1 also shows that the discrete conformation tensor given by Algorithm 3 is always symmetric and positive definite.

Theorem 8.2 (Positivity of the Discrete Conformation Tensor). *If the initial condition $\boldsymbol{c}_h^0$ is symmetric positive definite and the time step size k is small enough, then the discrete conformation tensor $\boldsymbol{c}_h^n$ is always symmetric positive definite for all $n = 1, 2, 3, \ldots,$*

Proof. It is trivial to the symmetry is kept for all n. We only need to check the positivity here. From the proof of Theorem 8.1, we have seen that if k is small enough, $\boldsymbol{F}_h^{n,\ell}$ is well defined. Since Π_h^S is a positivity preserving interpolation and $\beta > 0$, we can obtain that $\boldsymbol{c}_h^{n,\ell}$ is positive definite by induction. As this is true for all ℓ and n, it completes the proof. □

We are now ready to show the existence of the solution from the compactness argument. We will show that the sequence converges to a unique limit and conclude our main result in this section. To begin with, it is helpful to notice that for any invertible matrices $\boldsymbol{A}$ and $\boldsymbol{B}$, we have that

$$\boldsymbol{A}^{-1} - \boldsymbol{B}^{-1} = \boldsymbol{A}^{-1}(\boldsymbol{B} - \boldsymbol{A})\boldsymbol{B}^{-1}. \tag{8.31}$$

We arrive at the main result for this section as below.

Theorem 8.3 (Convergence of Algorithm 3). *The nonlinear iteration in Algorithm 3 converges if k small enough.*

Proof. For ease of our presentation, we define

$$\boldsymbol{e}_{\mathbf{u}}^{\ell+1} := \mathbf{u}_h^{n,\ell+1} - \mathbf{u}_h^{n,\ell} \quad \text{and} \quad \boldsymbol{e}_{\boldsymbol{c}}^{\ell+1} := \boldsymbol{c}_h^{n,\ell+1} - \boldsymbol{c}_h^{n,\ell}.$$

By subtracting the momentum equation for $\mathbf{u}_h^{n,\ell+1}$ from the equation for $\mathbf{u}_h^{n,\ell}$ in Algorithm 3 and taking integration by parts, we obtain that

$$\mathrm{Re}\,\|\boldsymbol{e}_{\mathbf{u}}^{\ell+1}\|_0^2 + k\|\nabla\boldsymbol{e}_{\mathbf{u}}^{\ell+1}\|_0^2 \le k\|\nabla\boldsymbol{e}_{\mathbf{u}}^{\ell+1}\|_\infty\|\boldsymbol{e}_{\boldsymbol{c}}^{\ell}\|_{L^1}.$$

Therefore, by the inverse inequality (8.27) and the Cauchy–Schwarz inequality, we conclude that

$$\mathrm{Re}\,\|\boldsymbol{e}_{\mathbf{u}}^{\ell+1}\|_0^2 \le C_3 k h^{-2} \|\boldsymbol{e}_{\boldsymbol{c}}^{\ell}\|_{L^1}^2, \quad \forall \ell = 0, 1, 2, \ldots. \tag{8.32}$$

By subtracting the constitutive equations for $\boldsymbol{c}_h^{n,\ell+1}$ and $\boldsymbol{c}_h^{n,\ell}$, we obtain the following inequality:

$$\|\boldsymbol{e}_{\boldsymbol{c}}^{\ell+1}\|_{L^1} \le \|\boldsymbol{F}_h^{n,\ell+1}\Pi_h^S(\boldsymbol{c}_h^{n,0}\circ\widetilde{\mathrm{y}}^n)(\boldsymbol{F}_h^{n,\ell+1})^T - \boldsymbol{F}_h^{n,\ell}\Pi_h^S(\boldsymbol{c}_h^{n,0}\circ\widetilde{\mathrm{y}}^n)(\boldsymbol{F}_h^{n,\ell})^T\|_{L^1}.$$

In the proof of Lemma 8.1, we have seen that $\boldsymbol{F}_h^{n,\ell}$ is well defined and also that the $\|\boldsymbol{F}_h^{n,\ell}\|_0 \le 2$ for $\ell = 0, 1, 2, \ldots$.

Therefore, we have

$$\begin{aligned}\|\boldsymbol{e}_{\boldsymbol{c}}^{\ell+1}\|_{L^1} \le{}& \|\boldsymbol{F}_h^{n,\ell+1}\Pi_h^S(\boldsymbol{c}_h^{n,0}\circ\widetilde{\mathrm{y}}^n)(\boldsymbol{F}_h^{n,\ell+1})^T - \boldsymbol{F}_h^{n,\ell}\Pi_h^S(\boldsymbol{c}_h^{n,0}\circ\widetilde{\mathrm{y}}^n)(\boldsymbol{F}_h^{n,\ell+1})^T\|_{L^1}\\ &+ \|\boldsymbol{F}_h^{n,\ell}\Pi_h^S(\boldsymbol{c}_h^{n,0}\circ\widetilde{\mathrm{y}}^n)(\boldsymbol{F}_h^{n,\ell+1})^T - \boldsymbol{F}_h^{n,\ell}\Pi_h^S(\boldsymbol{c}_h^{n,0}\circ\widetilde{\mathrm{y}}^n)(\boldsymbol{F}_h^{n,\ell})^T\|_{L^1}.\end{aligned}$$

Using an argument similar to that in the proof of Lemma 8.1, we obtain

$$\begin{aligned}\|\boldsymbol{e}_{\boldsymbol{c}}^{\ell+1}\|_{L^1} &\le 2(\|\boldsymbol{F}_h^{n,\ell+1}\|_\infty + \|\boldsymbol{F}_h^{n,\ell}\|_\infty)\|\boldsymbol{c}_h^{n,0}\|_{L^1}\|\boldsymbol{F}_h^{n,\ell+1} - \boldsymbol{F}_h^{n,\ell}\|_\infty\\ &\le 8\|\boldsymbol{c}_h^{n,0}\|_{L^1}\|\boldsymbol{F}_h^{n,\ell+1} - \boldsymbol{F}_h^{n,\ell}\|_\infty \le 32kh^{-1}\|\boldsymbol{c}_h^{n,0}\|_{L^1}\|\nabla\mathbf{u}_h^{n,\ell+1} - \nabla\mathbf{u}_h^{n,\ell}\|_0,\end{aligned}$$

where the last inequality is from the inverse inequality and the following fact:

$$\begin{aligned}\boldsymbol{F}_h^{n,\ell+1} - \boldsymbol{F}_h^{n,\ell} &= \boldsymbol{F}_h^{n,\ell+1}\left((\boldsymbol{F}_h^{n,\ell})^{-1} - (\boldsymbol{F}_h^{n,\ell+1})^{-1}\right)\boldsymbol{F}_h^{n,\ell}\\ &= \boldsymbol{F}_h^{n,\ell+1}\left(\boldsymbol{\delta} - k\Pi_h(\nabla\mathbf{u}_h^{n,\ell}) - \boldsymbol{\delta} + k\Pi_h(\nabla\mathbf{u}_h^{n,\ell+1})\right)\boldsymbol{F}_h^{n,\ell}\\ &= k\boldsymbol{F}_h^{n,\ell+1}\Pi_h(\nabla\mathbf{u}_h^{n,\ell+1} - \nabla\mathbf{u}_h^{n,\ell})\boldsymbol{F}_h^{n,\ell}.\end{aligned}$$

By invoking the inverse inequality again, we conclude that

$$\mathrm{Re}\,\|\boldsymbol{e}_{\mathbf{u}}^{\ell+1}\|_0^2 \le C_3 k h^{-2}\|\boldsymbol{e}_{\boldsymbol{c}}^{\ell}\|_{L^1}^2 \le C_4 k^3 h^{-4}\|\boldsymbol{c}_h^{n,0}\|_{L^1}^2\|\boldsymbol{e}_{\mathbf{u}}^{\ell}\|_0^2. \tag{8.33}$$

For sufficiently small k, more specifically $C_4\overline{C}^2k^3h^{-4} \le 1/2$, Eqn (8.33) implies that the sequences $\{\|\boldsymbol{e}_{\mathbf{u}}^{\ell}\|_0\}$ and $\{\|\boldsymbol{e}_{\boldsymbol{c}}^{\ell}\|_{L^1}\}$ are contractions. Hence, $\mathbf{u}_h^{n,\ell}$ converges in the L^2 sense and $\boldsymbol{c}_h^{n,\ell}$ converges in the L^1 sense. □

THEOREM 8.4 (Global Existence of the Discrete Solution). *For any initial guess $\mathbf{u}_h^0$ and $\boldsymbol{c}_h^0$, there is a positive constant κ_0, such that the discrete systems (8.2)–(8.4) have a unique solution for all $n \ge 0$ as long as $k \le \kappa_0 h^2$.*

PROOF. This theorem follows directly from Theorem 8.2 by noting that, in its proof, the time step size k and all other constants appearing in the proof of Theorem 8.2 are independent of the time level t^n. □

8.3. Computational complexity

So far, we have discussed all the details of the fully discrete scheme, Algorithm 3. We can now further investigate the computational complexity of Algorithm 3.

First, if k is small enough, then the nonlinear equation for the flow map in Step 1, Algorithm 3 is solvable. Specifically, Step 1 can be solved in a fixed number of iterations. Second, Theorem 8.3 guarantees that the fixed-point iteration for solving the coupled system in Step 2 can also be terminated in a finite number of iterations to any given tolerance tol. Finally, we have seen that Stokes-type systems can be solved by optimal multilevel methods independent of h, k, Re, and η_s. Based on these observations, we can easily see the following result:

COROLLARY 8.2 (Computation Complexity). *If the time step size k is small enough, Algorithm 1 converges uniformly with respect to* Re *and* Wi *and the computational complexity is $O(N \log N)$, where N is the total spatial degrees of freedom.*

9. Implementation details and numerical experiments

In this section, we will give details of our implementation of Algorithm 3. We will also offer some preliminary numerical experiments.

9.1. A benchmark problem

We consider the Poiseuille flow between two parallel plates around a cylinder with circular cross section for the numerical tests. The problem is well suited as a benchmark problem for understanding the viscoelastic models in a smooth flow without geometric singularity; see, for example, AFONSO, OLIVEIRA, PINHO and ALVES [2009], CORONADO, ARORA, BEHR and PASQUALI [2007], and SUN, SMITH, ARMSTRONG and BROWN [1999]. We start by describing the geometry and boundary conditions.

9.1.1. A two-dimensional model problem

Consider the computational domain $\Omega \subset \mathbb{R}^2$ as described in Fig. 9.1.

We use a symmetric domain with $R = 1$, $H_1 = H_2 = 2$, and $L_1 = L_2 = 15$. The ratio of the distance between the two plates and the diameter of the circular hole is 2.

As discussed in Section 3, the nondimensional Oldroyd-B model can be written as follows: find $(\mathbf{u}, p, \boldsymbol{c})$ for $x \in \Omega$ and $t \in (0, +\infty)$ such that

$$\begin{cases} \mathsf{Re}\left(\dfrac{\partial \mathbf{u}}{\partial t} + \mathbf{u} \cdot \nabla \mathbf{u}\right) + \nabla p - \eta_s \Delta \mathbf{u} = \nabla \cdot \boldsymbol{c} \\ \nabla \cdot \mathbf{u} = 0 \\ \dfrac{1}{\mathsf{Wi}} \boldsymbol{c} + \mathcal{L}_{\mathbf{u}, \nabla \mathbf{u}} \boldsymbol{c} = \dfrac{(1-\eta_s)}{\mathsf{Wi}^2} \boldsymbol{\delta}. \end{cases} \tag{9.1}$$

On the top and bottom walls, we impose the no-slip boundary condition for the flow velocity $\mathbf{u}$; at the outflow boundary, we give the Neumann boundary condition for $\mathbf{u}$. And the inflow

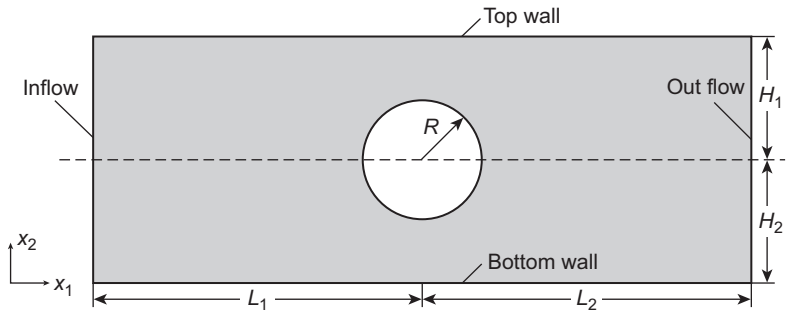

FIG. 9.1 Flow-past-cylinder domain

boundary condition for velocity is given by

$$\mathbf{u} = \begin{pmatrix} 1.5\left(1 - \left(\frac{x_2}{H}\right)^2\right) \\ 0 \end{pmatrix}.$$

Therefore, the average speed of the background inflow fluids is 1.0 in the horizontal direction and 0.0 in the vertical direction.

9.1.2. Drag coefficient

In order to compare with the established benchmark results in the literature, we focus on the dimensionless drag coefficient. The definition of the drag coefficient can be given as follows:

$$F_D = \frac{1}{U}\int_{\partial B} \left(-p\boldsymbol{\delta} + \eta_s(\nabla\mathbf{u} + \nabla\mathbf{u}^T) + \boldsymbol{c}\right)\mathbf{n}\cdot\mathbf{e}_1\,\mathrm{d}\Gamma, \tag{9.2}$$

where $\mathbf{n}$ is the outer unit normal vector for the boundary of circle ∂B (vector pointing outward from the circle) and $\mathbf{e}_1 = (1,0)^T$ and U is the mean background flow velocity.

There are two standard ways of computing the drag coefficient: one way is to compute the line integral directly on the curved boundary as in (9.2); an alternative is to do integration by parts and transform the integral into a volume integral (see JOHN [2004], for example.) Let $\boldsymbol{\varphi} = (\boldsymbol{\varphi}_1, 0)^T$ be a smooth function in Ω in which $\boldsymbol{\varphi}_1$ equals one on ∂B and vanishes on $\partial\Omega \setminus \partial B$. Multiplying $\boldsymbol{\varphi}$ on both ends of (9.1), we obtain that

$$\int_\Omega \mathrm{Re}\left(\frac{\partial\mathbf{u}}{\partial t} + \mathbf{u}\cdot\nabla\mathbf{u}\right)\cdot\boldsymbol{\varphi}\,\mathrm{d}x = \int_\Omega (-\nabla p + \eta_s\Delta\mathbf{u} + \nabla\cdot\boldsymbol{c})\cdot\boldsymbol{\varphi}\,\mathrm{d}x. \tag{9.3}$$

Applying integration by parts, we get

$$F_D = \frac{1}{U}\int_\Omega \left\{\mathrm{Re}\left(\frac{\partial\mathbf{u}}{\partial t} + \mathbf{u}\cdot\nabla\mathbf{u}\right) - \nabla p + \eta_s\Delta\mathbf{u} + \nabla\cdot\boldsymbol{c}\right\}\cdot\boldsymbol{\varphi}\,\mathrm{d}x. \tag{9.4}$$

9.2. Implementation details

In this section, we discuss the details for implementing Algorithm 3 step by step.

9.2.1. Flow map

We first discuss how to numerically approximate the departure foot of any point x in Step 1 of Algorithm 3 and how to find the value of certain functions at $\widetilde{y}^n$ using interpolation. Notice that in Step 1 of Algorithm 3, $\widetilde{y}^n$ appears on both sides of the equation for the midpoint rule. We can use a simple fixed-point iteration or the Newton–Raphson method to solve the nonlinear equation

$$G(y) = 0 \quad \text{with} \quad G(y) := y + k\mathbf{u}_h^n\left(\frac{x+y}{2}\right) - x.$$

In our experiments, we employ the Newton–Raphson method, and we stop the Newton–Raphson's iteration once the residual is less than 10^{-10}. In our experiments, the Newton–Raphson method usually converges in 2 to 4 iterations.

9.2.2. Feet searching

Once the coordinates of the departure foot $\widetilde{y}^n$ are computed as discussed in the previous section, we need to find the element in which $\widetilde{y}^n$ is located in order to perform interpolations in Step 2. Note that the time step size is usually small and the departure foot should not be too far away from the corresponding arrival point x. So it is natural to start searching for the host element by beginning with the element that contains x and then following the characteristics to locate the host element of each characteristic foot (Allievi and Bermejo [1997]). In order to describe the algorithm, we introduce two data structures first:

(i) PATCH(:,x) gives all elements that share a given point x, and PATCH(i,x) is the local index for the ith element in the patch.

(ii) NEIGH(:,E) gives the neighboring elements of a given element E, and NEIGH(s,E) is the neighbor of E opposite the side s.

Now, we are ready to describe the feet-searching algorithm.

Algorithm 4 Finding the Host Elements of Departure Feet

Step 0. Set the current element $E = \text{PATCH}(1, x)$ and $i = 1$.

Step 1. Find the reference coordinate r of y in E. If $r_1 + r_2 > 1$, then $s = 1$; else if $r_1 < 0$, then $s = 2$; else if $r_2 < 0$, then $s = 3$; otherwise, return E as the host element of y and stop.

Step 2. If NEIGH(s, E) has not yet been visited and it is not out-of-boundary, set $E =$ NEIGH(s, E); else if PATCH($i + 1$, x) is not empty, set $E = \text{PATCH}(i + 1, x)$ and $i = i + 1$. Go back to Step 1.

Step 3. Let E be the next nonvisited element and go to Step 1.

9.2.3. Stokes solvers

As stated in Section 7, the main computational cost at each iteration in Algorithm 3 is to solve the Stokes-like systems in Step 2. To date, we have only tested the Taylor–Hood $P_0^2 - P_0^1$ element; our implementation of the Scott–Vogelius $P_0^4 - P_{-1}^3$ is on going. We discussed two types of Stokes solvers in Section 7. Here, we test the preconditioned MinRes method using the flow-past-cylinder benchmark problem; we, therefore, (i) test the Stokes solvers for steady-state problems and (ii) test the time-marching scheme as a smoother to solve steady-state problems.

We report the dimensionless drag coefficient for various meshes in Tables 9.1 and 9.2 and for iteration numbers in Table 9.3. From Table 9.2, we note that the steady-state solution does not depend on time step size k. The differences between drag coefficients using different time step sizes k are less than 10^{-4}.

9.2.4. Using subdivisions to improve accuracy

In order to further improve accuracy, we divide each element $E \in \mathcal{T}_h$ into several subelements and then define the degree of freedom on each subelement for the piecewise constant

TABLE 9.1
Drag coefficient for steady-state Stokes flow between parallel plates

	DOF	$h_{\min}$	Drag coefficient	Difference
Mesh 1	33001	1.8e-3	132.24599	
Mesh 2	58979	7.1e-4	132.30130	5.5315e-02
Mesh 3	109729	3.2e-4	132.33079	2.9488e-02
Mesh 4	213575	2.0e-4	132.34571	1.4917e-02
Mesh 5	416409	7.1e-5	132.35255	6.8414e-03

The convergence rate for the drag coefficient is DOF^{-1} where DOF is the degrees of freedom. Reference value $= 132.34 \sim 132.36$.

TABLE 9.2
Steady limit of the drag coefficient for the time-dependent Stokes flow between parallel plates

	DOF	$h_{\min}$	$k = 0.5$	$k = 0.1$	$k = 0.01$
Mesh 1	33001	1.8e-3	132.24577	132.24577	132.24577
Mesh 2	58979	7.1e-4	132.30126	132.30125	132.30125
Mesh 3	109729	3.2e-4	132.33078	132.33078	132.33078
Mesh 4	213575	2.0e-4	132.34571	132.34571	132.34571
Mesh 5	416409	7.1e-5	132.35256	132.35256	132.35255

TABLE 9.3
Number of iterations for the MinRes solver with zero initial guess for the steady-state Stokes system

	Mesh 1	Mesh 2	Mesh 3	Mesh 4	Mesh 5
Number of iteration	106	106	109	112	113

The stopping criteria is that the relative residual is smaller than 10^{-8}.

tensor $\boldsymbol{c}_h^n$. We notice that Marchal and Crochet [1987] have employed a similar technique, which has been used to enhance stability.

Here, we have some different considerations due to the difficulties that inheres in the Eulerian–Lagrangian method:

- The integrand on the right-hand side of the momentum equation is usually nonsmooth (piecewise polynomial), and using subelements can improve the accuracy of numerical quadrature.
- When the velocity field is nonconstant, the deformed element $E(y)$ changes its shape, and using subelements can describe the shape of deformed triangles much better.

The extra cost of this approach is that, after locating the host element of y_q, we need to find in the subelement in which it is located and then evaluate interpolation on each subelement.

9.3. Numerical experiments

For the benchmark problem (the flow past a cylinder in a two-dimensional setting), the Newtonian viscosity η_s chosen is 0.59, and the Reynolds number is assumed to be 0. So the polymeric viscosity is $\eta_p = 1 - \eta_s = 0.41$. For the computational domain in Fig. 9.1, we take $R = 1$, $H = 2R$, and $L_1 = L_2 = 15$. Under this setting, many research groups have obtained results for Wi up to about 1.2, and they have agreed on the problems for $\mathrm{Wi} \leq 0.7$; see Afonso, Oliveira, Pinho and Alves [2009], for example. In this section, we test our algorithms using the two-dimensional benchmark problem above on different meshes, with various Weissenberg numbers. The main purpose is to validate the convergence of the proposed algorithms and the long-term stability of the computation.

First, we fix $\mathrm{Wi} = 0.1$ and 0.5; we use different meshes to test the convergence of the algorithm. We report drag coefficients in Table 9.4. Notice that the drag coefficients converge when we refine the mesh.

In order to reduce the error introduced by the interpolation, we employ the subelement technique introduced in Section 9.2.4. We divide each element into 4 and 16 congruent elements by applying regular refinement (by dividing each triangle into four smaller congruent triangles) once and twice, respectively. The numerical results for $\mathrm{Wi} = 0.1$ are reported in Table 9.5. We find that accuracy is improved by using more accurate interpolation.

We test the proposed algorithm using 16 subelements on a mildly refined mesh (Mesh 2) for various Weissenberg numbers. As discussed in Section 8, our algorithms remain stable as the time steps increase. The drag coefficients are reported in Fig. 9.2, and the results are consistent with the literature at least for Wi less than or equal to 0.75.

We find that the positivity of the conformation tensor can be preserved in the discrete sense. But we have yet to implement a discretization scheme that will maintain a strong

Table 9.4
Mesh dependence of the drag coefficient for low Weissenberg numbers

	Spatial DOF	k	$\mathrm{Wi} = 0.1$	$\mathrm{Wi} = 0.5$
Mesh 1	6269	2.5×10^{-3}	127.60	115.41
Mesh 2	25471	1.25×10^{-3}	129.33	117.23
Mesh 3	102674	6.25×10^{-4}	129.94	117.99
Mesh 4	412277	3.125×10^{-4}	130.11	118.35

TABLE 9.5
Comparison of drag coefficient for Wi = 0.1 numbers using different number of subelements

	Spatial DOF	1 subelement	4 subelements	16 subelements
Mesh 1	3477	121.96931	124.68434	125.62053
Mesh 2	15509	127.13945	128.40418	128.94619
Mesh 3	25763	128.08089	129.00947	129.28447
Mesh 4	50068	128.41062	129.19577	129.53881

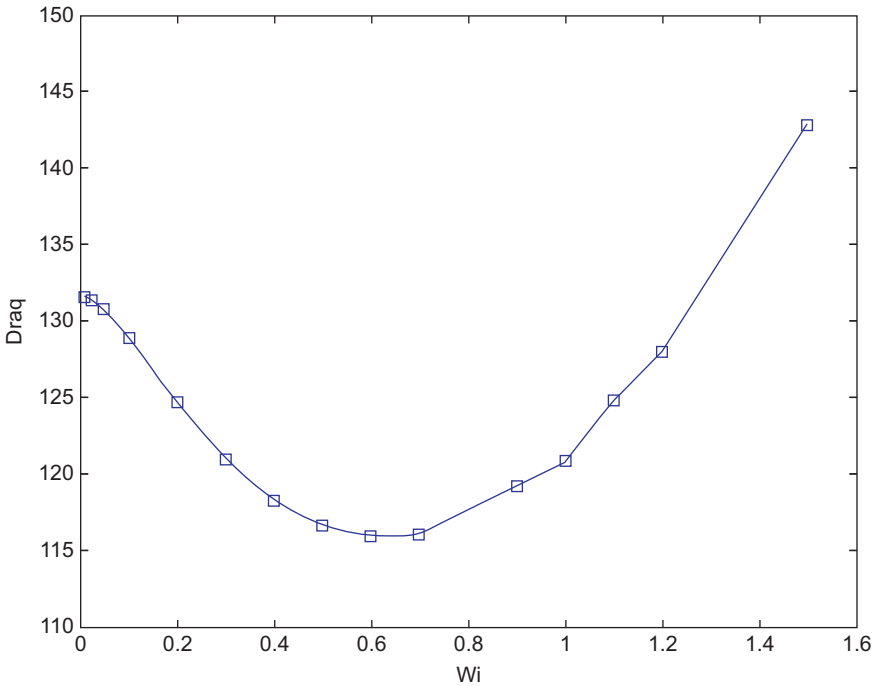

FIG. 9.2 Drag coefficients for various Weissenberg numbers.

divergence-free condition. Though the algorithm has not been fully realized, we obtained a stable numerical solution in time. We checked the grid convergence for different Weissenberg numbers, and we observed that the numerical solutions for Weissenberg numbers larger than 1.0 exhibit difficulties in grid convergence. In future research work, we will work to fully implement the proposed algorithms and study mesh convergence in high Weissenberg number regimes.

10. Concluding remarks

In this article, we reviewed the link between various constitutive equations from viscoelastic fluid models and symmetric matrix Riccati differential equations. We presented several

building blocks for the unified and stable numerical treatment of viscoelastic fluid models. We provided the proof that the resulting discrete problem admits a globally unique solution. We discussed how Stokes-type linear systems can be solved effectively using multigrid methods. We also presented some of our recent efforts to implement the designed algorithms in order to demonstrate some of our theoretical results.

Acknowledgments

The first author was supported in part by NSF DMS-0753111, DMS-0915028, and the Startup fund from the Rutgers University. The second and third authors were supported in part by NSF DMS-0749202, DMS-0915153, and the Center for Computational Mathematics and Application, the Pennsylvania State University.

References

Abou-Kandil, H., Freiling, G., Ionescu, V., Jank, G. (2003). *Matrix Riccati Equations: In Control and Systems Theory*, Systems and Control (Birkhäuser Verlag, Boston).

Adams, J., Fielding, S., Olmsted, P. (2008). The interplay between boundary conditions and flow geometries in shear banding: Hysteresis, band configurations, and surface transitions. *J. Non-Newton. Fluid Mech.* **151**, 101–118. 4th Annual European Rheology Conference.

Afonso, A., Oliveira, P., Pinho, F., Alves, M. (2009). The log-conformation tensor approach in the finite-volume method framework. *J. Non-Newton. Fluid Mech.* **157**, 55–65.

Allievi, A., Bermejo, R. (1997). A generalized particle search-locate algorithm for arbitrary grids. *J. Comput. Phys.* **132**, 157–166.

Alves, M.A., Oliveira, P.J., Pinho, F.T. (2003). Benchmark solutions for the flow of Oldroyd-B and PTT fluids in planar contractions. *J. Non-Newton. Fluid Mech.* **110**, 45–75.

Alves, M.A., Pinho, F.T., Oliveira, P.J. (2001). The flow of viscoelastic fluids past a cylinder: Finite-volume high-resolution methods. *J. Non-Newton. Fluid Mech.* **97**, 207–232.

Austin, T.M., Manteuffel, T.A., McCormick, S. (2004). A robust multilevel approach for minimizing $\mathbf{H}(\mathrm{div})$-dominated functionals in an $\mathbf{H}^1$-conforming finite element space. *Numer. Linear Algebra Appl.* **11**, 115–140.

Baaijens, F. (1993). An U-ALE formulation of 3-D unsteady viscoelastic flow. *Int. J. Numer. Methods Eng.* **36**, 1115–1143.

Baaijens, F.P. (1998). Mixed finite element methods for viscoelastic flow analysis: A review. *J. Non-Newton. Fluid Mech.* **79**, 361–385.

Bajaj, M., Bhat, P., Prakash, J.R., Pasquali, M. (2006). Multiscale simulation of viscoelastic free surface flows. *J. Non-Newton. Fluid Mech.* **140**, 87–107.

Bajaj, M., Pasquali, M., Prakash, J. (2008). Coil-stretch transition and the breakdown of computations for viscoelastic fluid flow around a confined cylinder. *J. Rheol.* **52**, 197–223.

Barrett, J., Süli, E. (2008). Existence of global weak solutions to dumbbell models for dilute polymers with microscopic cut-off. *M3AS*. **18**, 935–971.

Beris, A., Armstrong, R., Brown, R. (1984). Finite element calculation of viscoelastic flow in a journal bearing: I. small eccentricities. *J. Non-Newton. Fluid Mech.* **16**, 141–172.

Beris, A., Armstrong, R., Brown, R. (1986). Finite element calculation of viscoelastic flow in a journal bearing: II. moderate eccentricity. *J. Non-Newton. Fluid Mech.* **19**, 323–347.

Beris, A., Armstrong, R.C., Brown, R.A. (1983). Perturbation theory for viscoelastic fluids between eccentric rotating cylinders. *J. Non-Newton. Fluid Mech.* **13**, 109–148.

Beris A., Edwards, B. (1994). *Thermodynamics of Flow Systems, with Internal Mocrostructure* (Oxford Science Publication, New York).

Beris, A.N., Armstrong, R.C., Brown, R.A. (1987). Spectral/finite-element calculations of the flow of a Maxwell fluid between eccentric rotating cylinders. *J. Non-Newton. Fluid Mech.* **22**, 129–167.

Bird, R., Curtiss, C., Armstrong, R., Hassager, O. (1987). *Dynamics of Polymeric Liquids*, *Kinetic Theory* Volume 2 (Weiley Interscience, New York).

Black, W., Graham, M. (2001). Slip, concentration fluctuations, and flow instability in sheared polymer solutions. Macromolecules. **34**, 5731–5733.

Bonito, A., Picasso, M., Laso, M. (2006). Numerical simulation of 3D viscoelastic flows with free surfaces. *J. Comput. Phys.* **215**, 691–716.

Boyaval, S., Lelievre, T., Mangoubi, C. (2009). Free-energy-dissipative schemes for the Oldroyd-B model. *ESAIM:M2AN*. **43**, 523–561.

Bramble, J., Pasciak, J. (1997). Iterative techniques for time dependent Stokes problems. *Comput. Methods Appl. Mech. Eng.* **1–2**, 13–30.

Bramble, J.H. (1993). *Multigrid Methods*. Pitman Research Notes in Mathematical Sciences Volume 294. (Longman Scientific & Technical, Essex, England).

Brandt, A. (1977). Multi–level adaptive techniques (MLAT) for partial differential equations: ideas and software. In: Rice, J.R. (ed.), (Academic Press, New York), 277–318.

Brenner, S.C., Scott, L.R. (2002). *The mathematical theory of finite element methods*. Texts in Applied Mathematics Volume 15, (Springer-Verlag, New York), second ed.

Brezzi, F. (1974). On the existence, uniqueness and approximation of saddle point problems arising from Lagrange multipliers. *RAIRO Numer. Anal.* **8**, 129–151.

Brezzi, F., Fortin, M. (1991). *Mixed and hybrid finite element methods* (Springer-Verlag, New York).

Brockett, R.W. (1970). *Finite dimensional linear systems* (Wiley, New York).

Brown, R., Szady, M., Northey, P., Armstrong, R. (1993). On the numerical stability of mixed finite element methods for viscoelastic flows governed by differential constitutive equations. *Theor. Comput. Fluid Dyn.* **5**, 77–106.

Carreau, P., Grmela, M. (1987). Conformation tensor rheological models. *J. Non-Newton. Fluid Mech.* **23**, 271–294.

Chauvière, C., Owens, R. G. (2001). A new spectral element method for the reliable computation of viscoelastic flow. *Comput. Methods Appl. Mech. Eng.* **190**, 3999–4018.

Chemin, J.Y., Masmoudi, N. (2001). About lifespan of regular solutions of equations related to viscoelastic fluids. *SIAM J. Math. Anal.* **33**, 84–112.

Chilcott, M., Rallison, J. (1988). Creeping flow of dilute polymer solutions past cylinders and spheres. *J. Non-Newton. Fluids Mech.* **29**, 381–432.

Clermont, J., Pierrard, J. (1976). Experimental study of a non-viscometric flow: Kinematics of a viscoelastic fluid at the exit of a cylindrical tube. *J. Non-Newton. Fluid Mech.* **1**, 175–182.

Coronado, O.M., Arora, D., Behr, M., Pasquali, M. (2007). A simple method for simulating general viscoelastic fluid flows with an alternate log-conformation formulation. *J. Non-Newton. Fluid Mech.* **147**, 189–199.

Dealy, J., Vu, T. (1977). The Weissenberg effect in molten polymers. *J. Nonnewt. Fluid Mech.* **3**, 127–140.

Dieci, L. (1994). Structure preserving piecewise polynomial interpolation for definite matrices. *Lin. Alg. Appl.* **202**, 25–32.

Dieci, L., Eirola, T. (1994). Positive deffiniteness in the numerical solution of Riccati differential equations. *Numer. Math.* **67**, 303–313.

Dieci, L., Eirola, T. (1996). Preserving monotonicity in the numerical solution of Riccati differential equations. *Numer. Math.* **74**, 35–47.

Douglas, J., Russell, T.F. (1982). Numerical methods for convection-dominated diffusion problems based on combining the method of characteristics with finite element or finite difference procedures. *SIAM J. Numer. Anal.* **19**, 871–885.

Dupret, F., Marchal, J., Crochet, M. (1985). On the consequence of discretization errors in the numerical calculation of viscoelastic flow. *J. Non-Newton. Fluid Mech.* **18**, 173–186.

El-Kareh, A.W., Leal, L. (1989). Existence of solutions for all Deborah numbers for a non-Newtonian model modified to include diffusion. *J. Non-Newton. Fluid Mech.* **33**, 257–287.

Engler, H. (1987). On the dynamic shear flow problem for viscoelastic liquids. *SIAM J. Math. Anal.* **18**, 972–990.

Fattal, R., Kupferman, R. (2004). Constitutive laws for the matrix-logarithm of the conformation tensor. *J. Non-Newton. Fluid Mech.* **124**, 281–285.

Fattal, R., Kupferman, R. (2005). Time-dependent simulation of viscoelastic flows at high Weissenberg number using the log-conformation representations. *J. Non-Newton. Fluid Mech.* **126**, 23–37.

Feng, K., Shang, Z.-J. (1995). Volume-preserving algorithms for source-free dynamical systems. *Numer. Math.* **71**, 451–463.

Fortin, M., Esselaoui, D. (1987). A finite element procedure for viscoelastic flows. *Inter. J. Numer. Methods in Fluids.* **7**, 1035–1052.

Fortin, M., Fortin, A. (1989). A new approach for the FEM simulation of viscoelastic flows. *J. Non-Newton. Fluid Mech.* **32**, 295–310.

Fortin, M., Glowinski, R. (1982). *Méthodes de lagrangien augmenté*. Méthodes Mathématiques de l'Informatique Volume 9 (Gauthier-Villars, Paris). Applications à la résolution numérique de problèmes aux limites.

Fortin, M., Glowinski, R. (1983). *Augmented Lagrangian methods*. Studies in Mathematics and its Applications Volume 15. (North-Holland Publishing Co., Amsterdam). Applications to the numerical solution of boundary value problems, Translated from the French by B. Hunt and D. C. Spicer.

Fortin, M., Pierre, R. (1989). On the convergence of the mixed method of Crochet and Marchal for viscoelastic flows. *Comput. Methods Appl. Mech. Engrg.* **73**, 341–350.

Gelbart, W., Ben-Shaul, (1996). The "new" science of "complex fluids". *J. Phys. Chem.* **100**, 13169–13189.

Giesekus, H. (1982). A simple constitutive equation for polymer fluids based on the concept of deformation-dependent tensorial mobility. *J. Non-Newton. Fluid Mech.* **11**, 69–109.

Glowinski, R. (2003). Finite element methods for incompressible viscous flow. In: *Handbook of Numerical Analysis*, Volume IX (North-Holland, Amsterdam), 3–1176.

Glowinski, R., Le Tallec, P. (1989). *Augmented Lagrangian and operator-splitting methods in nonlinear mechanics*. SIAM Studies in Applied Mathematics Volume 9 (Society for Industrial and Applied Mathematics (SIAM), Philadelphia, PA).

Gordon, R., Schowalter, W. (1972). Anisotropic fluid theory: A different approach to the dumbbell theory of dilute polymer solutions. *Trans. Soc. Rheo.* **16**, 79–97.

Groisman, A., Steinberg, V. (1998). Mechanism of elastic instability in Couette flow of polymer solutions. *Experiment Phys. Fluids*, **10**, 2451–2463.

Guénette, R., Fortin, M. (1995). A new mixed finite element method for computing viscoelastic flows. *J. Non-Newton. Fluid Mech.* **60**, 27–52.

Guillope, C., Saut, J.-C. (1990a). Existence results for the flow of viscoelastic fluids with a differential constitutive law. *Nonlinear Anal.* **15**, 849–869.

Guillope, C., Saut, J.-C. (1990b). Global existence and one-dimensional nonlinear stability of shearing motions of viscoelastic fluids of Oldroyd type. *RAIRO Anal. Numér.* **24**, 369–401.

Hackbusch, W. (1985). *Multigrid Methods and Applications*. Computational Mathematics Volume 4. (Springer-Verlag, Berlin).

Hao, J., Pan, T.-W., Glowinski, R., Joseph, D.D. (2009). A fictitious domain/distributed Lagrange multiplier method for the particulate flow of Oldroyd-B fluids: A positive definiteness preserving approach. *J. Non-Newton. Fluid Mech.* **156**, 95–111.

He, L., Zhang, P. (2009). L2 decay of solutions to a micro-macro model for polymeric fluids near equilibrium. *SIAM J. Math. Anal.* **40**, 1905–1922.

Hu, H.H., Joseph, D.D. (1990). Numerical simulation of viscoelastic flow past a cylinder. *J. Non-Newton. Fluid Mech.* **37**, 347–377.

Hughes, T. (1984). Numerical Implementation of Constitutive Models: Rate-Independent Deviatoric Plasticity: Theoretical Foundation for Large-Scale Computations for Nonlinear Material Behavior. (Martinus Nijhoff Publisher, Dordrecht, The Netherlands).

Hughes, I., Brooks, A. (1982). A theoretical framework for Petrov-Galerkin methods with discontinuous weighting functions: Applications to the streamline upwind procedure. In: Gallagher, R., Norrie, D., Oden, D., Zienkiewicz, J. (eds.), *Finite Element in Fluids* Volume 4 (Wiley-Interscience Publisher, John Wiley and Sons, Inc., New York), pp. 47–65.

Hughes, T., Winget, J. (1980). Finite rotation effects in numerical integration of rate constitutive equations arising in large-deformation analysis. *Inter. J. Numer. Meth. Eng.* **15**, 1862–1867.

Hulsen, M. (1988). Some properties and analytical expressions for plane flow of Leonov and Giesekus models. *J. Non-Newton Fluid Mech.* **30**, 85–92.

Hulsen, M. (1990). A sufficient condition for a positive definite configuration tensor in differential models. *J. Non-Newton Fluid Mech.* **38**, 93–100.

Hulsen, M.A., Fattal, R., Kupferman, R. (2005). Flow of viscoelastic fluids past a cylinder at high Weissenberg number: Stabilized simulations using matrix logarithms. *J. Non-Newton. Fluid Mech.* **127**, 27–39.

Ilg, P., Karlin, I., Öttinger, H. (2002). Canonical distribution functions in polymer dynamics.(I). Dilute solutions of flexible polymers. *Physica A: Stat. Mech. Appl.* **315**, 367–385.

John, V. (2004). Reference values for drag and lift of a two-dimensional time-dependent flow around a cylinder. *Int. J. Numer. Methods Fluids.* **44**, 777–788.

Johnson, M., Segalman, D. (1977). A model for viscoelastic fluid behaviour which allows non-Newtonian deformation. *J. Non-Newton. Fluid Mech.* **2**, 255–270.

Joseph, D. (1990a). Fluid dynamics of viscoelastic liquids. *Applied Mathematical Sciences* Volume 84. (Springer, New York), p. 755.

Joseph, D., Saut, J. (1986). Change of type and loss of evolution in the flow of viscoelastic fluids. *J. Non-Newton. Fluid Mech.* **20**, 117–141.

Joseph, D.D. (1990b). Fluid dynamics of two miscible liquids with diffusion and gradient stresses. *Eur. J. Mech. B Fluids* **9**, 565–596.

Jourdain, B., Lelivre, T., Bris, C.L. (2004). Existence of solution for a micro-macro model of polymeric fluid: the FENE model. *J. Funct Anal.* **209**, 162–193.

Kabanemi, K., Bertrand, F., Tanguy, P., Ait-Kadi, A. (1994). A pseudo-transient finite element method for the resolution of viscoelastic fluid flow problems by the method of characteristics. *J. Non-Newt. Fluid Mech.* **55**, 283–305.

King, R.C., Apelian, M.N., Armstrong, R.C., Brown, R.A. (1988). Numerically stable finite element techniques for viscoelastic calculations in smooth and singular geometries. *J. Non-Newton. Fluid Mech.* **29**, 147–216.

Kreiss, H.-O. (2001). *Time-dependent partial differential equations and their numerical solution*. (Birkhuser Verlag, Basel).

Larin, M., Reusken, A. (2008). A comparative study of efficient iterative solvers for generalized Stokes equations. *Numer. Linear Algebra Appl.* **15**, 13–34.

Lee, Y.-J. (2004). Modeling and Simulations of Non-Newtonian Fluid Flows, PhD thesis (State College, Pennsylvania).

Lee, Y.-J. (2009). Uniform stability analysis of Austin, Manteuffel and McCormick finite elements and fast and robust iterative methods for the Stokes-like equations. *Numer. Linear Algebra Appl*. **17** (1), 109–138, January 2010.

Lee, Y.-J., Wu, J., Chen, J. (2009). Robust multigrid method for the planar linear elasticity problems. *Numer. Math.* **113**, 473–496.

Lee, Y.-J., Wu, J., Xu, J., Zikatanov, L. (2007). Robust subspace correction methods for nearly singular systems. *Math. Models Methods Appl. Sci.* **17**, 1937–1963.

Lee, Y.-J., Xu, J. (2006). New formulations, positivity preserving discretizations and stability analysis for non-Newtonian flow models. *Comput. Methods Appl. Mech. Engrg.* **195**, 1180–1206.

Lee, Y.-J. Xu, J., Zhang, C-S. On the global existence and uniqueness of solutions to discretized viscoelastic flow models. *Math. Models Methods Appl. Sci.* In press.

Lesaint, P., Raviart, P.A. (1979). Finite element collocation methods for first order systems. *Math. Comput.* **33**, 891–918.

Li, W.E.T., Zhang, P. (2004). Well-posedness for the dumbbell model of polymeric fluids. *Commun. Math. Phys.* **248**, 409–427.

Lielens, G., Halin, P., Jaumain, I., Keunings, R., Legat, V. (1998). New closure approximations for the kinetic theory of finitely extensible dumbbells. *J. Non-Newton. Fluid Mech.* **76** 249–279.

Lin, F.-H., Liu, C., Zhang, P. (2005). On hydrodynamics of viscoelastic fluids. *Comm. Pure Appl. Math.* **58**, 1437–1471.

Lin, F.-H., Liu, C., Zhang, P. (2007). On a micro-macro model for polymeric fluids near equilibrium. *Commun. Pure Appl. Math.* LX, 838–866.

Lions, P.L., Masmoudi, N. (2000). Global solutions for some Oldroyd models of non-Newtonian flows. *Chinese Ann. Math. Ser. B.* **21**, 131–146.

Liu, A.W., Bornside, D.E., Armstrong, R.C., Brown, R.A. (1998). Viscoelastic flow of polymer solutions around a periodic, linear array of cylinders: comparisons of predictions for microstructure and flow fields. *J. Non-Newton. Fluid Mech.* **77**, 153–190.

Lozinski, A., Owens, R.G. (2003). An energy estimate for the Oldroyd B model: Theory and applications. *J. Non-Newton. Fluid Mech.* **112**, 161–176.

Marchal, J., Crochet, M. (1987). A new mixed finite element for calculating viscoelastic flow. *J. Non-Newton. Fluid Mech.* **26**, 77–114.

Nochetto, R.H., Pyo, J.-H. (2004). Optimal relaxation parameter for the Uzawa method. *Numer. Math.* **98**, 695–702.

Nochetto, R.H., Wahlbin, L.B. (2002). Positivity preserving finite element approximation. *Math. Comp.* **71**, 1405–1419.

Oldroyd, J. (1950). On the formulation of rheological equations of state. *Proc. Roy. Soc.* **A200**, 523–541.

Oldroyd, J. (1958). Non-Newtonian effects in steady motion of some idealized elasto-viscous liquids. *Proc. R. Soc. A.* **245**, 278–297.

Oliveira, P.J., Pinho, F.T., Pinto, G.A. (1998). Numerical simulation of non-linear elastic flows with a general collocated finite-volume method. *J. Non-Newton. Fluid Mech.* **79**, 1–43.

Olshanskii, M.A., Peters, J., Reusken, A. (2006). Uniform preconditioners for a parameter dependent saddle point problem with application to generalized Stokes interface equations. *Numer. Math.* **105**, 159–191.

Owens, R., Phillips, T. (2002). *Computational Rheology* (Imperial College Press, London).

Paige, C.C., Saunders, M.A. (1975). Solutions of sparse indefinite systems of linear equations. *SIAM J. Numer. Anal.* **12**, 617–629.

Pan, T.-W., Hao, J., Glowinski, R. (2009). On the simulation of a time-dependent cavity flow of an Oldroyd-B fluid. *Int. J. Numer. Methods Fluids.* **60**, 791–808.

Pasquali, M., Scriven, L.E. (2002). Free surface flows of polymer solutions with models based on the conformation tensor. *J. Non-Newton. Fluid Mech.* **108**, 363–409.

Petera, J. (2002). A new finite element scheme using the Lagrangian framework for simulation of viscoelastic fluid flows. *J. Non-Newton. Fluid Mech.* **103**, 1–43.

Phillips, T.N., Williams, A.J. (1999). Viscoelastic flow through a planar contraction using a semi-lagrangian nite volume method. *J. Non-Newton. Fluid Mech.* **87**, 215–246.

Pironneau, O. (1981/82). On the transport-diffusion algorithm and its applications to the Navier-Stokes equations. *Numer. Math.* **38**, 309–332.

Rajagopalan, D., Armstrong, R., Brown, R. (1990). Finite-element methods for calculation of steady, viscoelastic flow using constitutive-equations with a Newtonian viscosity. *J. Non-Newton. Fluid Mech.* **36**, 159–192.

Reid, W. (1972). Riccati differential equations. Mathematics in Science and Engineering Voloume 86 (Academic Press, New York).

Remmelgas, J., Singh, P., Leal, L. (1999). Computational studies of nonlinear elastic dumbbell models of Boger fluids in a cross-slot flow. *J. Non-Newton. Fluid Mech.* **88**, 31–61.

Renardy, M. (1991). An existence theorem for model equations resulting from kinetic theories of polymer solutions. *SIAM J. Math. Anal.* **22**, 313–327.

Renardy, M. (2000a). Asymptotic structure of the stress field in flow past a cylinder at high Weissenberg number. *J. Non-Newton. Fluid. Mech.* **90**, 13–23.

Renardy, M. (2000b). *Mathematical Analysis of Viscoelastic Flows*. CBMS-NSF regional conference series in applied mathematics Volume 73 (SIAM, Philadelphia).

Renardy, M. (2006). A comment on smoothness of viscoelastic stresses. *J. Non-Newton. Fluid Mech.* **138**, 204–205.

Renardy, M. (2009). Global existence of solutions for shear flow of certain viscoelastic fluids. *J. Math. Fluid Mech.* **11**, 91–99.

Rusten, T., Winther, R. (1992). A preconditioned iterative method for saddlepoint problems. *SIAM J. Matrix Anal. Appl.* **13** (3), 887–904.

Scott, L., Vogelius, M. (1985a). *Conforming finite element methods for incompressible and nearly incompressible continua*. Lectures in Appl. Math., Large-scale computations in fluid mechanics, Part 2 (La Jolla, Calif., 1983) Volume 22-2 (Amer. Math. Soc., Providence, RI).

Scott, L., Vogelius, M. (1985b). Norm estimates for a maximal right inverse of the divergence operator in spaces of piecewise polynomials. *RAIRO Modél. Math. Anal. Numér.* **19**, 111–143.

Simo, J., Hughes, T. (1998). *Computational inelasticity*. Interdisciplinary Applied Mathematics Volume 7 (Springer, New York).

Sun, J., Phan-Thien, N., Tanner, R.I. (1996). An adaptive viscoelastic stress splitting scheme and its applications: AVSS/SI and AVSS/SUPG. *J. Non-Newton. Fluid Mech.* **65**, 75–91.

Sun, J., Smith, M.D., Armstrong, R.C., Brown, R.A. (1999). Finite element method for viscoelastic flows based on the discrete adaptive viscoelastic stress splitting and the discontinuous Galerkin method: DAVSS-G/DG. *J. Non-Newton. Fluid Mech.* **86**, 281–307.

Sureshkumar, R., Beris, A. (1995). Effect of artificial stress diffusivity on the stability of numerical calculations and the flow dynamics of time-dependent viscoelastic flows. *J. Non-Newton. Fluid. Mech.* **60**, 53–80.

Sureshkumar, R., Beris, A. (1997). Direct numerical simulation of the turbulent channel flow of a polymer solution. *Phys. Fluids* **9**, 743–755.

Szady, M., Salamon, T., Liu, A., Bornside, D., Armstrong, R., Brown, R. (1995). A new mixed finite-element method for viscoelastic flows governed by differential constitutive-equations. *J. Non-Newton. Fluid. Mech.* **59**, 215–243.

Szeri, A. (2000). A deformation tensor model for nonlinear rheology of FENE polymer solutions. *J. Non-Newton. Fluid Mech.* **92**, 1–25.

Taylor, C., Hood, P. (1973). A numerical solution of the Navier-Stokes equations using the finite element technique. *Int. J. Comput. Fluids.* **1**, 73–100.

Thien N., Tanner, R. (1977). A new constitutive equation derived from network theory. *J. Non-Newton. Fluid Mech.* **2**, 353–365.

Thiffeault, J.-L. (2001). Covariant time derivatives for dynamical systems. *J. Phys. A* **34**, 5875–5885.

Thomases, B., Shelley, M. (2007). Emergence of singular structures in Oldroyd-B fluids. *Phys. Fluids* **19**, 103103.

Thomases, B., Shelley, M. (2009). A transition to mixing and oscillations in a Stokesian viscoelastic flow. *Phys Rev. Lett.* **103**, 094501.

Vaithianathan, T., Robert, A., Brasseur, J.G., Collins, L.R. (2006). An improved algorithm for simulating three-dimensional viscoelastic turbulence. *J. Non-Newton. Fluid Mech.* **140**, 3–22.

Vaithianathan, T., Robert, A., Brasseur, J.G., Collins, L.R. (2007). Polymer mixing in shear-driven turbulence. *J. Fluid Mech.* **585**, 487–497.

Wapperom, P., Renardy, M. (2005). Numerical prediction of the boundary layers in the flow around a cylinder using a fixed velocity field. *J. Non-Newton. Fluid Mech.* **125**, 35–48.

Xie, X., Xu, J., Xue, G. (2008). Uniformly-stable finite element methods for Darcy-Stokes-Brinkman models. *J. Comput. Math.* **26**, 437–455.

Xu, J. (1992). Iterative methods by space decomposition and subspace correction. *SIAM Rev.* **34**, 581–613.

Xu, J. (2009). Optimal algorithms for discretized partial differential equations. In: ICIAM 07—6th International Congress on Industrial and Applied Mathematics. *Eur. Math. Soc*, (Zürich), pp. 409–444.

Xu, J. (2010). Fast Poisson-based solvers for linear and nonlinear PDEs. In: *Proceedings of International Congress of Mathematicians* (World Scientific Publishing Company, Hyderabad, India).